Inaugural dissertation

for

obtaining the doctoral degree

of the

Combined Faculty of Mathematics, Engineering and Natural Sciences

of the

Ruprecht - Karls - University

Heidelberg

Presented by

Sonja Ildiko Herter, MSc

Born in Böblingen, Germany

Oral Examination: 18.09.2024

Multi-Parametric Drug Screening identifies Vulnerabilities and Combination Treatment Strategies for Neuroblastoma Subtypes

Referees: Prof. Dr. Peter Angel

Apl.-Prof. Dr. Ina Oehme

Declaration

I hereby declare that I have written this dissertation myself, using only the cited literature and sources.

I hereby declare that I have not applied to be examined at any other institution, nor have I used the dissertation in this or any other form at any other institution as an examination paper, nor submitted it to any other faculty as a dissertation.

Sonja Ildiko Herter

Summary

Neuroblastoma is the most common extracranial solid tumor in children and shows variable clinical outcomes. Neuroblastoma comprises epigenetically regulated subtypes, sustained by super enhancer networks and characterized by subtype specific gene sets. The adrenergic subtype shows a more differentiated, adrenal linage committed identity while the mesenchymal subtype displays a more undifferentiated stem cell like phenotype. This diversity contributes to the clinical heterogeneity as mesenchymal cells show elevated resistance to conventional chemotherapy drugs and occur more often in relapses. However, comprehensive analysis of subtype-specific vulnerabilities and optimal therapeutic interventions remain an ongoing challenge.

Drug sensitivity profiling based on metabolic activity for 75 clinically relevant drugs for a panel of 24 neuroblastoma cell lines showed varying drug sensitivity profiles across the subtypes. Elevated sensitivity to chemotherapeutic drugs was confirmed for the adrenergic subtype, whereas increased sensitivity to MEK inhibitors was revealed as novel vulnerability for the mesenchymal subtype.

Neuroblastoma subtypes differ in their cellular phenotype, therefore I developed a high-content imaging pipeline to quantify distinct morphological characteristics. Mesenchymal neuroblastoma cells showed an enlarged cellular phenotype and increased lysosomal content. Using changes in lysosomal content as readout for an image-based drug screen, I highlighted differences in the lysosomal stress response among neuroblastoma subtypes and demonstrated a higher increase in lysosome amount in response to chemotherapy treatment for mesenchymal neuroblastoma.

To test, if higher lysosomal content in combination with the previously identified drug hits such as the MEKi could serve as a targetable vulnerability in the mesenchymal subtype, I did synergy combination screens, including image-based and metabolic readouts. Here, the lysosome was targeted by lysomotropic drugs and inhibitors of lysosomal acid sphingomyelinase. Although the results revealed synergistic effects for some combinations, a general heightened sensitivity for the mesenchymal subtype could not be demonstrated.

Gene expression analysis revealed an upregulation of senescence secretome-associated pathways in mesenchymal neuroblastoma cells. Moreover, senescence was induced upon treatment of mesenchymal cells with inhibitors of the MAPK pathway, suggesting a metabolic alteration, which is druggable by senolytic treatments. The combination of senescence inducing drugs and senolytic agents was indeed synergistic in a sequential synergy screen setting.

In summary, metabolic and morphological drug screens identified subtype-specific differences in drug sensitivity and phenotypic adaptation to drug treatment. Targeting lysosomal acid sphingomyelinase or senolytic signaling in combination with inhibitors of the MAPK pathway may be a possible therapeutic approach for neuroblastoma and will have to be evaluated in further studies.

Zusammenfassung

Das Neuroblastom ist ein Tumor des sympathischen Nervensystems und ist der häufigste maligne extrakranielle Tumor im Kindesalter. Neuroblastome bestehen aus Zellen verschiedener epigenetisch regulierter Subtypen. Das sind zum einen Zellen des adrenergen Subtyps, die einen höheren Differenzierungsgrad zu adrenergen Nervenzellen aufweisen, sowie stammzellähnliche, mesenchymale Zellen mit einem niedrigeren Grad an Differenzierung. Die Subtypen sind durch Expression spezifischer Gene charakterisiert, deren Transkription durch super enhancer Netzwerke veranlasst wird. Diese Heterogenität der Tumore spiegelt sich in den klinischen Verläufen wieder. So sind Zellen mit mesenchymalen Charakteristika häufiger in Rezidiven zu finden und zeigen eine höhere Resistenz gegenüber der klassischen Chemotherapeutika, die standardmäßig in der Neuroblastomtherapie Anwendung finden. Darüber hinaus gibt es jedoch keine Daten wie die Subtypen auf weitere, in der Krebstherapie eingesetzte, Medikamente reagieren.

In dieser Doktorarbeit habe ich Sensitivitätsprofile für 75 verschiedene Medikamente von 24 verschieden Neuroblastomzelllinien, die diese verschiedenen Subtypen widerspiegeln, erstellt. Die adrenergen Zelllinien zeigten wie erwartet eine höhere Sensitivität gegenüber der Behandlung mit klassischen Chemotherapeutika. Zusätzlich zeigte sich eine Sensitivität des mesenchymalen Subtyps gegenüber MEK-Inhibitoren. Mit dem High-Content Imaging Verfahren konnte ich die verschiedenen morphologischen Merkmale der Subtypen quantifizieren. Hier zeigten die mesenchymalen Zellen vergrößerte Zellkörper und eine höhere Anzahl an Lysosomen gegenüber den adrenergen Zellen. In einem selbstentwickelten Screening, das Änderungen der Lysosomenzahl quantifiziert, zeigte sich, dass die Subtypen unterschiedliche lysosomale Stressreaktionen auf medikamentöse Behandlung zeigen. Die Lysosomenzahl steigt stärker in mesenchymalen Zellen bei Behandlung mit Chemotherapeutika als in adrenergen Zellen. Um zu testen, ob die höhere Lysosomenzahl der mesenchymalen Zellen ein neuer Angriffspunkt für Wirkstoffe sein könnte, wurden lysosomale Inhibitoren in Kombination mit den bereits als wirksam identifizierten MEK-inhibitoren getestet. Zu diesen lysosomalen Inhibitoren zählen Medikamente die ursprünglich aus der Malariabehandlung kommen, sowie Inhibitoren der lysosomalen Sphingomyelinase. Einige dieser Kombinationen zeigten Synergieffekte, jedoch waren diese Effekte nicht spezifisch für einen Subtyp oder eine Wirkstoffklasse.

Eine Analyse der Genexpressionsprofile der Neuroblastomsubtypen zeigte eine erhöhte Expression der Gene des Seneszenz-assoziierten sekretorischen Phänotyps in den mesenchymalen Zelllinien. Seneszenz konnte außerdem durch MEK-Inhibitor Behandlung in den mesenchymalen Zellen induziert werden. Diese biologische Veränderung könnte mit Wirkstoffen, die in die Signalwege seneszenter Zellen eingreifen, als therapeutischer Angriffspunkt gesehen werden. Kombinationen aus Seneszenz induzierenden und senolytischen Wirkstoffen in einem sequentiellen Behandlungsplan zeigen Synergieeffekte.

Zusammenfassend wurden in diesem Projekt metabolische und bildbasierte Screening-Verfahren zur Wirkstofftestung mit Fokus auf Kombinationsbehandlungen entwickelt, welche die unterschiedlichen Sensitivitäten der Neuroblastomsubtypen zeigten. Hierbei wurden die MEK Inhibitoren als spezifische Behandlungsstrategie für den mesenchymalen Subtyp identifiziert. Wirkstoffe, die die lysosomale Sphingomyelinase hemmen oder Seneszenz Signalwege stören, könnten eine Möglichkeit zur Kombinationsbehandlung für Neuroblastome darstellen und sollten weiter erforscht werden.

Abbreviations

ALK	Anaplastic lymphoma kinase
ASM	Acid sphingomyleinase
ASMi	Acid sphingomyelinase inhibitor
ATP	Adenosine triphosphate
AUC	Area under the curve
BCL-2	B-cell lymphoma-2
BCL-XL	B-cell lymphoma-extra large
BF	Bright field
BETi	Bromodomain and extra-Terminal inhibitor
BSA	Bovine serum albumin
BztCL	Benzethoniumchloride
CAR-T	Chimeric antigen receptor T-cell therapy
CDK	Cyclin dependent kinase
ChIP-seq	Chromatin immunoprecipitation sequencing
CLEAR	Coordinated Lysosomal Expression and Regulation
CSS	Combined sensitivity score
CTG	Cell-Titer-Glo (Promega)
DAPI	4’,6-diamidino-2-phenylindole
DNA	Deoxyribonucleic acid
DMSO	Dimethyl sulfoxide
EDTA	Ethylenediaminetetraacetic Acid
EGF	Epidermal growth factor
ERK	Extracellular regulated kinase
FCS	Fetal calf serum
FGFR	Fibroblast growth factor receptor
FIMM	Institute for Molecular Medicine Finland
FITC	Fluorescein isothiocyanate
GO	Gene ontology
HCM	High content imaging
IC50	50% inhibitory concentration

IDRF	Image derived risk factors
IF	Immunofluorescence
IgG	Immune globulin G
INFORM	INdividualized Therapy FOr Relapsed Malignancies in Childhood
INRG	International neuroblastoma risk group
INSS	International neuroblastoma staging system
iTreX	interactive Therapy Response eXploration
LAMP	Lysosomal membrane associated protein
LMP	Lysosomal membrane permabilization
LT	Lysotracker
MAPK	Mitogen-activated protein kinase
MB	Medulloblastoma
MEK	Mitogen-activated protein kinase kinase
MPAS	MAPK pathway activity score
mRNA	Messenger ribonucleic acid
MSS	MAPK inhibitor sensitivity score
mTOR	Mammalian target of rapamycin
NB	Neuroblastoma
NEAA	Non-essential amino acids
NF1	Neurofibromin 1
NF-kB	Nuclear factor kappa-light-chain-enhancer of activated B cells
NGS	Next-generation sequencing
OIS	Oncogene-induced senescence
PBS	Phosphate-buffered saline
PC	Principal component
PCA	Principal component analysis
PCR	Polymerase chain reaction
PFA	Paraformaldehyde
RAF	Proto-oncogene serine/threonine-protein kinase
RAS	Rat sarcoma virus
Rpm	Rounds per minute

RT	Room temperature
SASP	Senescence-associated secretory phenotype
SD	Standard deviation
ssGSEA	Single-sample gene set enrichment analysis
STR	Straurosporine
TERT	Telomere reverse transcriptase
TME	Tumor microenvironment
TMRE	Tetra-methyl-rhodamin- ethylester
TNF	Tumor necrosis factor
UMAP	Uniform manifold approximation and projection
WHO	World health organization
WT	Wildtype
ZIP	Zero Interaction Potency

Table of Contents

List of Tables

List of Figures

List of supplementary figures

1 Introduction

1.1 Neuroblastoma

Neuroblastoma is an embryonal tumor arising from developing neural crest cells within the sympathetic nervous system during embryonal development. It is the most common extracranial solid tumor in children, with an average age at diagnosis of two years; approximately 90% of all cases are diagnosed below the age of five[1]. Neuroblastoma tumors are very heterogeneous, ranging from cases of spontaneous regression over low or intermediate risk tumors that can be surgically resected, to high-risk tumors associated with fatal outcomes despite intensive therapy[1].

1.2 Neuroblastoma clinical characterization

Neuroblastomas develop in the tissues of the sympathetic nervous system, such as the adrenal medulla and paraspinal ganglia, leading to the formation of masses and lesions in neck, chest, abdomen and pelvis. The symptoms experienced vary depending on the specific location of the tumor[2]. The course of the disease is quite heterogeneous for neuroblastoma. The median age at diagnosis stands at 17 months[3]. At the time of diagnosis, approximately 50% of cases show metastases, with bone, bone marrow, and lymph nodes being the most frequent sites[4].

The diagnostic and staging procedures for neuroblastoma use histological, biochemical, and imaging methods. Radiological imaging is performed to identify image-defined risk factors and metastatic sites. Biopsies support and confirm a diagnosis. The histology of the tumor is categorized as either favorable or unfavorable[5]. Molecular characterization involves analyzing the *MYCN* copy number, assessing ploidy, and evaluating segmental chromosomal aberrations such as 11q23 [6].

1.2.1 Disease staging

The International Neuroblastoma Staging System (INSS) from 1986 is a post-surgical staging system based on spread and resectability of the tumor. It was amended by International Neuroblastoma Risk Group (INRG) staging in 2004 that allows pre-surgical staging of tumors [7-9]. This system distinguishes for patients with locoregional tumors the absence or presence (staged as L1 or L2) of one of 20 possible image derived risk factors (IDRF). These are identified with imaging and are surrogates of aggressive tumor behavior such as vascular encasement and organ infiltration and are markers for tumor resectability. Tumor staging M is for distant metastasis and MS for tumors with specific metastasis patterns in infants younger than 18 months with metastasis limited to bone marrow, liver and skin. Tumors from this group can undergo spontaneous regression[8,9].

The risk of neuroblastoma tumors is classified according to their INRG stage. Additional markers that are considered are age, histopathology, resectability of the tumors and biomarkers such as MYCN amplification, ploidy and the presence of segmental chromosomal aberrations[10]. Half of all newly diagnosed neuroblastomas are classified as high-risk disease[1].

1.2.1.1 Genetic alterations in Neuroblastoma

Most neuroblastomas occur without a specific pattern of molecular risk factors or familial inheritance; however, genetic alterations can modify the risk of developing neuroblastoma. Compared to other, especially adult, cancer entities, neuroblastoma presents with a very low amount of somatic mutations, but commonly with chromosomal alterations[1]. The familial predisposition for neuroblastoma is relatively low, with only 2-3% of all cases having predisposing factors. In 80% of familial cases, these factors involve an activating alteration in *ALK*, a receptor tyrosine kinase, or an inactivating mutation in *PHOX2B*, a transcription factor crucial for the development of both the central and peripheral nervous systems[11,12].

1.2.1.2 Chromosomal alterations

Chromosomal alterations are observed in approximately 90% of all neuroblastoma cases[13]. Among these alterations, whole chromosome gains, particularly hyperploidy, are associated with a more favorable outcome compared to diploidy. Conversely, segmental chromosomal alterations such as loss of 1p, loss of 11q, and gain of 17q are generally linked to an unfavorable prognosis. The poor prognosis is attributed to tumor suppressor gene inactivation from segmental loss or the creation of enhancer structures that promote tumorigenesis[1]. Alterations, that are frequently identified at relapse are losses of 1p or 6q[14].

1.2.1.3 MYCN

MYCN is a transcription factor and a proto-oncogene that is well known for its role in embryonal development and affects many hallmarks of cancer, such as growth, metabolism and cellular differentiation[15]. Amplification of *MYCN* is one of the recurrent somatic alterations found in around 25% of sporadic neuroblastomas[16]. It is an established driver of high-risk neuroblastoma and a major prognostic factor as it has a high predictive value for neuroblastoma prognosis and is associated with aggressive tumors with an overall poor outcome[17,18].

1.2.1.4 ALK

The receptor tyrosine kinase ALK is constitutively activated through a point mutation in 6-12% of sporadic neuroblastomas in addition to genomic amplification of *ALK* in 1-2 % of neuroblastoma cases[11,19,20]. Relapsed neuroblastomas show activating *ALK* mutations in 20% of the cases[21]. *ALK* alterations also occur in other cancer entities, like non-small cell lung cancer, inflammatory myofibroblastic tumors and anaplastic large cell lymphomas. For treatment of non-small cell lung cancer, five ALK inhibitors are approved by the FDA, the ALK inhibitor crizotinib is also approved for the other two cancer entities[22]. For neuroblastoma, ALK inhibitors lorlatinib and crizotinib are studied in clinical trials, also in combination with chemotherapy as treatment option for ALK-driven high-risk classified tumors[23]

1.2.1.5 Telomere maintenance mechanisms

Other genomic alterations that are frequently present in high-risk neuroblastoma affect the telomere maintenance mechanisms. This include defects in ATRX that cause alternative lengthening of telomeres or chromosomal rearrangements that lead to activation of telomere reverse transcriptase (TERT)[23,24].

1.2.1.6 Immune system

In general, neuroblastomas have low immunogenicity and use various mechanisms to evade the immune system. This includes low levels of cytotoxic t cell infiltration and limited expression of MHC I which leads to evasion of T-cell mediated toxicity[25]. Natural killer cell function is inhibited in neuroblastoma by tumor associated macrophages and myeloid derived suppressor cells in the tumor micro environment[1]. Immunotherapy for neuroblastoma is a challenge, check point inhibitors that were successful for other entities are not effective[26]. Antibodies targeting GD2, a highly expressed disialoganglioside in neuroblastoma tumors, are approved by FDA and EMA for high risk neuroblastoma[26-28]. CAR-T cells targeting GD2 were also tested in phase I/II trials, unfortunately this treatment showed high toxicity[29].

1.2.2 Neuroblastoma tumor subtypes

During development of the sympathetic nervous system, precursor cells derived from the neural crest, including neuroblasts, chromaffin cell precursors, and Schwann cell precursors, undergo differentiation to give rise to structures such as the adrenal medulla and sympathetic trunk[30,31]. Neuroblastomas form in the adrenal gland or along the sympathetic chain resembling the differentiation stages of developing adrenal neuroblasts. These stages of differentiation have implications on therapy response and prognosis[1]. Low-risk tumors resemble the committed

neuroblasts, whereas high-risk tumors, particularly those amplified with MYCN, contain features of early neuroblasts[32].

This intra-tumor heterogeneity was already examined in 1983 in isogenic tumor-derived cell lines and their subclones and revealed the presence of tumor cells with different phenotypes. These were historically named neuroblastic, substrate adherent, and intermediate stem cell-like cells[33,34]. Subsequent research in gene expression and epigenetic profiling of neuroblastoma tumors and cell lines provided more insight into the intra-tumoral heterogeneity. These studies demonstrated that neuroblastomas are comprised of epigenetically regulated subtypes that range continuously between undifferentiated, more mesenchymal, neural crest-like cells and differentiated cells, committed to the sympathetic adrenergic linage[35,36]. These mesenchymal and adrenergic subtypes are characterized by the extent of expression of mesenchymal and adrenergic markers and their linage-specific super enhancers[37,38].

The epigenetic regulation is reprogrammable. Both cell types have the capability to reversibly transdifferentiate in cell culture, highlighting the plasticity of these neuroblastoma subtypes[36,39]. The identified epigenetic signatures are associated with different clinical outcomes, with relapsed tumors having increased mesenchymal properties[37]. Sensitivity to drug treatment is also different across the tumor subtypes. Super enhancers that overlap genes coding for drug targets, such as *ALK* in adrenergic cells, result in linage-specific sensitivity to targeted therapies, in this case to ALKi treatment[40]. In vitro, mesenchymal cells demonstrate increased resistance to standard chemotherapy agents such as doxorubicin, cis-platin, and etoposide[35,36]. Mesenchymal linage is also associated with resistance to immune therapy[41,42].

1.2.3 Neuroblastoma treatment

Depending on the risk status, neuroblastoma standard of care treatment ranges from observation only and surgical resection in low risk patients to multi modal therapy for high risk neuroblastomas. As low risk tumor can spontaneously regress, minimal therapeutic intervention is preferred. Neuroblastomas of the intermediate risk group are resected by surgery and treated with chemotherapy regimens of lower intensity. High-risk tumor treatments include intensive multi-agent chemotherapy with autologous hematopoietic stem-cell rescue, surgery and radiotherapy[43,44]. Immunotherapy with anti-GD2 antibodies such as dinutuximab and naxitamab is also used for high risk disease.[28,45]

Despite the intensive therapies, refractory disease and relapses are still a challenge in neuroblastoma treatment. Clinical trials from COG and SIOPEN explore intensification of the therapy regimens for neuroblastoma in the fields of immunotherapy and radiotherapy as well as targeted approaches[44]. Clinical trials that test targeted approaches are applying ALK inhibitors lorlatinib, certinib and crizotinib in treatment of relapsed neuroblastomas[1,46].

1.3 Lysosomes

Lysosomes are acidic organelles in the cytoplasm surrounded by a single lipid-bilayer membrane and are responsible for the degradation of biological macromolecules[47]. The organelles contribute to maintenance of cellular homeostasis and mediate adaptation of cell metabolism to environmental cues[48]. First described by Christian de Duve in the 1950s, lysosomes for a long time have only been regarded as cellular recycling bins for their role in disposal of cellular waste[49]. However, they also contribute to various signaling processes needed for cellular metabolism and homeostasis, such as autophagy, exocytosis, plasma membrane repair, cholesterol homeostasis and cell death[50,51].

1.3.1 Lysosomal regulation

Lysosomal biogenesis and lysosomal function are regulated by global transcription regulation involving the lysosomal transcription factors of the MiT/TFE family: MITF, TFEB, TFE3, TFEC[52,53]. All four transcription factors recognize an enhancer box DNA motif CLEAR within promotors of lysosomal and autophagy related genes[54].

The activity of the MiT/TFE transcription factors is regulated by shuttling between cytosol and nucleus. Dephosphorylated TFEB/TF3 translocate to the nucleus and activate gene expression. TFEB/TFE3 are phosphorylated by kinases such as mTOR, ERK GSK3beta, AKT and PKC and dephosphorylated by calcineurin phosphatase or protein phosphatase 2A. Phosphorylated TFEB/TFE3 get exported into the cytoplasm[55-57].

1.3.2 Lysosomal function

The two main classes of proteins that are essential for lysosomal functions are integral membrane proteins and hydrolases in the lysosomal lumen. Lysosomal membrane proteins are involved in the transport of substances in and out of the lysosome. For maintaining the acidity of the lysosomal lumen, vacuolar ATPases (v-ATPases) in the lysosomal membrane pump protons from the cytosol into the lysosome[58]. The most abundant proteins in the lysosomal membrane are the lysosomal membrane proteins LAMP1 & LAMP2. The luminal part of these proteins is highly glycosylated and protects the lysosomal membrane from digestive enzymes[52]. The lysosomal lumen has an acidic pH between 4.5 and 5 and contains more than 60 acid hydrolases, such as proteases, lipases and nucleases that digest macromolecules of all kind[59]. These hydrolases play an important role in cell death mechanisms. When the lysosomal membrane is permeabilized, hydrolases leak into the cytosol and induce apoptosis or other types of cell death independent of apoptosis pathways[59-61].

The main function of the lysosome is degradation of macromolecules within the cell. Intracellular components reach the lysosome by autophagy, a cellular catabolic process, which is distinguished in macroautophagy, microautophagy and chaperone mediated autophagy. In macroautophagy, cytoplasmic material is delivered to the lysosome by the autophagosome, whereas in microautophagy

the lysosomal membrane gets internalized to sequester cytoplasmic materials. In chaperone mediated autophagy, cytoplasmic proteins are recognized by chaperone proteins on the lysosomal membrane[62,63].

Extracellular material that is destined for degradation arrives to the lysosome by the endocytic pathway. The macromolecules are internalized in early endosomes that mature into late endosomes. Cargo that is destined for degradation arrives at the lysosome and the organelles fuse to form an endolysosome and mature to a dense lysosome[64]. Products of lysosomal digestion leave the lysosome through diffusion or carrier-mediated transport and are reused by the cell as building blocks or are released from the cell by lysosomal exocytosis[50,65].

1.3.3 Lysosomes in cancer

Lysosomes are highly dynamic organelles that adapt to changing metabolic needs in the malignant transformation of cancer cells. Many cancer cells have an increased metabolism and require more nutrients and energy to sustain their enhanced proliferation rate. Increased autophagy rates and elevated number of lysosomes are common metabolic changes to maintain homeostasis and support survival of cancerous cells in nutrient-stress conditions[66]. Increased aerobic glycolysis changes the pH of cancer cells leading to increased proton concentration in the cytosol. This dysregulation in cellular pH levels is stabilized by the lysosomes, through pumping cytosolic protons into the lysosomal lumen[67].

Lysosomal processes are also involved in metastatic growth of cancer cells. During lysosomal exocytosis, lysosomes release cathepsins into the extra cellular space, supporting the remodeling of the extracellular matrix. Since lysosomes are also involved in degradation of cell surface molecules that are recognized by immune cells, they also support immune evasion[67].

The lysosomal membrane of cancer cells is less stable compared to non-malignant cells. This makes cancer cells more susceptible to lysosomal membrane permeabilization, leading to release of lysosomal cathepsins into the cytosol[68]. This process was already discovered in 1959 by Christian deDuve, who described the lysosomes as potential suicide bags that cause autolysis of tissues when ruptured[49]. Lysosomal membrane permeabilization can be induced by oxidative stress, lipid accumulation or lysomotropic agents[66,69]. Depending on the mechanism that caused the membrane permeabilization and the extend of hydrolase release into the cytosol, lysosomal membrane permeabilization can either lead to apoptosis or induce other cell death types like necrosis[70]. The release of cathepsins B and D activates Bid and leads to mitochondrial outer membrane permeabilization followed by cytochrome c release which induces caspase dependent apoptosis[68]. Extended release of cathepsins leads to uncontrolled breakdown of cellular molecules and results in necrosis[71,72].

In addition to the lysosomal changes that are relevant for maintaining metabolic homeostasis of cancer cells, lysosomes play an important role in cancer drug resistance. Drugs with a lipophilic, weak basic molecular structure such as doxorubicin, sunitinib, and mitoxantrone can pass the lysosomal membrane and get protonated in the lysosomal lumen. Due to this additional charge, the drugs are trapped and accumulate in the lysosome not reaching their nuclear or cytosolic targets [73-75].

1.3.4 Targeting lysosomes in cancer

Recognizing the contribution of lysosomes to cancer cell survival and drug resistance has raised interest in strategies to pharmacologically inhibit lysosomal functions. The most common strategy to interfere with lysosomes is to use lysomotropic drugs with lipophilic, weak basic or amphiphilic molecular structure. These drugs accumulate in the lysosome and interfere with pH levels, disrupt lysosomal membrane stability, induce lysosomal membrane permeabilization, and inhibit lysosomal functions including autophagy[76].

Examples for lysomotropic drugs are chloroquine and chloroquine derivates, which accumulate in the lysosome, increase lysosomal pH and impair autophagosome formation and therefore are also considered autophagy inhibitors[77]. Another group of drugs that accumulate in lysosomes are inhibitors of the lysosomal acid sphingomyelinase, which converts sphingomyelin into ceramide and phosphocholine. Inhibition of that enzyme causes accumulation of sphingomyelin, which can destabilize the lysosomal membrane[57,78].

Another target is the v-ATPase in the lysosomal membrane that pumps protons into the lysosome and maintains the lower pH of the lysosomal lumen. Inhibition of this proton pump would also lead to an increase in lysosomal pH. Targeting lysosomal cathepsins with protease inhibitors could also be a treatment option, since their release into the tumor environment supports metastatic growth[77,79].

1.4 Senescence

Senescence is a biological process where cells exit the cell cycle but remain metabolically active. It was initially discovered by Hayflick and Moorhead in the 1970s and was described as a state where cells cease to proliferate in culture[80]. Senescence has its role in tissue remodeling, wound healing, and developmental processes such as embryogenesis. It also contributes to tumorigenesis and aging processes of tissues by reducing the regenerative potential. [81].

Senescence is categorized by the different stimuli of induction. Replicative senescence is characterized by a decrease in proliferation potential and is observed in cell culture. Repeated cell divisions result in telomere erosions and eventually cause the growth arrest[82]. Aberrant oncogenic signaling such as activation of BRAF, activation of Ras or inactivation of PTEN lead to oncogene induced senescence[83,84]. Stress induced, premature senescence occurs due to hypoxia, oxidative stress or DNA damage as a result of radiation or chemotherapy treatment[85]. Cellular stress can either induce apoptosis or senescence depending on the extend of the damage. Other senescence inducting stimuli are epigenetic dysregulation or mitochondrial dysfunction. Drug treatments targeting cyclin dependent kinases (CDK) or epigenetic regulators such as histone deacetylase (HDAC) can induce senescence as well[86].

Paradoxically, senescence can be beneficial or detrimental for tumor growth. It acts as early barrier for tumorigenesis by stopping the proliferation of damaged and malignant cells. Senescent cells further activate immune surveillance, which then clears the accumulated senescent cells[83]. However, senescence does not solely have beneficial effects for tumor suppression. Senescent cells secrete

cytokines, for example, IL-1α, IL-1β, IL-6 and IL-8, chemokines, for example, CCL2, CCL5 and CXCL1, and other inflammatory factors, collectively termed the Senescence-Associated Secretory Phenotype (SASP)[87]. Signaling pathways initiating SASP are the NF-κB, p38, mTOR and C/EBPβ signaling pathways[88]. SASP reinforces the senescent state in an autocrine fashion and fosters inflammation in the tumor micro environment. Inflammatory signaling enhances immune evasion, angiogenesis and metastasis and thereby contributes to cancer progression[89,90].

Identifying specific senescence markers proves challenging due to the complexity and heterogeneity of the senescent phenotype[91]. The expression and secretion of markers can vary significantly between cell types, tissues, and the different senescence types, which activate different pathways, markers or secretome factors [81,82]. However, senescent cells exhibit certain characteristics that proliferative cells lack[92]. These distinctive traits can be used for detecting senescent cells or as targets for therapeutic intervention. Senescent cells often exhibit phenotypic changes in cell structure, including flattened and enlarged cell morphology, along with an increase in lysosomal mass[93]. Senescence-associated beta-galactosidase (β-gal) staining has been a long-standing marker, as well as gene expression of p16 and p21. P21 expression is part of the cell cycle regulation and gets transactivated by p53 upon DNA damage. Since p21 also gets activated independently of p53 and is not exclusively expressed in senescence cells, p21 expression should only be used as senescence marker in combination and in context with other markers. P16 inhibits CDK4/6 and epigenetic alterations can lead to the upregulation of p16 through the p16-INK4a-RB pathway[94-96]. The lack of sensitivity and specificity of individual senescence markers underscores the necessity of employing more than one marker to detect senescent cells.

1.4.1 Targeting senescence with senolytic drugs

Premature stress induced senescence caused by anticancer treatments is also known as therapy induced senescence. This induction of senescence as an initial drug response is a favorable outcome because it stops the proliferation of damages cells and prevents genomic instability[97]. However, persistence and accumulation of senescent cells creates a proinflammatory environment that contributes to cancer growth. Senolytic therapy aims to selectively target this cell type. Targeting the pathologically accumulated senescent cells is challenging due to the vital functions senescent cells serve in the body. Senolytic drugs target cellular senescence by inducing apoptosis by interfering with upregulated anti-apoptotic pathways. For example, BCL-2 family inhibitor navitoclax inhibits BCL-X_L members[88,98,99]. Senomorphic drugs interfere with SASP signaling. For example, mTOR inhibitor rapamycin could be an option to inhibit the proinflammatory signaling of the SASP[100]. In addition to targeted therapies, efforts are being made to develop a new generation of senescence targeting drugs by conjugating established senolytics with antibodies or applying cell therapy with CAR-T cells[101,102]. Surface proteins such as B2M and Apolipoprotein D that are specifically expressed in senescent cells are targeted by Antibody drug conjugates[101]. Urokinase-type plasminogen activator receptor was identified as a target for CAR-T cells to treat senescence associated diseases[103].

1.5 Functional precision medicine

Precision medicine is a significant advancement in cancer research, because it applies individual therapeutic approaches, tailored to the unique biological features and distinct vulnerabilities of individual tumors and patients[104]. Historically, cancers have been treated based on the diagnosed cancer type. Precision oncology offers a transition from this generalized approach towards treatment guided by patient-specific molecular, cellular and functional analysis in addition to the classic diagnosis. The underlying concept is to identify the optimal drug for each patient and to tailor therapies to individual profiles[105,106]. However, genomic data alone provides reliable markers only for a subset of patients with tumors driven by clear molecular drivers, for example NTRK-fusion, BRAF mutations and ALK mutations[107].

Functional drug sensitivity profiling of *ex-vivo* tumor samples is an important tool for precision oncology approaches where large libraries of different compounds are tested in an automated manner to identify effective drugs[107]. It is adding a functional layer complementing the genetic profiling to provide a comprehensive assessment of vulnerabilities and allows for a personalized treatment approach beyond targeting specific mutations. It also might be useful in cases without any known actionable target[108].

Screening format, tumor model and readout are important considerations in the design of drug screens, balancing complexity of used tumor models and screening throughput. In this project, the chosen cell model consists of tumor spheroids. These structures are self-assembled spherical clusters of cell lines, cultivated in an environment where cell-cell interactions are more prominent compared to cell-substrate interactions[109,110]. They replicate avascular tumors with metabolic gradients, such as oxygen and nutrient gradients, providing more meaningful readouts and increased translational potential[111,112].

Readouts for drug screens include measuring metabolic activity, fluorescence staining intensity and phenotypic changes or a combination of readouts. Compared to classical endpoint readouts, phenotypic screens provide an in-depth assessment of morphological differences in addition to growth. In two-dimensional assays, changes in cell shape and size as well as organelle features and distributions can be analyzed. In three-dimensional assays, imaging gives information about spheroid size and integrity[113].

1.5.1 Synergy screening

Cancer is a highly heterogeneous disease with significant variability in drug sensitivity between tumor entities, patients and within the tumor itself. Drug resistance can be intrinsic or acquired through genetic and epigenetic changes during tumor growth[114]. This can lead to activation of compensatory pathways and the emergence of cells and subpopulations that show resistance to treatment[115]. Addressing this complexity often requires the use of drug combinations to achieve effective and sustained inhibition of cancer cell growth[116].

Combination treatment became standard practice in the 1960s, as it was demonstrated to further improve patient outcomes in tumor therapy[117]. The rationale for using drug combinations is to enhance killing of tumor cells while minimizing side effects, toxicity, and the emergence of drug resistance[118,119].

Evaluating the effect of combination treatments is complex. In general, synergistic, additive and antagonistic effects are distinguished. Simplified, synergy describes a higher effect than expected for a drug combination, additivity would be the expected effect and in an antagonistic combination, the drugs reduce the effect of each other[120]. There are various models to address the question of quantifying drug synergy over drug additivity. The most common synergy models are the Bliss independence model, the loewe additivity and the zero interaction potential (ZIP) model[120,121].

The Bliss independence model assumes that drugs act independently form each other, which is also its biggest limitation as drug effects, especially in cancer treatment, are often the result of secondary processes such as induced stress, oxidation and cell death which can hardly be independent for cotreatment with two therapeutic agents[122].

The loewe model assumes that drug effects are the same but with different potency. However, this model can over estimate antagonism because some drugs do not meet this assumption and act partially independently form each other [123].

The ZIP model is an approach to harmonize the issues of the previous two models. It compares the changes in potency between the single drug curves and the combinations, however also this model relies heavily on dose response curve fitting and requires high quality drug screen data to produce reliable synergy scores[124,125].

The efficacy of drug combinations needs to be evaluated in addition to synergy. Evaluating only the synergy scores gives information about the degree of the interactions and might lead to false positives. The combined sensitivity score (CSS) is a relative inhibition based on the area under the curves at the IC50 doses for the combinations and shows the total efficacy of the combination treatment[126].

2 Aim

Neuroblastoma is a heterogeneous tumor comprising epigenetically regulated subtypes that present a considerable clinical challenge. The specific drug sensitivities of these subtypes are poorly characterized. Additionally, the subtypes show differences in their cell morphology which indicates underlying molecular changes that influence the growth, proliferation, and invasiveness of these cells.

Therefore, the aim of my PhD project was to thoroughly analyze drug sensitivities and morphological changes of these subtypes in a panel of neuroblastoma cell lines by applying phenotypic and metabolic drug screens.

To characterize subtype specific vulnerabilities, I used drug sensitivity profiling based on metabolic activity.

I further aimed to characterize the differences in morphology between the subtypes, especially in regard to lysosomes, which are essential in cancerous metabolic changes and to identify the consequences of these differences in regard to drug sensitivity. Therefore, my goal was to develop a confocal high content imaging pipeline with lysosomal stainings and to establish a lysosomal score reflecting the range of lysosomal phenotypes in untreated cells and in response to drug treatment.

I wanted to explore if the observed changes in lysosomal quantity, that occur in response to drug treatment, create a new druggable target and if additional inhibition of lysosomal functions can be used as combination treatment strategy for neuroblastoma.

In addition, I examined gene expression data of the subtypes in regard to senescent signaling and senescence induction. To analyze potential vulnerabilities caused by observed changes in senescent signaling, I tested combination treatments of senescence inducing drugs and senolytics in 3D image-based and metabolic synergy screens.

3 Materials and Methods

3.1 Materials

3.1.1 Cell lines

Table 1: Neuroblastoma cell lines

Cell lines	#RRID	Culture media	Supplier
BE-(1)	CVCL_9898	RPMI, 10% FCS	F.Westermann, DKFZ, Heidelberg, Germany
CHP-134	CVCL_1124	RPMI, 10% FCS	F.Westermann, DKFZ, Heidelberg, Germany
Gi-ME-N	CVCL_1232	RPMI, 10% FCS	F.Westermann, DKFZ, Heidelberg, Germany
HDN33		RPMI, 10% FCS	F.Westermann, DKFZ, Heidelberg, Germany
IMR-32	CVCL_0346	DMEM, 10% FCS, 1% NEEA	German Collection of Microorganisms and Cell Cultures (Leibnitz institute DMSZ), Braunschweig, Germany
IMR-575	CVCL_M473	RPMI, 10% FCS	F.Westermann, DKFZ, Heidelberg, Germany
Kelly	CVCL_2092	RPMI, 10% FCS	German Collection of Microorganisms and Cell Cultures (Leibnitz institute DMSZ), Braunschweig, Germany
KP-N-Si9s	CVCL_1340	RPMI, 10% FCS	F.Westermann, DKFZ, Heidelberg, Germany
LAN-1	CVCL_1827	RPMI, 10% FCS	F.Westermann, DKFZ, Heidelberg, Germany
LAN-5	CVCL_0389	RPMI, 10% FCS	F.Westermann, DKFZ, Heidelberg, Germany
NB-1	CVCL_1440	RPMI, 10% FCS	Rieken BRC cell bank
NMB	CVCL_2143	RPMI, 10% FCS	F.Westermann, DKFZ, Heidelberg, Germany
SHEP	CVCL_0524	RPMI, 10% FCS	F.Westermann, DKFZ, Heidelberg, Germany
SH-SY5Y	CVCL_0019	RPMI, 10% FCS	German Collection of Microorganisms and Cell Cultures (Leibnitz institute DMSZ), Braunschweig, Germany
SIMA	CVCL_1695	RPMI, 10% FCS	F.Westermann, DKFZ, Heidelberg, Germany
SJ-NB-1	CVCL_8812	RPMI, 10% FCS	F.Westermann, DKFZ, Heidelberg, Germany
SJ-NB-12	CVCL_1442	RPMI, 10% FCS	F.Westermann, DKFZ, Heidelberg, Germany
SK-N-AS	CVCL_1700	RPMI, 10% FCS	M. Schwab, DKFZ, Heidelberg, Germany
SK-N-BE-(1)	CVCL_9898	RPMI, 10% FCS	F.Westermann, DKFZ, Heidelberg, Germany

SK-N-BE-(2)	CVCL_0528	RPMI, 10% FCS	German Collection of Microorganisms and Cell Cultures (Leibnitz institute DMSZ), Braunschweig, Germany
SK-N-BE-(2)-C	CVCL_0529	RPMI, 10% FCS	German Collection of Microorganisms and Cell Cultures (Leibnitz institute DMSZ), Braunschweig, Germany
SK-N-DZ	CVCL_1701	RPMI, 10% FCS	F.Westermann, DKFZ, Heidelberg, Germany
SK-N-SH	CVCL_0531	RPMI, 10% FCS	F.Westermann, DKFZ, Heidelberg, Germany

Table 2: Other cell lines

Cell line	**#RRID**	**Culture media**	**Entity**	**supplier**
D425	CVCL_1275	DMEM, 10% FCS, 1% NEEA	MB	T.Milde, DKFZ, Heidelberg, Germany
HDMB03	Milde, T. *et al.*[127]	RPMI, 10% FCS	MB	T.Milde, DKFZ, Heidelberg, Germany
KNS-42	CVCL_0378	RPMI, 10% FCS	pHGG	Kyushu Neuosurgery, Japan
MED8A	CVCL_M137	DMEM, 10% FCS, 1% NEEA	MB	R. Gilbertson, Memphis, TN, USA
ONS76	CVCL_1624	DMEM, 10% FCS, 1% NEEA	MB	Institute for Fermentation, Osaka, Japan
UW-2282	CVCL_0572	DMEM, 10% FCS, 1% NEEA	MB	John Silber, Seattle, WA, USA
UW-2283	CVCL_0573	DMEM, 10% FCS, 1% NEEA	MB	Steven Clifford, Newcastle, United Kingdom

Cell culture reagents

Table 3: Cell culture reagents

Article	Cat. no.	Supplier
0.05 % Trypsin-EDTA	25300054	ThermoFisher Scientific, Waltham, MA, USA
10x NEAA	11140035	ThermoFisher Scientific, Waltham, MA, USA
DMEM	41965-062	Gibco, ThermoFisher Scientific, Waltham, MA, USA
FCS	F7524	Sigma-Aldrich, St. Louis, MO, USA
Matrigel™ Matrix	354234	ThermoFisher Scientific, Waltham, MA, USA
PBS	D8537	Sigma-Aldrich, St. Louis, MO, USA
RPMI-1640	21875-091	Gibco, ThermoFisher Scientific, Waltham, MA, USA
Vi-Cell XR Cell Viability Analyzer™ solutions	B94987	Beckmann Coulter, Krefeld, Germany

3.1.2 Drugs

3.1.2.1 Drug library for metabolic and phenotypic screen

The drugs from the drug library are tested in 5 concentrations on the cells. The library for the metabolic spheroid screens consists of 75 drugs. The library for the lysosomal adaptation screen has 11 drugs more to a total of 86 drugs. Drugs dissolved in DMSO were stored in nitrogen atmosphere at room temperature. Water soluble drugs were stored at -80°C. To dispense drugs solved in water, Tween 20 is added to a final concentration of 0.3%.

Table 4: Drug library

Substance	Sol-vent	c1 [nM]	c2 [nM]	c3 [nM]	c4 [nM]	c5 [nM]	Company	Cat. No.	Part of metabolic drug screen library
A-1155463	DMSO	10000	1000	100	10	1	ChemieTek	CT-A115	yes
A-1210477	DMSO	50000	5000	500	50	5	Active Biochem	A-9036	yes
A-1331852	DMSO	1000	100	10	1	0,1	ChemieTek	CT-A133	yes
Afatinib	DMSO	1000	100	10	1	0,1	Selleck	S1011	yes
Alectinib	DMSO	1000	100	10	1	0,1	ChemieTek	CT-CH542	yes
Alpelisib	DMSO	10000	1000	100	10	1	Medchem Express	HY-15244	no
AMG-232	DMSO	10000	1000	100	10	1	ChemieTek	CT-AMG232	yes
APR-246	DMSO	10000	1000	100	10	1	Tocris Biosciences	3710	yes
APR-246 2nd concentration range	DMSO	100000	10000	1000	100	10	Tocris Biosciences	3710	yes
Axitinib	DMSO	10000	1000	100	10	1	LC Labora-tories	A-1107	yes

Bortezomib	DMSO	1000	100	10	1	0,1	ChemieTek	CT-BZ001	yes
Busulfan	DMSO	10000	1000	100	10	1	Sigma-Aldrich	B2635	yes
Cabozan-tinib	DMSO	1000	100	10	1	0,1	ChemieTek	CT-XL184	yes
Carboplatin	AQ	10000	1000	100	10	1	Hospital pharmacy Heidelberg	Cay13112-25	no
CCNU (Lomus-tine)	DMSO	10000	1000	100	10	1	Medchem Express	HY-13669	no
Ceritinib	DMSO	2500	250	25	2,5	0,25	Selleck	S7083	yes
Chloro-quine	AQ	100000	10000	1000	100	10	Sigma-Aldrich	C6628	yes
Cisplatin	AQ	100000	10000	1000	100	10	Hospital pharmacy Heidelberg	-	yes
Cobime-tinib	DMSO	1000	100	10	1	0,1	Medchem Express	HY-13064	yes
Copanlisib	AQ	1000	100	10	1	0,1	Medchem Express	HY-15346	no
Crizotinib	DMSO	10000	1000	100	10	1	Selleck	S1068-5	yes
Cytarabine	DMSO	10000	1000	100	10	1	Medchem Express	HY-13605	yes
Dabrafenib	DMSO	2500	250	25	2,5	0,25	ChemieTek	CT-DABR	yes

Dactino-mycin	DMSO	1000	100	10	1	0,1	Medchem Express	HY-17559	yes
Dasatinib	DMSO	1000	100	10	1	0,1	LC Labora-tories	D-3307	yes
Dauno-rubicin	DMSO	1000	100	10	1	0,1	Medchem Express	HY-13062	yes
Decitabine	DMSO	10000	1000	100	10	1	Selleck	S1200	yes
Doxo-rubicin	DMSO	1000	100	10	1	0,1	Sigma-Aldrich	D1515	yes
Entinostat	DMSO	10000	1000	100	10	1	ChemieTek	CT-MS275	yes
Entrectinib	DMSO	1000	100	10	1	0,1	Medchem Express	HY-12678	yes
Erdafitinib	DMSO	10000	1000	100	10	1	Medchem Express	HY-18708	no
Erlotinib	DMSO	10000	1000	100	10	1	Medchem Express	HY-50896	yes
Etoposide	DMSO	10000	1000	100	10	1	Medchem Express	HY-13629	yes
Everolimus	DMSO	100	10	1	0,1	0,01	LC Laboratories	E-4040	yes
Foretinib	DMSO	1000	100	10	1	0,1	Selleck	S1111	yes
Gemcita-bine	DMSO	1000	100	10	1	0,1	Medchem Express	95058-81-4	yes
I-BET151	DMSO	10000	1000	100	10	1	ChemieTek	CT-BET151	yes

Idasanutlin	DMSO	10000	1000	100	10	1	Medchem Express	HY-15676	yes
Imatinib	DMSO	10000	1000	100	10	1	Medchem Express	HY-50946	yes
Irinotecan	DMSO	10000	1000	100	10	1	LC Laboratories	I-4122	yes
Isotretionin	DMSO	10000	1000	100	10	1	Hölzel	TMO-T1611	no
Lapatinib	DMSO	1000	100	10	1	0,1	LC Laboratories	L-4804	yes
Larotrectinib	DMSO	1000	100	10	1	0,1	Medchem Express	HY-12866	yes
Lorlatinib	DMSO	10000	1000	100	10	1	Medchem Express	HY-12215	yes
Melphalan	AQ	10000	1000	100	10	1	Sigma-Aldrich	M2011	yes
Mercaptopurine	DMSO	10000	1000	100	10	1	Medchem Express	HY-13677	yes
Merestinib	DMSO	1000	100	10	1	0,1	Medchem Express	HY-15514A	yes
Methothrexate	DMSO	5000	500	50	5	0,5	Selleck	S1210	yes
Mitoxantrone	DMSO	1000	100	10	1	0,1	Medchem Express	HY-13502A	yes
Navitoclax	DMSO	10000	1000	100	10	1	Medchem Express	HY-10087	yes
Nilotinib	DMSO	10000	1000	100	10	1	LC Laboratories	N-8207	yes
Olaparib	DMSO	10000	1000	100	10	1	LC Laboratories	O-9201	yes

ONC201	DMSO	10000	1000	100	10	1	Selleck	S7963	no
Paclitaxel	DMSO	1000	100	10	1	0,1	Medchem Express	HY-B0015	yes
Palbociclib	AQ	10000	1000	100	10	1	Selleck	S1116-10	yes
Panobino-stat	DMSO	1000	100	10	1	0,1	LC Laboratories	P-3703	yes
Pazopanib	DMSO	10000	1000	100	10	1	LC Laboratories	P-6706	yes
Ponatinib	DMSO	1000	100	10	1	0,1	Selleck	S1490	yes
Pralsetinib	DMSO	10000	1000	100	10	1	BIOZOL	TMO-TQ0277	no
Rapamycin	DMSO	100	10	1	0,1	0,01	LC Labora-tories	R-5000	yes
Ribociclib	DMSO	10000	1000	100	10	1	Selleck	S7440	yes
Romidepsin	DMSO	1000	100	10	1	0,1	Medchem Express	HY-15149	no
Ruxolitinib	DMSO	10000	1000	100	10	1	ChemieTek	CT-INCB-2	yes
Selinexor	DMSO	10000	1000	100	10	1	Selleck	S7252	yes
Selume-tinib	DMSO	10000	1000	100	10	1	Medchem Express	HY-50706	yes
SN-38	DMSO	100	10	1	0,1	0,01	Medchem Express	Hy-13704	no
Sorafenib p-Toluene-sulfonate Salt	DMSO	1000	100	10	1	0,1	LC Labora-tories	S-8502	yes

Sunitinib	DMSO	1000	100	10	1	0,1	LC Laboratories	S-8803	yes
Talazoparib	DMSO	1000	100	10	1	0,1	Medchem Express	HY-16106	yes
Tazemetostat	DMSO	10000	1000	100	10	1	ChemieTek	CT-EPZ438	yes
Temozolomide	DMSO	100000	10000	1000	100	10	Selleck	S1237	yes
Temsirolimus	DMSO	100	10	1	0,1	0,01	LC Laboratories	T-8040	yes
Thioguanine	DMSO	10000	1000	100	10	1	Medchem Express	HY-13765	yes
Thiotepa	DMSO	50000	5000	500	50	5	Sigma-Aldrich	T6069	yes
Topotecan	DMSO	10000	1000	100	10	1	Medchem Express	HY-13768A	yes
Trametinib	DMSO	2500	250	25	2,5	0,25	ChemieTek	CT-GSK112	yes
Valproic acid	AQ	1000000	100000	10000	1000	100	Sigma-Aldrich	P4543	yes
Vandetanib	DMSO	1000	100	10	1	0,1	LC Laboratories	V-9402	yes
Vemurafenib	DMSO	10000	1000	100	10	1	ChemieTek	CT-P4032-2	yes
Venetoclax	DMSO	1000	100	10	1	0,1	ChemieTek	CT-A199-2	yes

Vinblastine	DMSO	1000	100	10	1	0,1	Medchem Express	HY-13780	yes
Vincristine	DMSO	1000	100	10	1	0,1	Selleck	S1241	yes
Vinorelbine	DMSO	10000	1000	100	10	1	Selleck	S4269	yes
Vismodegib	DMSO	10000	1000	100	10	1	LC Laboratories	V-4050	yes
Volasertib	DMSO	1000	100	10	1	0,1	ChemieTek	CT-BI6727	yes
Vorinostat	DMSO	10000	1000	100	10	1	LC Laboratories	V-8477	yes

3.1.2.2 Drugs and treatment reagents

Table 5: Additional drugs

Substance	Solvent	Company	Cat. No.
Amitriptyline	DMSO	Sigma-Aldrich	BP016
Artesunate	DMSO	Selleckchem	S2265
Bafilomycin A1	DMSO	Selleckchem	S1413
Benzethonium chloride	DMSO	Selleckchem	S4162
Binimetinib	DMSO	Selleckchem	S7007
Fluoxetine	DMSO	BIOZOL	SEL-S1333
GW4869	DMSO	Medchem Express	HY-19363
LY3214996	DMSO	Selleckchem	S8534
Nortriptyline	DMSO	Sigma-Aldrich	BP269
Pimasertib	DMSO	Selleckchem	S1475
Ravoxertinib	DMSO	Selleckchem	S7554
SCH772984	DMSO	Selleckchem	S7101
Staurosporine	DMSO	Selleckchem	S1421
Ulixertinib	DMSO	Selleckchem	S7854

3.1.3 Antibodies used for Immunofluorescence

3.1.3.1 Primary Antibodies

Table 6: Primary Antibodies

Antibody	Dilution for primary incubation	Source	Cat. No.	Supplier
LAMP1	1:1000	Mouse monoclonal	H3A4	Developmental Studies Hybridoma Bank
LAMP2	1:1000	mouse	sc-18822 (H4B4)	Santa Cruz, Dallas, TX, USA
PHOX2b	1:200	Mouse monoclonal	sc-376997 AF488	Santa Cruz, Dallas, TX, USA
PRRX1	1:200	rabbit polyclonal	nbp2-68808	Novus/R&D, Centennial, CO, USA
SNAI2	1:200		9585T	Cell Signaling, Danvers, MA, USA
YAP1	1:200	Rabbit monoclonal	14074T	Cell Signaling, Danvers, MA, USA

3.1.3.2 Secondary Antibodies

Table 7: Secondary Antibodies

Antibody	Cat. No.	Supplier
Anti-mouse IgG (Alexa Fluor(R) 488 Conjugate)	4408S	Cell Signaling, Danvers, MA, USA
Donkey anti-Rabbit IgG (Alexa Fluor™ 568)	A10042	ThermoFisher Scientific, Waltham, MA, USA

3.1.4 Biochemical reagents

Table 8: Biochemical reagents

Article	Cat. No.	Supplier
16% formaldehyde solution (methanol free)	28908	ThermoFisher Scientific, Waltham, MA, USA
BSA	A4612	Sigma-Aldrich, St. Louis, MO, USA
DMSO, cell culture grade	M6323.0100	Genaxxon bioscience, Ulm, Germany
Ethanol, absolute	20821.321	VWR chemicals, Radnor, PA, USA
Isopropanol	20842.33	VWR chemicals, Radnor, PA, USA
Triton X-100	A4975.0500	AppliChem, Darmstadt, Germany
Tween 20	500-018-3	MP Biomedicals, Santa Ana, CA, USA

3.1.5 Fluorescent live-cell imaging stains

Table 9: Imaging dyes

Article	Cat. No.	Supplier
Cell Mask	C10046	ThermoFisher Scientific, Waltham, MA, USA
Hoechst 33342	H1399	ThermoFisher Scientific, Waltham, MA, USA
LysoTracker™ Red DND-99	L7528	ThermoFisher Scientific, Waltham, MA, USA
Reddot	40061	Biotium, Fremont, CA 94538
TMRE	ab113852	Abcam, Cambridge, UK

3.1.6 Buffers and solutions

Table 10: Buffers and solutions

Solution (storage)	Final concentration	Recipe
70% ethanol (RT)	70% Ethanol	70 ml 99.9% absolute ethanol 30 ml de-ionized H_2O

4% PFA (up to 1 week at 4°C, long time storage -20°C)	4% Formaldehyde	10 ml 16% formaldehyde solution (methanol free) 30 ml PBS
10% Triton X (RT)	10% Triton X-100	5 ml 100% Triton X-100 45 ml PBS
IF blocking solution (4°C)	5% BSA, 0.05% Triton X-100	5g BSA, 500 µL 10% triton-100, ad 100 mL PBS
Freezing media	50% FCS, 40% media, 10 % DMSO	5 ml FCS, 40% of respective culture media of the cell line,

3.1.7 Consumables

Table 11: Consumables

Article	**Supplier**
Cell scraper	Sarstedt, Nürnbrecht, Germany
Conical tubes, 15 ml and 50 ml	ThermoFisher Scientific, Waltham, MA, USA
Corning half area high content imaging plates CLS4517	Corning, NY, USA
Corning ultra-low attachment plates 4516	Corning, NY, USA
Cryovials	Carl Roth, Karlsruhe, Germany
D300e Digital dispenser dispenshead casettes D4+	Tecan, Männerdorf, Switzerland
D300e Digital dispenser dispenshead casettes T8+	Tecan, Männerdorf, Switzerland
Glassware	SCHOTT AG, Mainz, Germany
Greiner Bio-One 384-well sterile cell culture plate with flat bottom, black with transparent bottom	Greiner Bio-One, Frickenhausen, Germany
Greiner Bio-One 96-well sterile cell culture plate with flat bottom, black with transparent bottom	Greiner Bio-One, Frickenhausen, Germany
Kimtech wipes	Kimberly-Clark Kimtech Science, Irving, TX, USA

Parafilm® M	Benis, Braine-l'Alleud, Belgium
Pipette filter tips, 10 µL, 20 µL, 100 µL, 200 µL, 1000 µL	Nerbe plus, Winsen/Luhe, Germany
Safe-Lock reaction tubes, 0.5 ml, 1.5 ml, 2.0 ml, 5 ml	Eppendorf, Hamburg, Germany
Serological pipettes, 5 ml, 10 ml, 25 ml, 50 ml	Sigma-Aldrich, St. Louis, MO, USA
Sterile filter, 0.2 µm	Merck Millipore, Burlington, MA, USA
Syringe 10 ml, 10 ml	Terumo, Tokyo, Japan
Tissue culture dishes, 6 cm, 10 cm	TPP Techno Plastic Products AG, Trasadingen, Switzerland
Tissue culture flasks, 25 cm2, 75 cm2, 175 cm2	Greiner Bio-One, Frickenhausen, Germany
Tissue culture plates, 6 well, 24 well	Corning, Kaiserslautern, Germany
ViCell 4 ml tubes	Beckmann Coulter, Brea, CA, USA

3.1.8 Kits

Table 12: Kits

Article	**Cat. no.**	**Supplier**
Venor® GenM Classic Mycoplasma Detection Kit	11-1250	Minerva Biolabs, Berlin, Germany
CellEvent™ Senescence Green Detection Kit	C10850	ThermoFisher Scientific, Waltham, MA, USA
CellTiterGlo 2.0	G9243	Promega, Madison, WI, USA

3.1.9 Instruments and devices

Table 13: Instruments and devices

Instrument	**Supplier**
BarnsteadTM GenPureTM xCAD Plus Ultrapure water purification system	ThermoFisher Scientific, Waltham, MA, USA

Benchtop centrifuge Micro Star 17R	VWR International, Radnor, PA, USA
CellCamper® Mini	neoLab Migge GmbH, Heidelberg, Germany
Centrifuge 5810 R	Eppendorf, Hamburg, Germany
Cryo freezing container Nalgene® Cryo 1°C "Mr. Frosty"	ThermoFisher Scientific, Waltham, MA, USA
D300e Digital dispenser	Tecan, Männerdorf, Switzerland
Einkanal-Mikroliterpipette Transferpette® S, 0.1-2.5 µl, 0.5-10 µl, 2-20 µl, 20-200 µl, 100-1000 µl	BRAND GMBH + CO KG, Wertheim, Germany
Fluorescence microscope Eclipse Ts2	Nikon, Minato, Japan
FLUOstar Omega automated plate reader	BMG Labtech, Ortenberg, Germany
FLUOstar OPTIMA automated plate reader	BMG Labtech, Ortenberg, Germany
Hamilton syringe	Hamilton Company, Reno, NV, USA
Heat sealer "Folio"	Severin Elektro, Sundern, Germany
Heating block Thermomixer® Comfort	Eppendorf, Hamburg, Germany
ImageXpress Micro Confocal High-Content Imaging System	Molecular devices, San Jose,CA , USA
Incubator Heraeus B6420	Heraeus, Leverkusen, Germany
Light microscope CKX31	Olympus, Hamburg, Germany
LSM 710 confocal microscope	Zeiss, Oberkochen, Germany
Magnetic stirrer with heating MR-3001	Heidolph Instruments, Schwabach, Germany
Mosquito LV	Spt labtech Melbourn Hertfordshire, UK
Multi-axle rotating mixer TRM 56	IDL GmbH, Nidderau, Germany
Nano-Drop ND-1000 spectrophotometer	PEQLab, Erlangen, Germany
NovaSeq 6000 System	Illumina, San Diego, CA, USA
pH meter SevenCompact	Mettler-Toledo, Gießen, Germany
PHERAstar FSX	BMG Labtech, Ortenberg, Germany
Picus® 2 elektronische Pipette, 8-Kanal, 10 - 300 µl	Sartorius, Goettingen, Germany
Pipetboy acu 2	INTEGRA Biosciences, Zizers, Switzerland
Plate sealer	MolGen BV, Veenendaal, Netherlands
Power supply EV231	PEQLab, Erlangen, Germany

Power supply PowerPacTM Basic Power Supply	Bio-Rad, Hercules, CA, USA
Precision balance 440-47N	Kern & SOHN, Balingen, Germany
Refrigerator with freezer	Liebher, Biberach and der Riß, Germany
Rocking platform WT 16	Biometra, Göttinger, Germany
Storage pod	Roylan Developments Ltd., Fetcham Leatherhead, Surrey, UK
TECAN Spark microplate reader	Tecan, Männerdorf, Switzerland
Tip probe sonicator "Sonopuls HD2070"	Bandelin, Berlin, Germany
Tissue culture incubator "C200"	Labotect, Rosdorf, Germany
Tissue culture incubator "CB220"	Binder GmbH, Tuttlingen, Germany
Tissue culture sterile bench "MaxiSafe 2030i"	ThermoScientific, Waltham, MA, USA
Tissue culture sterile bench "Safe2020"	ThermoScientific, Waltham, MA, USA
Ultra-low temperature freezer	ThermoFisher Scientific, Waltham, MA, USA
Vi-CELL XR automated cell counter	Beckmann Coulter, Brea, CA, USA
Vortexer IKA VF2	IKA Janke & Kunkel, Staufen im Breisgau, Germany
VWR ® Shaking water bath (18L)	VWR chemicals, Radnor, PA, USA

3.1.10 Databases and datasets

Table 14: Databases

Database	**Website address**
R2 platform	https://hgserver1.amc.nl/cgi-bin/r2/main.cgi?open_page=login
Molecular signature databases	https://www.gsea-msigdb.org/gsea/msigdb/index.jsp

Table 15: Datasets

Dataset	Author	Reference
Neuroblastoma cell line data set	F. Westermann	ensh37e75

INFORM data set	INFORM	ps_inform_pedinform1056_u133p2_box1635450459
Jansky single cells	S. Jansky	S.Jansky et al, Nat Genet. 2021 May;53(5):683-693. doi: 10.1038/s41588-021-00806-1

Table 16: Gene lists

Gene list	Reference
MSS	R. Sigaud et al, Nat Commun. 2023 Jul 27;14(1):4533. doi: 10.1038/s41467-023-40235-8. PMID: 37500667; PMCID: PMC1037457
MPAS	M.C. Wagle et al, NPJ Precis Oncol. 2018 Mar 7;2(1):7. doi: 10.1038/s41698-018-0051-4. PMID: 29872725; PMCID: PMC5871852.
SASP	J.P. Coppe et al, PLoS Biol. 2008 Dec 2;6(12):2853-68. doi: 10.1371/journal.pbio.0060301. PMID: 19053174; PMCID: PMC2592359.
GO senescence	Subramanian A et al,. Proc Natl Acad Sci U S A. 2005 Oct 25;102(43):15545-50. doi: 10.1073/pnas.0506580102. Epub 2005 Sep 30. PMID: 16199517; PMCID: PMC1239896.

3.1.11 Online tools

Table 17: Online tools

Online tool	**Website**
iTReX	https://itrex.kitz-heidelberg.de/iTReX/
SynergyFinder+	https://synergyfinder.org/

3.1.12 Software

Table 18: Software

Software	**Supplier**
BioRender	BioRender
CellProfiler v.4.1.3	Broad Institute, Cambridge, MA, USA

CellProfiler Analyst v.3.0.4	Broad Institute, Cambridge, MA, USA
ChatGPT	Open AI, San Francisco, CA, USA
D300e Digital dispenser control software	Tecan, Männerdorf, Switzerland
ImageJ v2.9.0	National Institutes of Health
Microsoft Office 2019	Microsoft, Redmond, WA, USA
RStudio v2023.12.0	RStudio, Boston, MA, USA
Vi-CELLTM XR 2.03 software	Beckmann Coulter, Brea, CA, USA
MetaExpress 6.5.559	Molecular devices, San Jose,CA , USA
Endnote21	Clarivate, Philadelphia, PA, USA
Mosquito software	Spt labtech Melbourn Hertfordshire, UK
R4.2.2	The R Foundation, Vienna, Austria

3.2 Methods

3.2.1 Cell culture

Cell lines were authenticated by single nucleotide polymorphism or short tandem repeats profiling done by Multiplexion GmbH (Heidelberg, Germany). Potential bacterial, fungal and mycoplasma contaminations were regularly checked with mycoplasma kit.

3.2.1.1 Thawing, Maintenance, Freezing

To thaw cells, the respective culture media was pre-warmed to 37°C. Cryovials containing frozen cells were thawed in a 37°C water bath and the cells were transferred to a 25 cm^2 cell culture flask with pre-warmed media. After 24h media was changed.

For passaging of adherent cells after reaching a confluency of 70 -90%, media was removed from the flask and cells were washed with 3 ml PBS. 2.5 ml Trypsin EDTA solution was added to the flask and incubated at 37°C for 3 min. Cells were detached by slight patting on the flask and fresh media was added to stop the enzymatic trypsin reaction. To remove excess EDTA, cell suspension was transferred to a 50 ml conical tube and centrifuged at 206 rfc for 3 minutes. Supernatant was discarded and the cell pellet resuspended in fresh media. The desired ratio of the resuspended cells was transferred to a new cell culture flask containing fresh media. Cells were kept at 37°C, 5% CO_2.

Semi-adherent cells (NBS 124) were kept in flasks coated with Matrigel. To coat plates or cell culture flasks with matrigel, 100µL of matrigel was diluted in 15 mL media and poured in the usual quantity of the media into the flasks or the wells. After 1h of incubation at 37°C, media can be removed and the flasks or plates can directly be used. Alternatively, the sealed plates can be kept at 4°C up to 2 weeks.

To freeze cells, the desired number of cells is resuspended in freezing media after the centrifugation step described above and transferred to a cryovial, placed into a Mr. Frosty to ensure a consistent freezing rate and put into a -80°C freezer.

Table 19: Vi-Cell Settings

Parameter	Setting
Cell brightness	85%
Cell sharpness	100
Viable cell spot brightness	65%
Viable cell spot area	5%
Minimum circularity	0
Decluster degree	Medium

Minimum diameter	5 microns
Maximum diameter	50 microns
Images	50
Aspirate cycles	1
Trypan blue mixing cycles	3

3.2.1.2 Counting and Seeding

To count the cells prior to seeding an experiment a ViCELL XR counter with the settings listed in **Table 19** was used to count and analyze cell viability with trypan blue exclusion assay.

3.2.2 Drug libraries and treatments

3.2.2.1 Drug library for metabolic screens

The drug library for the metabolic screens is adapted from Peterziel *et al*. and contains 75 clinically relevant drugs (**Table 4**) for cancer treatment[128]. 80% of the drugs are approved by the FDA, around 10% are in late clinical trials. Assay plates are 384 well u-bottom ultra-low attachment plates containing the respective drugs of the plate layout design in each well. The plate design is a set of 3 plates with the drugs printed in five concentrations (**Table 4**) mostly centered around the c_{max} of the respective drugs. Each plate has staurosporine in a concentration range from 0.1 nM to 1000 nM and at a concentration of 250 nM as well as 100 µM benzethonium chloride as dead controls. DMSO treated wells are used as negative control. The assay plates were obtained from the Institute for Molecular Medicine Finland (FIMM) or multiplicated from source plates obtained from FIMM using the Mosquito LV liquid handling system.

3.2.2.2 Drug library for lysosomal adaptation screen

The drug library used for the lysosomal adaptation screen is an extended version of the metabolic screen library and contains the additional drugs listed in **Table 4**. To prepare the source plates, a total of 5 µl of the drugs in respective concentrations is dispensed into deep-well plates. With the Mosquito LV liquid handling system, the plate layout from the source plate is transferred in two replicates onto 384 flat bottom plates by aspirating 25 nL of each source plate well and dispensing the liquid to the assay plates. For drugs dissolved in water, concentration and dispensed liquid are adapted to the available concentrations of the stock dilution. Assay plates and sealed source plates are stored in a

nitrogen atmosphere at room temperature in storage pods. Source plates containing drugs dissolved in water are sealed and stored at -80°C.

3.2.2.3 Drug treatments without pre-dispensed library

Other drug treatments were applied directly after seeding the cells by dispensing the drugs with a D300e Digital dispenser. All treatments concentrations are normalized to the drug solvent DMSO to ensure no solvent effect in the drug screening assays.

3.2.3 Metabolic activity assay

Metabolic activity assay was done as a primary readout or additionally after imaging as described by Peterziel *et al*[128]. 15µL of Cell titer glo 2.0 reagent was added to each well and incubated shaking (250 rpm) for 20 min before luminescence was measured with the PHERAstar or TECAN Spark plate readers. Raw luminescence signal data was either used directly to calculate percent inhibition using positive and negative controls or analyzed with iTreX[129]. This web application fits a five-parameter dose response curve to the dose response data and calculates drug sensitivity scores (DSSasym) based on the asymmetric curve fit[130].

3.2.4 High-content imaging staining methods

3.2.4.1 Live cell imaging stainings

Stainings for live cell imaging were directly applied to the assay plates in the concentrations indicated in **Table 20**. After adding the stains to the media, the plates were incubated at 37°C for 30 minutes and imaged using the Image Express High content confocal microscope.

Table 20: Imaging stains

Stain	**Stained structure**	**Final concentration**	**Channel setting High content Microscope**
Hoechst 33342	Nucleus	1:10000	DAPI
Cell Mask	Cell membrane	1:4000	Cy5
LysoTracker™ Red DND-99	Lysosomes	1:10000	Cy3
Reddot	Dead cells	1:200	Cy5

TMRE	Mitochondrial membrane potential	1:10000	Cy3

3.2.4.2 Immunofluorescence staining

To perform Immunofluorescence staining cells were fixed in PFA at a final concentration of 4% in the well for 30 minutes at RT and were permeabilized with 0.1% TritonX for 10 minutes at RT. After 1h of blocking with 3% BSA, 0.005% TritonX in PBS, the primary Antibodies, diluted in 3% BSA, 0.005% TritonX in PBS in the dilution according to **Table 6** were added. The plate was incubated overnight at 4°C and washed 3 times with PBS before 1h incubation at RT with the secondary antibodies diluted to a final concentration according to **Table 7**. Plates were imaged with the high content microscope.

3.2.5 High content imaging assays

3.2.5.1 Basal lysosome imaging

Cells were seeded in a 96-well half area plate at different cell numbers according to the size of the cells (2500-3500 cells/well) in 50 µL of their respective culturing media. The cells were kept at 37°C for 24h and stained with Hoechst, Lysotracker and Cell Mask as described above. Without removing the staining media, the cells were fixed in PFA at a final concentration of 4% in the well for 30 minutes at RT. The plate was then imaged with the HCM, 4 sites per well with 40x magnification. After the first imaging round the cells were permeabilized and IF staining for LAMP1 and LAMP2 was performed as described above, each for half of the plate. The plate was imaged again with the HCM at 40x magnification at the same sites.

3.2.5.2 Immunofluorescence lysosomal adaptation screen

The drug library of the lysosomal adaptation screen (**Table 4**) was pre-dispensed on flat-bottom 384 well plates and cells were seeded at 3000 cells/well and incubated for 24h. IF staining and Hoechst staining was performed as described and plates were imaged with the HCM in 20x magnification.

3.2.5.3 Functional lysosomal adaptation

Cells were seeded into flat bottom 384-well plates (2500 cells/well) and treated with a Tecan D300 drug printer. After incubation for 72h, Live cell imaging with Hoechst and lysotracker staining was done. Plates were imaged with 40x magnification.

3.2.5.4 3D Spheroid synergy screens with imaging readout

Cells were seeded into 384 well u-bottom, ultra-low attachment plates (1000 cells/well) and centrifuged at 206 rcf for 3 min. Drug treatment was dispensed with a Tecan D300 drug printer and plates were incubated at 37°C for 72h. Live cell stainings TMRE and Reddot were added as described and plates were imaged with the HCM at 10x magnification. Metabolic activity assay was performed directly after imaging with the same plates.

3.2.5.5 Sequential senolytic combination screen

For this synergy screen, cells were seeded at a density of 500 cells/well and treated with the first drug of the combination using the Tecan D300e. Plates were incubated for 72h and the second drug of the combination treatment was added, then the plates were incubated for another 72h. Spheroids were stained with TMRE and Reddot and imaged at 10x magnification. Metabolic activity assay was performed directly after imaging.

3.2.5.6 Immunofluorescence co-staining of LAMP1 and YAP1

The neuroblastoma cell line SK-N-SH was seeded into 384 well flat bottom plates and drug treatment was added with the Tecan D300e. After incubation of 72h, cells were fixed and IF staining was performed as described. The antibodies for YAP1 and LAMP1 were added at the same time in the indicated dilutions. After incubation and washing steps, the secondary antibodies were added to the plate. Wells with each combination of primary and secondary antibodies were added to the plate to test for cross reactivity between the primary and the secondary antibodies. Hoechst staining was added and plates were imaged at 20x magnification.

3.2.6 Senescence induction assay

Fluorescent beta-gal staining was performed according to the instructions of the kit. Cells were seeded in a 384 well flat bottom plate and treated with senescence inducing drugs for 6 days. To perform the staining, cells were washed with PBS and fixed in 2 % PFA for 10 minutes at RT. Cells were washed and 25 µL of the pre-warmed working solution of the kit was added. Plates were sealed with parafilm to avoid moisture loss and incubated at 37°C without CO_2. Cells were washed with PBS 3 times and the plate was imaged at 20x magnification using the FITC channel of the HCM.

3.2.7 Image analysis

The image analysis for all experiments was done with the Broad Institute Software Cell profiler. The Z-stacks of each channel were projected into a maximum intensity projection. This projection image was separately segmented and measured for each channel.

3.2.7.1 Segmentation, feature extraction and measurement of 2D screens

To segment nuclei, a median smoothing filter was applied to the image of the nuclear stain. A threshold (Otsu or minimum cross entropy) was applied to segment the nuclei as primary objects. If a cell membrane stain was used in the experiment, the cell body was also segmented in the images containing the signal from the cell mask channel (Otsu three classes method) as secondary object using the identified nuclei as seed objects.

To quantify lysosomes, images of the lysosomal stain were enhanced and background signal was reduced by the enhance speckle module of the software, and objects were segmented with robust background thresholding method. Size and fluorescence intensity were measured for all objects. To obtain measurements on a single cell level, the cell body objects were defined as parent object and the measurements of the lysosome objects were attributed to each respective parent object. Per-parent means were calculated.

3.2.7.2 Phenotypic analysis

For the clustering analysis of morphological features, 18 features (**Table 21**) for each of the neuroblastoma cell lines were measured. For the clustering analysis the measurements were scaled and centered.

Table 21: phenotypic features measured

Feature	Description
AreaShape_FormFactor	circularity of object
AreaShape_Solidity	proportion of pixels of convex hull area that are also part of the object
AreaShape_Extend	proportion of pixels in bounding box that are also in the object
Children_Lysos_Count	Number of objects per cell identified by Lysotracker staining

Intensity_MeanIntensity_LT	Mean Intensity of Lysotracker staining
Intensity_IntegratedIntensity_LAMP	Intensity summed up for all LAMP stained objects
Intensity_MeanIntensity_LAMP	Mean Intensity of LAMP staining
AreaShape_Orientation	angle between the x axis and major axis of an ellipse that has same second moments as the object
AreaShape_Eccentricity	Ratio of the distance between the foci on an ellipse that has the same second moment as the object and its major axis length
AreaShape_Area	number of pixels of object
AreaShape_ConvexArea	area of a polygon containing the whole object
AreaShape_Perimeter	Perimeter of the whole cell object
AreaShape_MinFeretDiameter	Minimum distance between two parallels at the closest points of the object
AreaShape_MaxFeretDiameter	Maximum distance between two parallels at the closest points of the object
AreaShape_MajorAxisLength	Longest axis of object
Children_LAMPstain_Count	Number of objects per cell identified by LAMP staining
AreaShape_MeanRadius	Mean radius of cell object
Intensity_IntegratedIntensity_LT	Intensity summed up for all Lysotracker stained objects

3.2.7.3 Segmentation, feature extraction and measurement of 3D cultures

For analysis of spheroid images, the whole spheroid was considered one object. To segment the spheroid object from the background, the images of the TMRE stain were smoothed and Otsu two classes thresholding method was applied. Size and fluorescence intensity of the identified objects were measured.

3.2.7.4 Lysosomal score

To calculate the combined lysosomal score, the scores of the three lysosomal measurements (LT, LAMP1, LAMP2) of the single cells for each cell line were normalized to the Gi-M-EN cell line for each plate to factor out variations in experimental procedure. The means for each measurement were summed up to obtain one combined score for each cell line.

3.2.7.5 Lysosomal adaptation score

To compare changes of the lysosomal amount in cells in response to drug treatment, a lysosomal adaptation score was calculated for each of the 87 drugs for each cell line. For each drug concentration the mean number of lysosomes per cell was divided by the number of lysosomes per cell for the DMSO control to calculate the fold change. This change was summed up for all concentrations of one drug to get one value for each cell-drug combination. This score was then used to create the heatmap and for the clustering analysis.

3.2.7.6 Classification of mes/adr markers in immunofluorescence assay

To distinguish between mesenchymal and adrenergic cells, immune fluorescence staining of cell lines representing both tumor subtypes was done as described above. Nuclei were segmented and intensity of the nuclei objects was measured. The classifier function of the cell profiler analyst application[131,132] was used to classify the cells into two classes: staining positive and negative cells. Random images of cells were fetched from the whole experiment and assigned to the respective class by hand to create a training set. With this training set a random forest classifier was trained, accuracy was checked, and the cells from the whole experiment were classified. To distinguish adrenergic and mesenchymal cell different markers for the subtypes were tested. The adrenergic marker was PHOX2B, mesenchymal markers were YAP1, PRRX1, SNAI2[36]. To check the classification accuracy confusion matrices were compared, the accuracy is listed in **Table 22**.

Table 22: Confusion matrix results

Mes/adr marker	Classification accuracy
PRRX1	66.7%
PHOX2b	70.0%
SNAI2	54.2%
YAP1	96.0%

3.2.8 Gene expression analysis

3.2.8.1 Single sample gene set enrichment analysis (ssGSEA)

Calculation of ssGSEA scores was adapted from Barbie *et al*[133].The gene lists that were used to calculate the ssGSEA scores are listed databases and datasets.

3.2.8.2 MAPKi sensitivity score (MSS)

To calculate the MSS score, the gene signature "ME1/2i_dualERKi" of Sigaud *et al* was used[134]. To calculate the expression score for this signature, the ssGSEA method was used[133].

3.2.8.3 MAPK pathway activity score (MPAS)

MPAS score was calculated based on the expression of 10 MAPK pathway specific genes as described in Wagle *et al*[114].

3.2.8.4 Mesenchymal/adrenergic (mes/adr) score

The mesenchymal/adrenergic (mes/adr) score is calculated from the top 10 neuroblastoma super enhancers assigned to the mesenchymal identity that were identified in ChiP seq analysis by Gartlgruber *et al*[37]. Based on this gene list, the score was calculated with the method described by Barbie et al.

3.2.9 Graphics and statistics

Graphical representations are done with R package ggplot2 3.4.4 and its extension for imputation of statistical and correlation analysis ggpmisc 0.5.5, heatmaps were done with pheatmap 1.0.12 and ComplexHeatmap 2.18.0. Clustering analysis was done with pheatmap with clustering distance row = manhattan, clustering distance rows = euclidean and clustering method ward.D2. Code writing was supported by the AI tool ChatGPT.

3.2.9.1 Principal component analysis

PCA analysis was done with R package factoextra 1.0.7.

3.2.9.2 Quantile ranks

To calculate the quantile rank, the DSSasym scores of all cell lines in the cohort for a drug are ranked and the sum of DSSasym scores below the cell line is divided by the number of cell lines. If a drug effect has a quantile rank above 75% it is classified as a hit, over 95% it is classified as top hit.

3.2.9.3 Synergy analysis

Synergy analysis was done with the BioConductor version of Synergyfinder+[121]. The synergy layout used in this project, was based on the matrix combination design where each drug concentration of drug 1 is combined with each drug concentration of drug 2. To achieve a higher throughput in the combination drug screens and to increase the number of tested drug combinations, a reduced matrix design was used. The missing values of the synergy matrix are then imputed by predictive mean matching. To quantify synergistic drug effects, the Zero Interaction Potency (ZIP) score was used. This synergy model calculates the effect of a combination treatment while assuming the drug effects do not potentiate each other. Therefore, it considers both assumptions of the Bliss and Loewe models.

In addition to the synergy scores that quantify the degree of interaction, the efficacy of a drug combination is calculated with the combined sensitivity score (CSS). The CSS score is calculated assuming that one drug is used at a fixed concentration (relative IC50) and the other one in a variable concentration. This is done again with the drugs switched between fixed and variable. The drug responses are fitted to a 4-parameter log-logistic curve and area under the curve (AUC) values are calculated. To summarize the scores from the whole drug screen and to identify the most promising drug combinations, Sensitivity-Synergy plots were used. To evaluate the success of a drug combination, the efficacy represented by the CSS score as well as the synergy score, that shows the extend of interaction, need to be considered. Therefore, the most promising drug combinations show high values for both and are located in the upper-right corner of the plot.

4 Results

4.1 Drug sensitivity profiling of pediatric cancer cell lines

To systematically test for differences in vulnerabilities of neuroblastoma subtypes, I screened a library of 75 clinically relevant drugs. The cell line panel used in this project comprised 23 neuroblastoma cell lines, four of them classified as mesenchymal and seven of them as adrenergic based on gene expression data[37]. Additionally, other pediatric cancer cell lines were examined, including six medulloblastomas and one pediatric high-grade glioma. The cell lines were screened as spheroids to resemble the physiological 3D structure. As a robust viability readout, metabolic activity through bulk ATP measurement was chosen.

Drug sensitivity was calculated as DSSasym for all the 75 drugs for all cell lines (**Figure 1A**). The upper cluster of the heatmap, that contains mostly chemotherapeutic drugs, shows higher values for DSSasym. This is expected since chemotherapeutic drugs are usually quite effective due to their nonspecific mechanism of action, leading to DNA damage. There was no drug for which the other pediatric cancer cell lines reacted notably different than the neuroblastomas (**Supplemental Figure 1**).

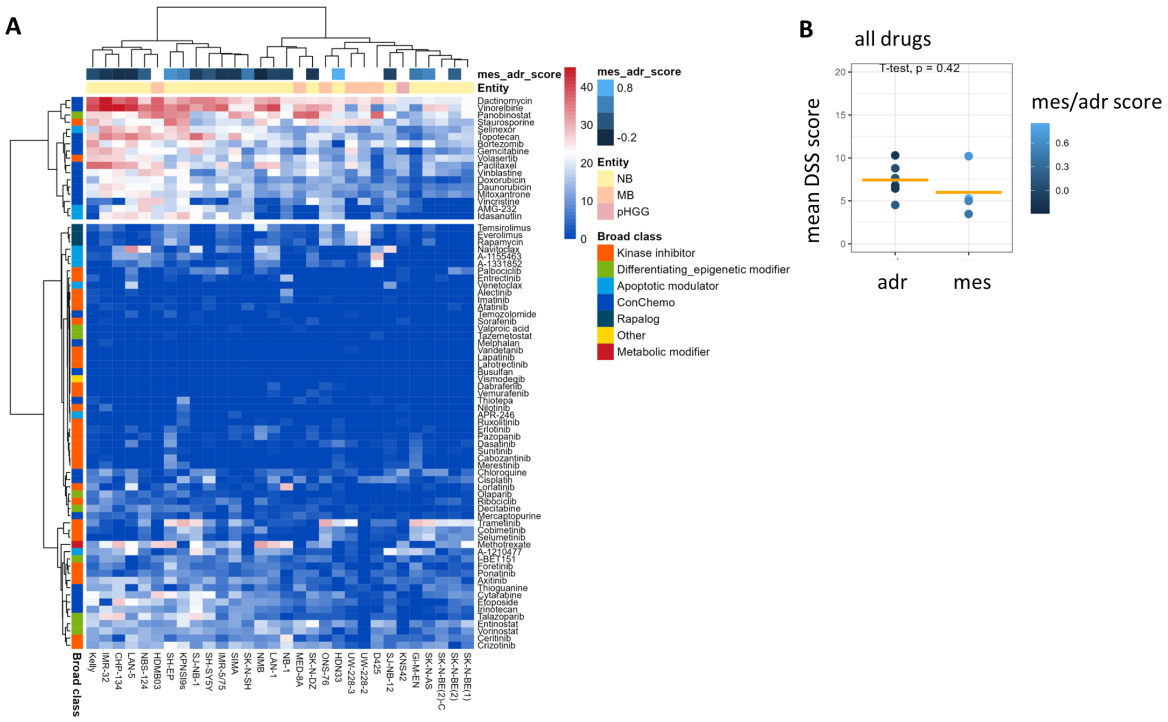

Figure 1: Drug sensitivity profiles of pediatric cancer cell lines. (A) Heatmap with hierarchical clustering summarizing drug sensitivity scores (DSSasym) based on metabolic activity from 31 pediatric cancer cell lines from 3 different entities. (B) Mean DSSasym for neuroblastoma cell lines classified into mesenchymal and adrenergic subgroups (n = 7 adrenergic cell lines; n = 4 mesenchymal cell lines).

4.1.1 Comparison of drug sensitivity in drug classes for neuroblastoma subtypes

Comparison of the overall mean DSSasym did not reveal a difference between the subtypes (**Figure 1B**). This changes when comparing different drug classes. Specifically, for conventional chemotherapeutic compounds, there was a trend towards higher sensitivity in the adrenergic subtype. This is in line with literature that shows higher resistance of the mesenchymal subtype to chemotherapy. However, no significant difference between the classified subtypes was observed for any of the other drug classes (**Figure 2**).

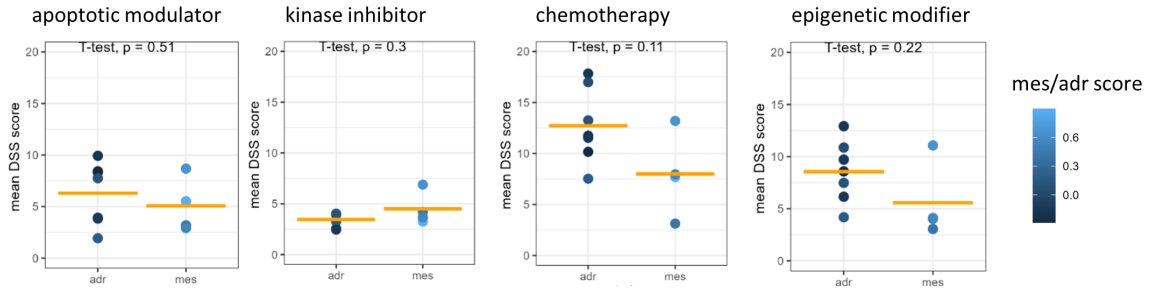

Figure 2: Comparison of drug class mean DSSasym between neuroblastoma subtypes. Mean DSSasym of neuroblastoma cell lines classified as adrenergic or mesenchymal (n = 7 adrenergic cell lines; n = 4 mesenchymal cell lines) for 4 drug classes. Statistical analysis was performed using unpaired two tailed t-test.

4.1.2 Sensitivity towards MEKi differs in neuroblastoma subtypes

Besides the binary classification of neuroblastoma subtypes into mesenchymal and adrenergic, a score can be calculated based on gene expression of the super enhancer target genes that are characteristic for the mesenchymal subtype. This approach avoids binarization and provides a continuous variable, the mes/adr score, that reflects the spectrum of the two subtypes better than a classification[37].

To assess if the cell lines can be grouped based on their drug sensitivity, a principal component analysis (PCA) was employed. The PCA is a dimension reduction method that condenses the variability between the cell lines in principal components. The two principal components that capture the majority of the dataset's variability are visualized in the plot. The cell lines with a high mes/adr score group in the upper part compared to the more adrenergic cell lines that group in the lower left of the plot (**Figure 3A**). Thus, the neuroblastoma subtypes can be separated based on their drug sensitivity.

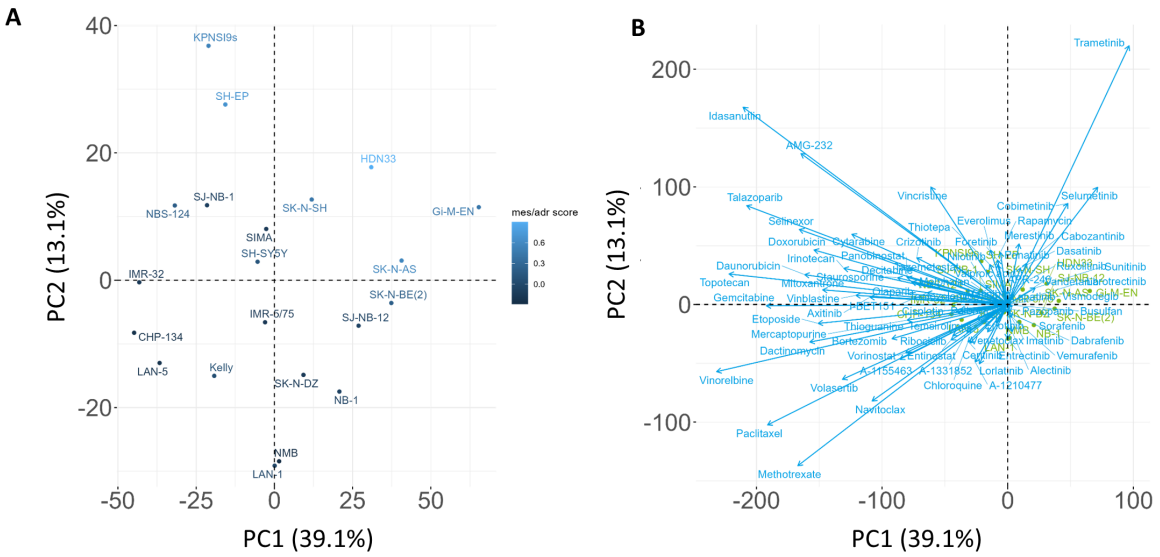

Figure 3: Grouping of neuroblastoma cell lines based on DSSasym. (A) Principal component analysis based on DSSasym for comparison of 24 neuroblastoma cell lines, colored according to mes/adr score (B) Biplot of principal components and overlay of loading plot. The arrows represent the weight of the drug responses for each drug on the principal components 1 and 2.

The loading plot of a PCA represents the weight of each drug's reactions across all cell lines to the principal components. Notably, in this plot (**Figure 3B**), the loadings for trametinib, selumetinib and cobimetinib, diverged from the others and point towards the upper right quadrant, contributing to the variability represented by PC1. All of these drugs belong to the same drug class, the MEK inhibitors (MEKi). In conclusion, drug response to MEKi caused the separation of the two neuroblastoma subtypes in the PCA.

4.1.3 Mesenchymal neuroblastoma cell lines are sensitive to MEKi treatment

The examination of spheroids from mesenchymal and adrenergic neuroblastomas after treatment with MEKi revealed a decrease in metabolic activity and shrinkage of the tumor spheroids (**Figure 4A**). The absence of spheroids at the highest trametinib concentration in mesenchymal cell lines compared to the minimally shrunken spheroids of adrenergic cell lines suggests, that MEKi are not only cytostatic but also possess cytotoxic effects, leading to the death of mesenchymal neuroblastoma cells.

Given that the diverse drug responses of mesenchymal and adrenergic neuroblastoma to MEKi led to the separation of the two subtypes, the correlation between drug sensitivity and mes/adr score was assessed. The MEKi are the only drugs that show a positive correlation for the mes/adr score and DSSasym (**Figure 4B**). For all other drugs the correlation was neutral or negative (**Supplemental Figure2**). Therefore, the only drug class, for which the mesenchymal cells are more sensitive than the adrenergic cells, are MEKi. This result is further confirmed by the correlation of MEKi sensitivity score (MSS) with the mes/adr score, which indicates a higher sensitivity for MEKi in mesenchymal neuroblastoma[134] (**Figure 4C**).

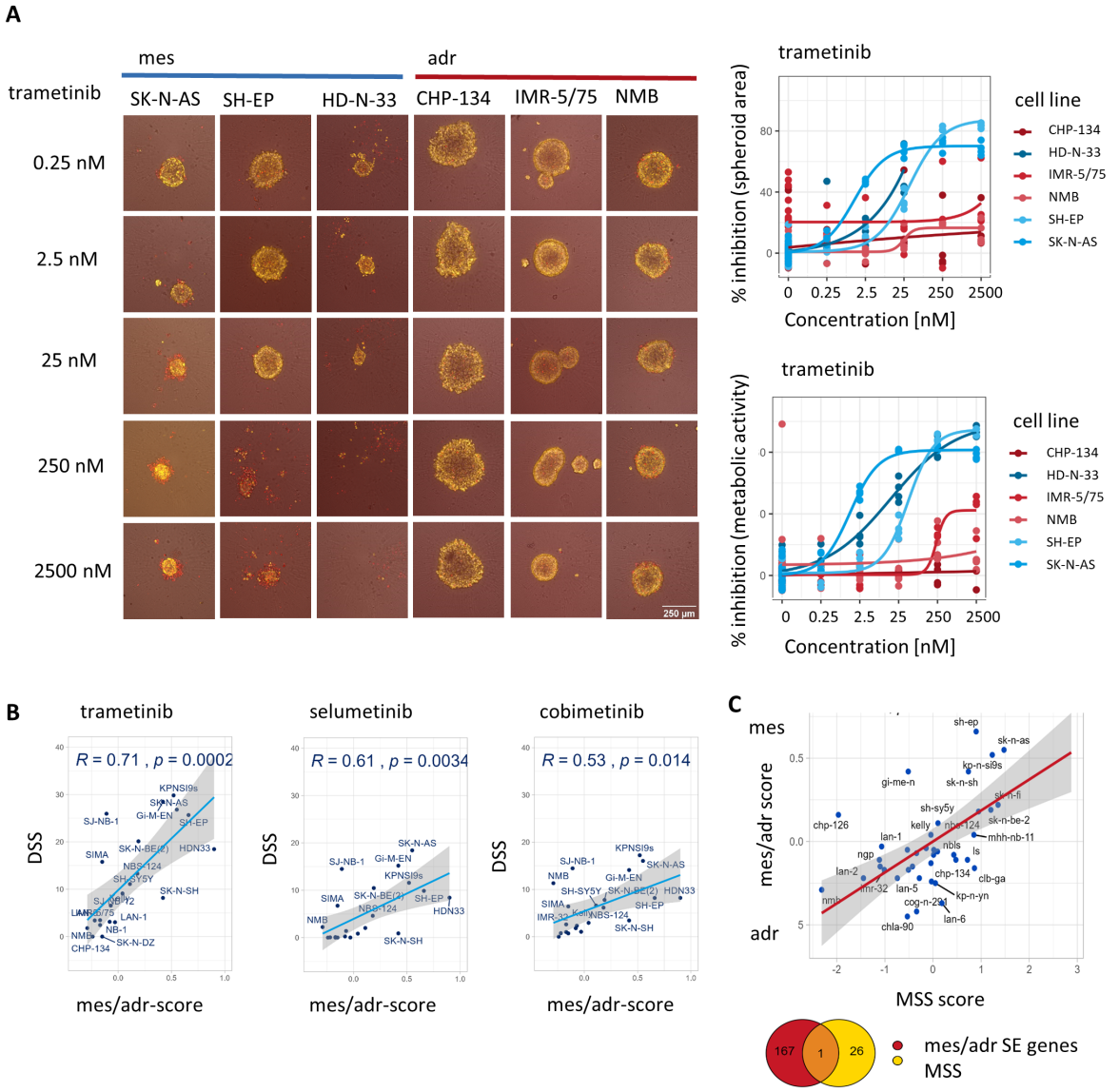

Figure 4: MEKi sensitivity in neuroblastoma subtypes. (A) Example images of 3D tumor spheroids of 6 neuroblastoma cell lines (n= 3 adrenergic and n= 3 mesenchymal) treated with increasing concentrations of trametinib. Viable cells are stained with the membrane potential indicator TMRE (yellow) and dead cells with reddot (red), scare bar 250 µm. Quantification of metabolic activity and spheroid area are shown as percent inhibition calculated based on DMSO (negative) and benzethonium chloride (positive) treated controls. (B) Pearson's correlation calculated for mes/adr score and DSSasym of 24 neuroblastoma cell lines. (C) Pearson's correlation of MSS and mes/adr score. Venn diagram indicates overlap between gene lists the mes/adr score and the MSS are based on.

4.1.4 MAPK pathway activity is upregulated in mesenchymal neuroblastoma cell lines

Since mesenchymal cells are more sensitive to MEKi, I hypothesized, that MAPK pathway activity is higher in in this subtype. Therefore, I calculated the MAPK pathway activity score (MPAS), from expression of 10 key MAPK target genes[114]. MAPK pathway activity differs between cell lines harboring the same MAPK alteration, therefore a score, calculated based on gene expression, is suggested to be

a more accurate way to analyze MAPK pathway activity[135]. Mesenchymal neuroblastoma cell lines have a higher MAPK pathway activity which is shown by the correlation of MPAS and mes/adr score (**Figure 5**). The gene list of the mes/adr score does not overlap with the gene list the MPAS is based on (**Figure 5**). This demonstrates, that none of the MAPK activity genes was identified as marker for mesenchymal cells and shows the independence of the correlation. The above identified high sensitivity of the mesenchymal cells towards MEKi might results from higher MAPK activity in these cells.

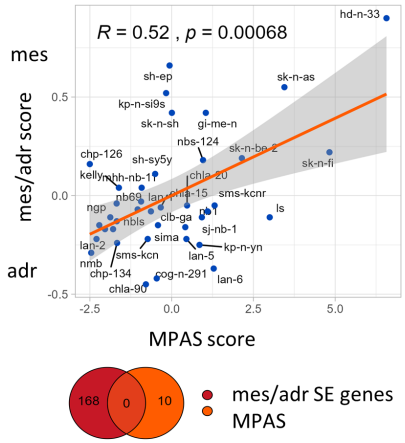

Figure 5: MAPK pathway activity in neuroblastoma subtypes. Pearson's correlation of MPAS and mes/adr score calculated based on gene expression of respective gene sets in 39 neuroblastoma cell lines. Venn diagram indicating the overlap of the gene sets.

4.1.5 Drug hit comparison in the neuroblastoma cohort confirms MEKi among the hits for mesenchymal neuroblastoma cell lines

To identify drug hits for each of the cell lines, an outlier analysis with the whole neuroblastoma cell line cohort was done. With this method, it was analyzed if a cell line shows a particularly high sensitivity towards a drug using quantile values. Drugs are ranked based on their quantile value to identify hits, which are drugs in the upper 75% quantile. For the four tested mesenchymal cell lines Gi-M-EN, HD-N-33, SK-N-AS and SH-EP, the MEKis show above average response. For the SK-N-AS cell line, selumetinib is considered a top hit since this cell line shows higher sensitivity for selumetinib than 95% of all other cell lines in the cohort (**Figure 6A and Supplemental Figure 3**). Comparing the mean quantile scores for MEKi shows that mesenchymal cell lines have significantly higher scores compared to adrenergic ones (**Figure 6B**).

In conclusion, in this first drug screen, the drug sensitivity profiles of pediatric cancer cell lines were compared, with particular focus on the difference between adrenergic and mesenchymal neuroblastoma subtypes. The entities were not separated into distinct clusters. However, a notable trend was observed in the neuroblastoma cell lines, showing grouping of the adrenergic and the mesenchymal subtypes based on drug sensitivity profiles. Moreover, higher MAPK pathway activity and greater sensitivity to MEKi for mesenchymal compared to adrenergic neuroblastomas were demonstrated. The specific sensitivity for MEKi is a potential target for mesenchymal neuroblastomas.

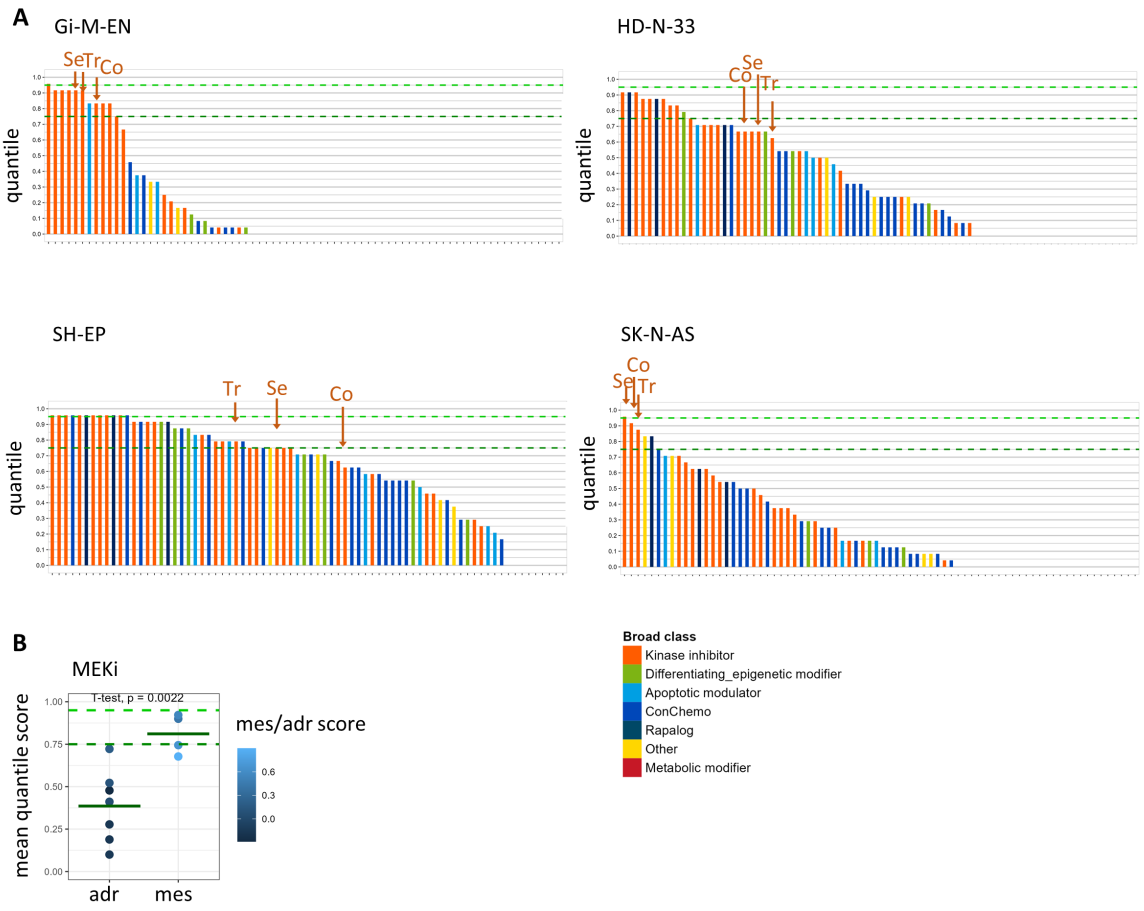

Figure 6: Cohort comparison of MEKi sensitivity. (A) Waterfall plots of 4 mesenchymal neuroblastoma cell lines with drugs ranked based on their quantile score. The quantile score of each drug represents the drug response of the cell line to that drug compared to the drug reaction of all the cell lines in the cohort and allows a comparison of the drugs in one cell line. (B) Mean quantile score for three MEKi of neuroblastoma cell lines classified as adrenergic or mesenchymal (n = 7 adrenergic cell lines; n = 4 mesenchymal cell lines) dashed lines indicate the 0.75 and 0.95 quantiles defining hits. Statistical analysis was performed using unpaired two tailed t-test.

4.2 High content imaging analysis characterizes differences in cell morphology and lysosomal compartment of neuroblastoma subtypes

Neuroblastoma subtypes not only vary in their gene expression and drug sensitivity but also have distinct morphological characteristics. Therefore, I established a high content imaging pipeline to quantify morphological differences using confocal fluorescence microscopy and correlate them with previously obtained metabolic drug screening data.

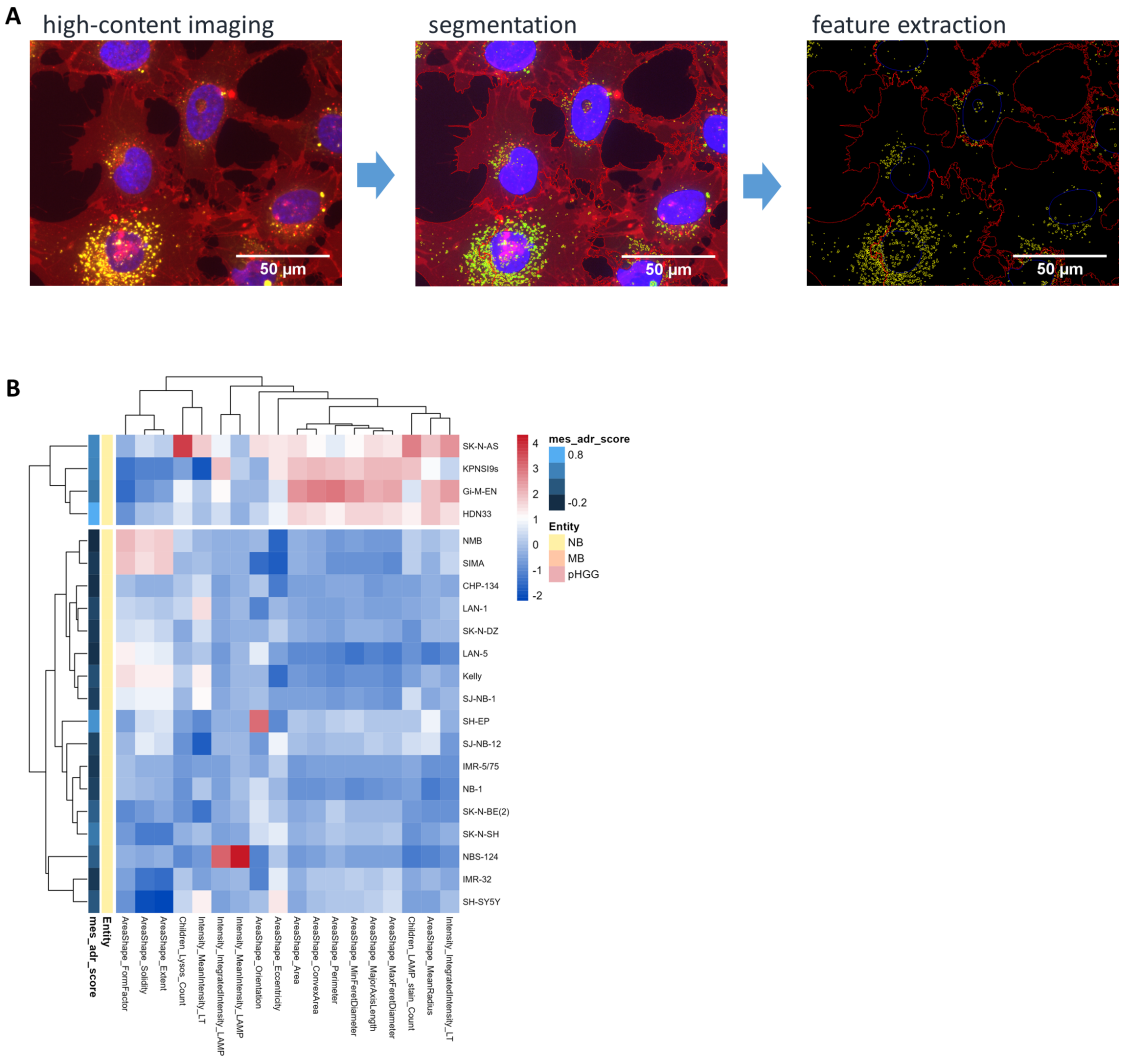

Figure 7: Phenotypic analysis of lysosomal compartment in neuroblastoma cell lines. (A) Example images describing the workflow of the phenotypic image analysis, overlay of three channels (red = cell membrane, blue = nuclei, yellow = lysosomes) of fixed cells, overlay of outlines of segmentation of the identified objects and outlines without images. (B) Heatmap summarizing normalized and scaled phenotypic measurements of cell body, nucleus and lysosomes of 18 phenotypic features for 21 neuroblastoma cell lines. Hierarchical clustering separating cell lines in 2 clusters.

For this, a membrane stain and a nucleus stain were used to compare morphological variances in the nucleus and cell body. Lysosomes were stained with lysotracker (LT), a stain that accumulates in acidic

organelles and therefore specifically stains functional lysosomes. To analyze structural lysosomal proteins LAMP1 and LAMP2, immunofluorescence staining was done after fixation of the LT staining. With this approach, various morphological features, such as cell size and shape as well as lysosomal number and intensity were measured for each segmented object (**Figure 7A and Supplemental Figure 4**).

Based on the morphological measurements, mesenchymal and adrenergic cell lines clustered together respectively (**Figure 7B**). Mesenchymal and adrenergic cell lines differ most in measurements related to cell size and lysosomes. Mesenchymal cell lines are characterized by larger cell bodies and a higher quantity of lysosomes.

4.2.1 Basal lysosomal score correlates with mes/adr score

To summarize all lysosomal measurements and to compare lysosomal quantity to other results, a lysosomal score was calculated. To ensure comparability and rule out plate effects, the lysosomal numbers were normalized to the lysosomal number of the cell line Gi-M-EN that was included on each plate.

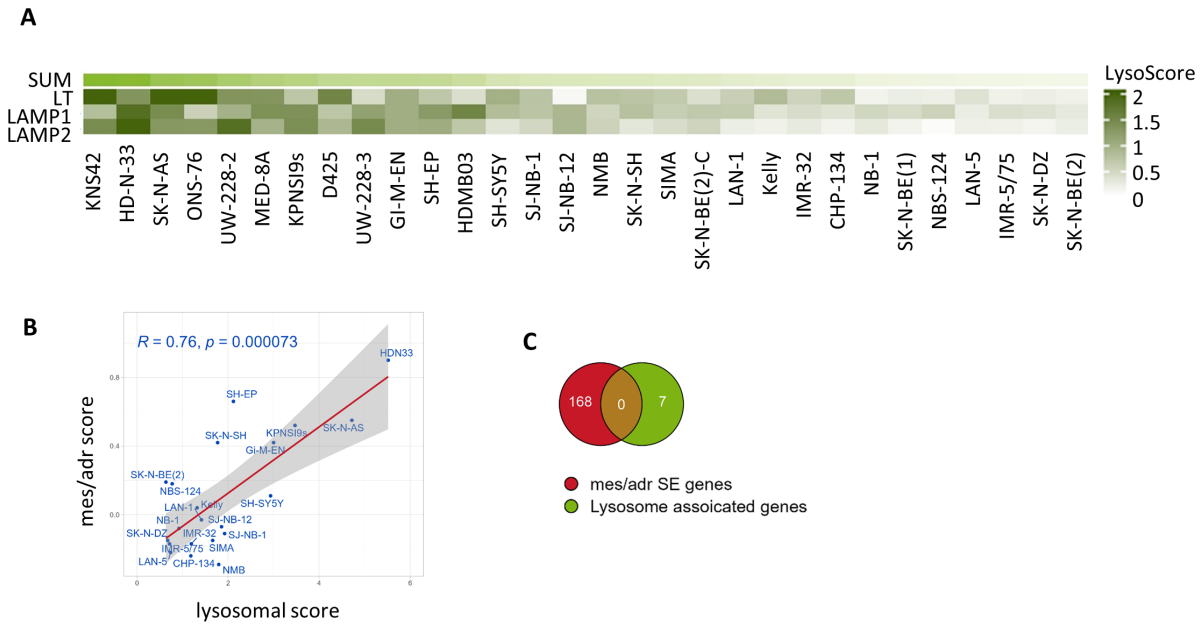

Figure 8: Comparison of basal lysosomal score in neuroblastoma subtypes. Heatmap summarizing normalized number of lysosomes of the three measurements (LT, LAMP1, LAMP2) and the lysosomal score summarizing these three measurements (B) Pearson's correlation between mes/adr score and lysosomal score of 24 neuroblastoma cell lines (C) Venn diagram showing overlap between lysosomal genes and mes/adr gene list.

For each cell line, the mean lysosome number of all cells in the images was calculated and the means for each stain were summed up into a lysosomal score (**Figure 8A, Supplemental Figure 5**). Correlation analysis showed, that mesenchymal neuroblastoma cell lines have a higher lysosomal score than

adrenergic cell lines (**Figure 8B**). The lysosomal score also correlates with the expression of some genes associated with lysosomal function and biogenesis like the master transcription factors TFEB and TFE3 but not all of them (**Supplemental Figure 6**). This shows, that measuring expression of these genes is not necessarily an indicator of a high lysosomal level. Additionally, none of these lysosomal genes and transcription factors associated with lysosomal biogenesis overlap with the mesenchymal super enhancer gene list, demonstrating the independence of the phenotypic lysosomal score from subtype specific gene expression (**Figure 8C**). This makes the number of lysosomes a novel marker to distinguish mesenchymal and adrenergic neuroblastoma without access to genomic data.

4.2.2 The correlation between basal lysosomal score and MEKi sensitivity is specific for neuroblastoma

Lysosomes can be involved in drug resistance processes. To investigate, if a high lysosomal score could serve as a marker for drug resistance or drug sensitivity, the connection between lysosomes and drug sensitivity was investigated. Pearson correlation analysis revealed a strong positive correlation between basal lysosomal levels and MEKi drug sensitivity (**Figure 9B**). A high lysosomal score therefore indicates a sensitivity towards MEKi in neuroblastoma. Interestingly, the positive correlation is stronger when the analysis is done with only neuroblastoma cells compared to the correlation of DSSasym and lysosomal score for all tested entities (**Figure 9A &B**). This result suggests, that this effect is specific for neuroblastoma, however more cell models need to be tested to confirm this.

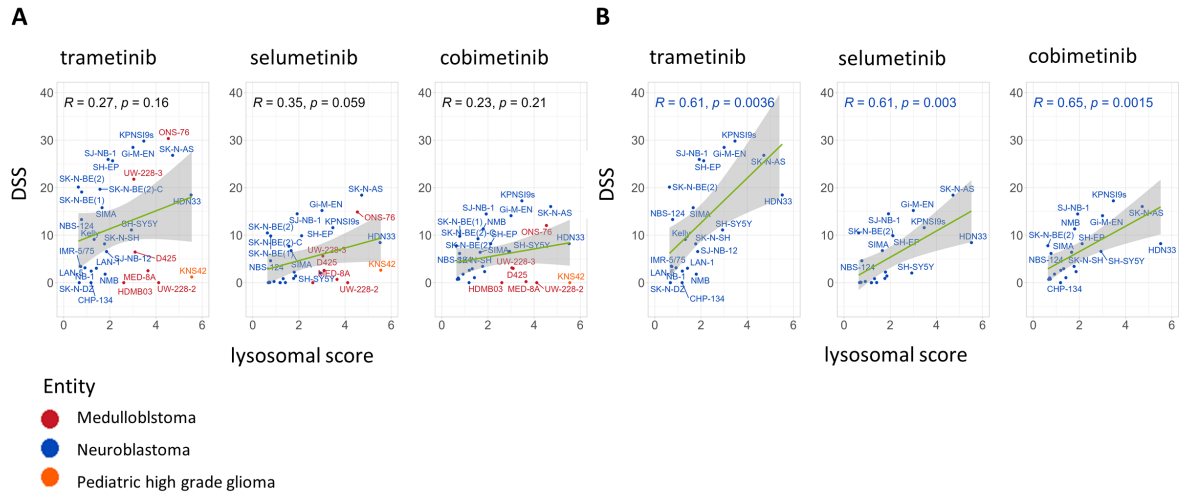

Figure 9: Connection between drug sensitivity and lysosomal score. (A) Pearson's correlation of lysosomal score and drug sensitivity score for three MEKi for all cell lines, color indicating tumor entity. (B) Correlation for only neuroblastoma cell lines.

In conclusion, mesenchymal and adrenergic cells show a difference in their morphology, with mesenchymal cells being bigger, showing less elongation and a higher number of basal lysosomes. The lysosomal score calculated from the three lysosomal measurements is a marker for mesenchymal neuroblastoma cells as it correlates with the mes/adr score. A High lysosomal score also points towards higher drug sensitivity towards MEKi, which this seems to be a neuroblastoma specific effect.

4.3 Phenotypic adaptation of the lysosomal compartment to drug treatment in neuroblastoma subtypes

Lysosomes are highly dynamic organelles which adapt to various environmental changes and stresses. In such altered conditions, cells modify and adjust the quantity of lysosomes to provide nutrients for cellular function in this changed condition[57]. The aim was to analyze and compare differences in lysosomal adaptation upon drug treatment. The lysosomal drug response was also compared to drug sensitivity as this indicates a drug or cell line specific stress reaction.

4.3.1 Image based drug screen characterizes lysosomal changes in neuroblastoma subtypes

To compare the adaptation of lysosomes to drug treatment between the neuroblastoma subtypes, I did a screening experiment with 8 neuroblastoma cell lines that were exposed to 86 different drugs (**Figure 10**). For this screen, number of lysosomes per cell was the readout. Immunofluorescence staining of LAMP1 was used to analyze number of lysosomes.

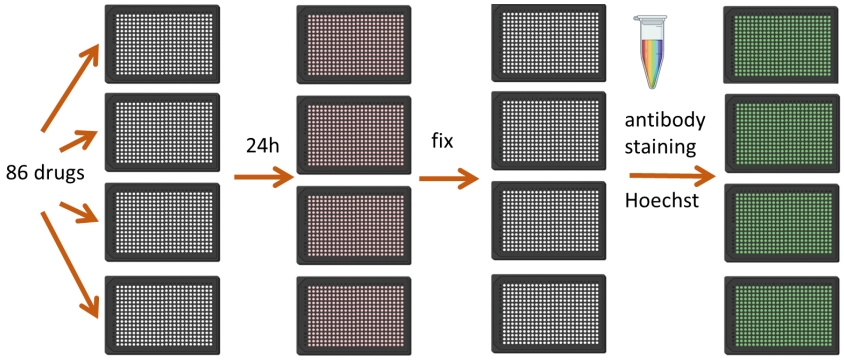

Figure 10: Experimental setup of cellular lysosomal adaptation screen. Schematic overview of experimental design, drug library with 86 drugs in 5 concentrations predispensed on 4 flat bottom plates. After 24h of drug treatment of cells in 2D culture, immunofluorescence staining against LAMP1 and staining of nuclei was performed and plates were imaged.

To compare the adaptation of lysosome numbers to drug treatment between the cell lines, a lysosomal adaptation score was calculated. Clustering analysis of the quantified lysosomal adaptation grouped the two most adrenergic cell lines (CHP-134 and IMR-32) together, showing that lysosomal adaptation is different between the subtypes (**Figure 11**).

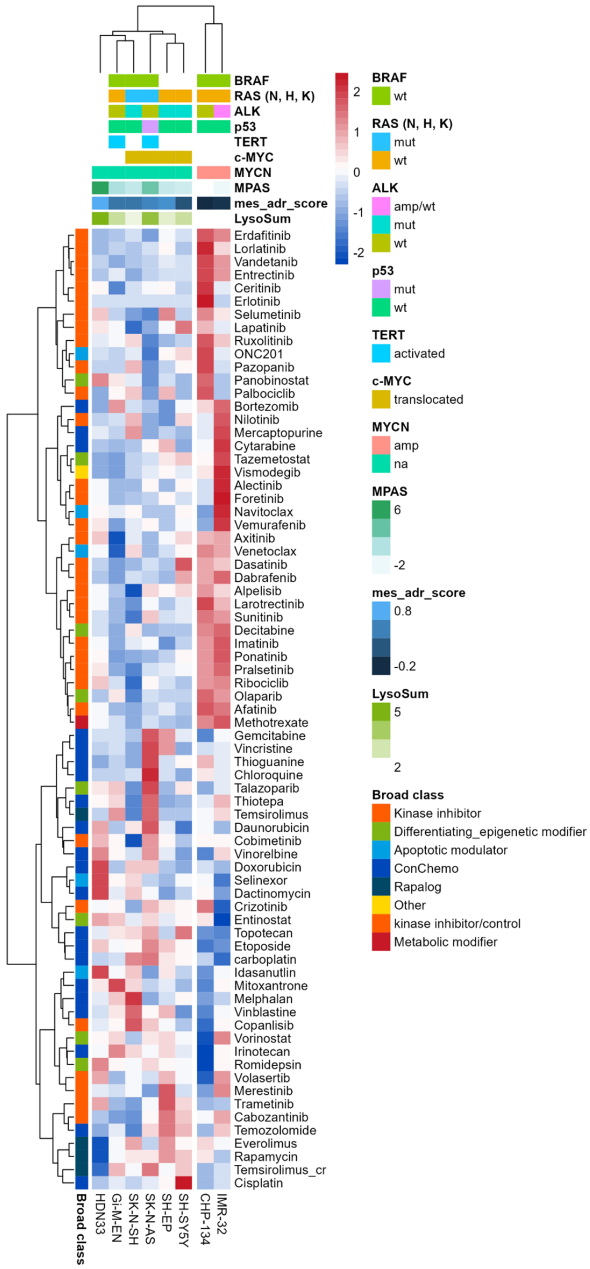

Figure 11: Adaptation of lysosomal numbers to drug treatment. Heatmap representing lysosomal adaptation score calculated by summing up the fold changes of lysosomal numbers based on LAMP1 immunofluorescence staining from DMSO treated control to five drug concentrations for 8 neuroblastoma cell lines. Hierarchical clustering separating cell lines into two groups.

Notably, the two cell lines in the adrenergic cluster both contain a *MYCN* amplification, however this was not common for all adrenergic cell lines, the *MYCN* amplified cell lines are a sub group among the adrenergic cell lines. *MYCN* amplification is usually not observed in mesenchymal cells[37,136].

4.3.2 Lysosomal adaptation increases with prolonged drug exposure

Above described experiments showed an elevated sensitivity of mesenchymal neuroblastoma cells to MEKi. Focusing on the cellular lysosomal changes in response to MEKi treatment, the adaptation of lysosomes at different time points for the mesenchymal cell line SH-EP was analyzed. The change in lysosome numbers could be an early response to drug treatment or occur at later time points, when cells are stressed or dying due to the drug treatment. The numbers of lysosomes increased strongly at the later timepoint of 72h (**Figure 12 A & B**).

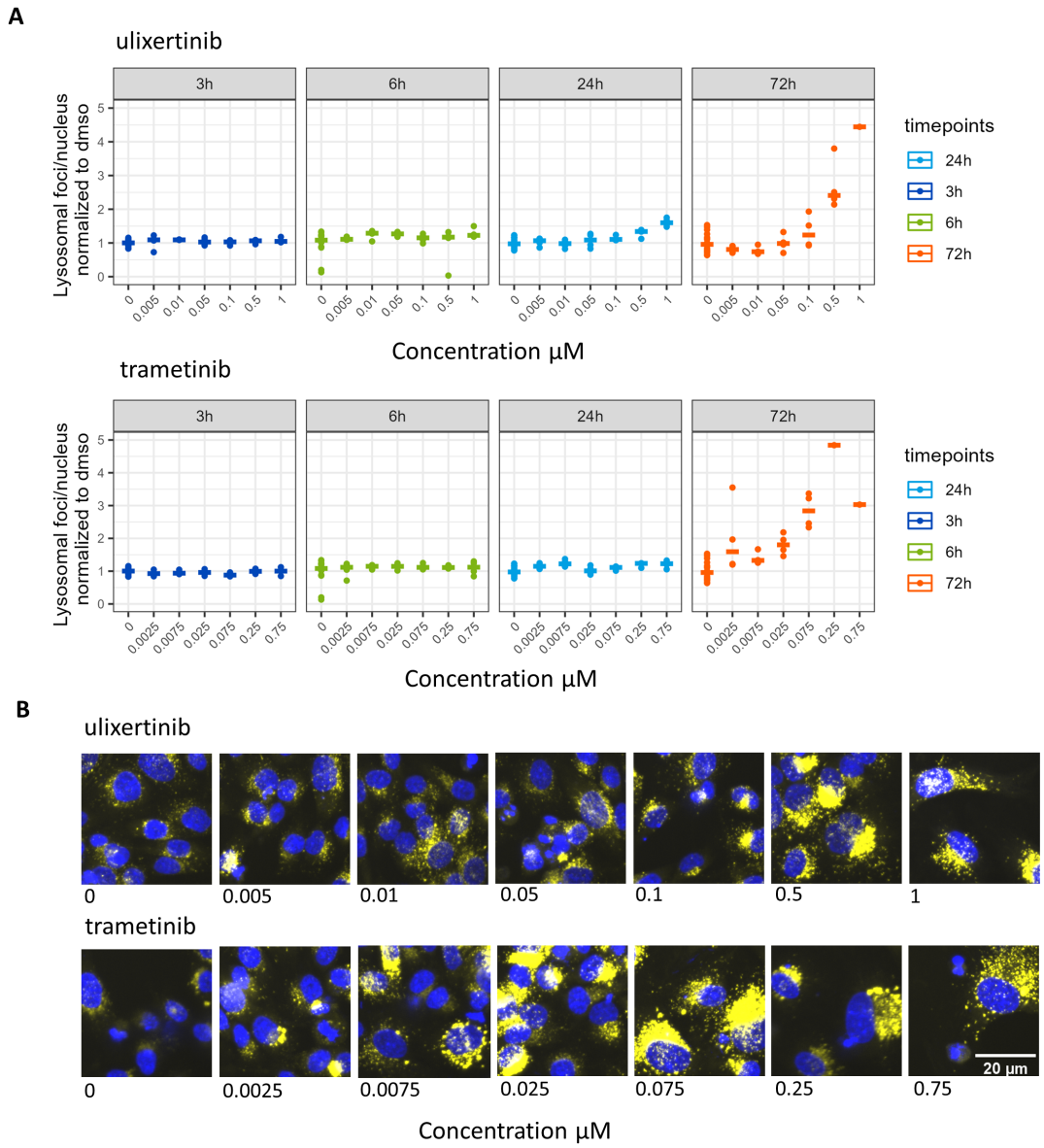

Figure 12: Lysosomal adaptation across multiple time points. (A) Mesenchymal SH-EP cell line treated with MEKi trametinib and ERKi ulixertinib for indicated time points. Number of lysosomes per nucleus was normalized to DMSO treatment for each time point. (B) Example images of SH-EP cell line treated with ERKi ulixertinib and MEKi trametinib for 72h. Nuclei = blue, Lysotracker = yellow.

As the strong lysosomal phenotype occurred at the latest timepoint, the lysosomal reaction seems to be part of a stress response to drug treatment rather than being an initial response. An increase or decrease at early timepoints would indicate a direct effect of the drug to the lysosomal pH and would hint changes in lysosomal functionality[137].

4.3.3 Mesenchymal neuroblastoma cells show strong increase in lysosome quantity in response to chemotherapy and MEKi treatment

To further examine the differences in lysosomal stress response between mesenchymal and adrenergic cell lines, both subtypes were exposed to DNA damage induced by 72h treatment with chemotherapeutic drugs. Both cell lines reacted with an increase in lysosomal numbers (**Figure 13**). Mesenchymal cells showed an increase up to four-fold of the number of lysosomal foci per cell compared to the adrenergic cell line that showed a two-fold increase at concentrations shortly below the toxic concentrations where cells died (**Figure 13**). The mesenchymal cells, which already have higher basal lysosomal levels showed a stronger lysosomal stress response.

Since MEKi were the only drugs of the drug library for which mesenchymal cells showed a higher sensitivity than the adrenergic cells, I next addressed the question if adaptation of lysosomal numbers is different between the subtypes for MEKi treatment. As depicted in **Figure 14**, the lysosomal number in mesenchymal cells increases for all MAPKi but Pimasertib. The number of lysosomes was always the highest at the drug concentration where nuclei numbers begin to decrease, indicative for starting cell death. At drug concentrations where nuclei numbers approach zero, indicating most cells are already dead, lysosomal numbers drop as well. For the adrenergic cells, lysosome numbers only increased for cobimetinib. This is unexpected since nuclear numbers are not decreasing, indicating that this increase is not due to a stress reaction of dying cells.

In conclusion, lysosomal adaptation is a stress response of neuroblastoma cells to treatment that shows the strongest effects after prolonged drug exposure and shortly before the cells start to die. Neuroblastoma subtypes differ in their lysosomal adaptation to drug treatment. Mesenchymal cells, which have already high basal lysosomal levels demonstrated a higher increase in lysosomal numbers to both chemotherapy and MEKi treatment.

This effect is independent of the drug sensitivity of the cells as mesenchymal cells are more sensitive to MEKi but less sensitive to chemotherapy and adrenergic cells are more sensitive to chemotherapy but do not show the same extend of cellular lysosomal adaptation. Lysosomal adaptation seems to be a general stress response of mesenchymal neuroblastoma cells to drug treatment, which might not be directly linked to mechanism of action of the active compounds.

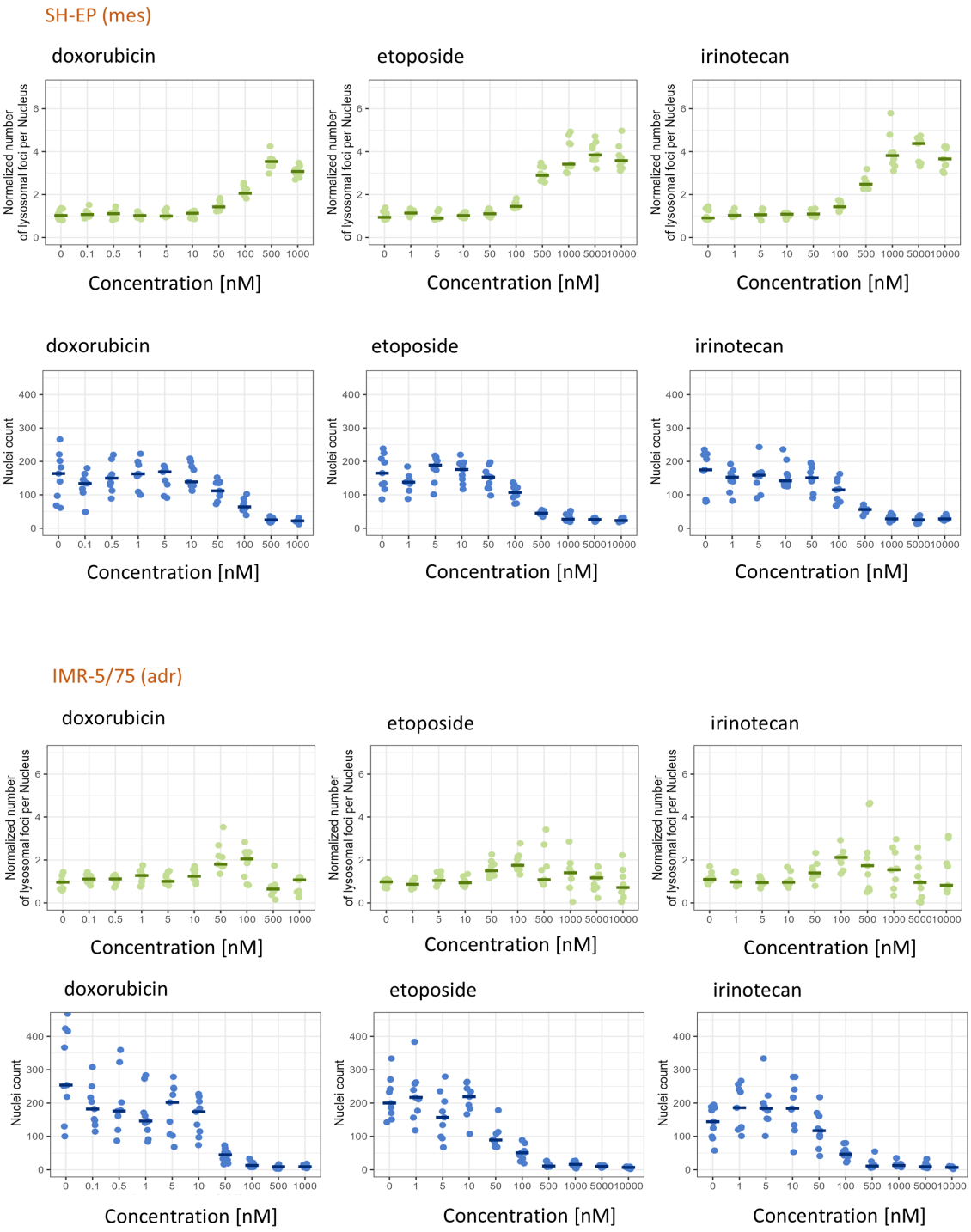

Figure 13: Functional lysosomal changes as response to chemotherapy. Adrenergic (IMR 5/75) and mesenchymal (SH-EP) cells treated with multiple concentrations of chemotherapy drugs for 72h. Normalized number of lysosomes per cell and Nuclei count are plotted.

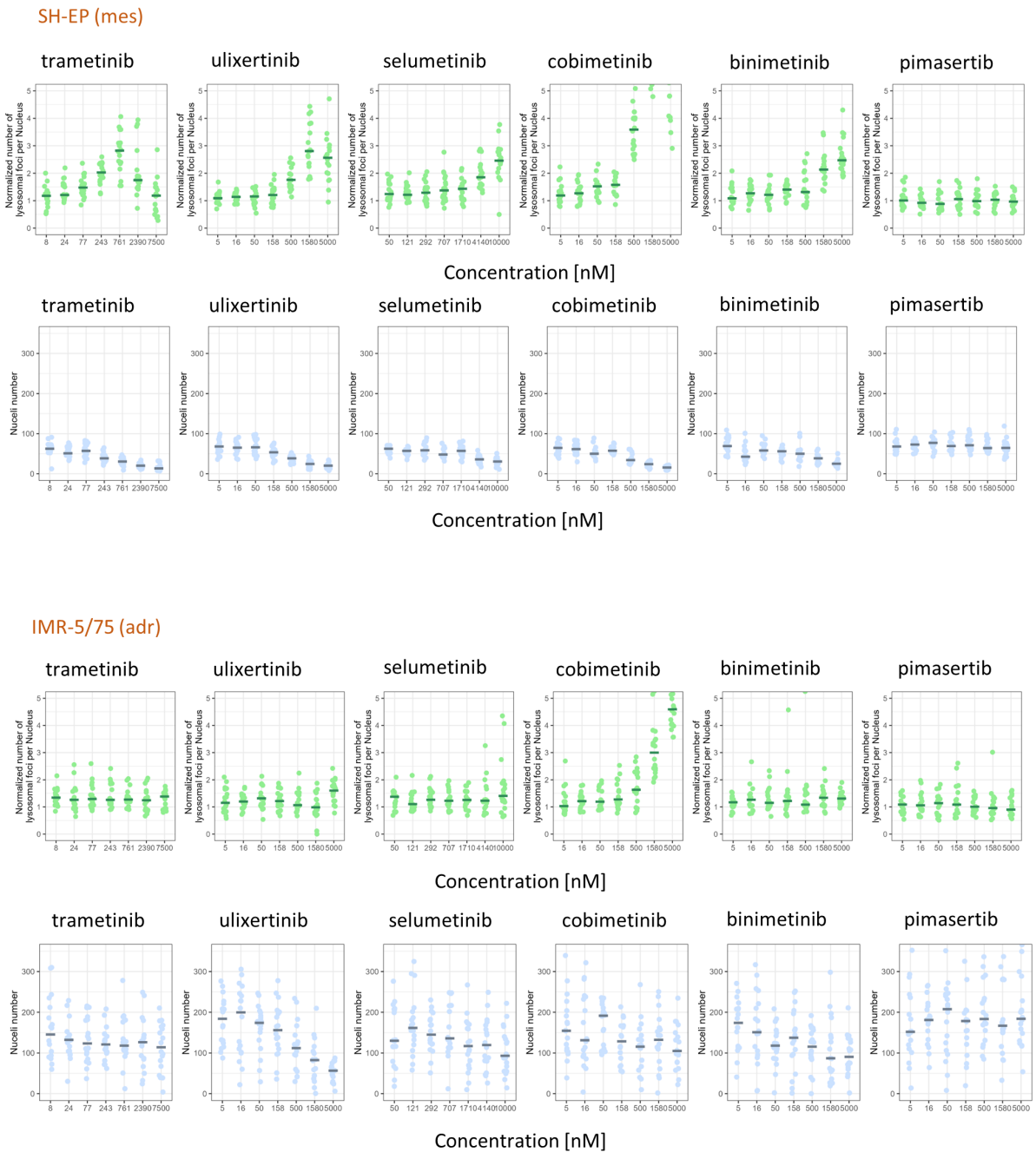

Figure 14: Functional lysosomal changes as response to MAPKi treatment. Mesenchymal (SH-EP) and adrenergic (IMR 5/75) cells treated with multiple concentrations of MAPKi for 72h. Number of lysosomes were normalized to DMSO control treatment of each cell line.

4.4 Targeting lysosomes as a potential combination treatment with MAPK inhibition

To test if the increased number of lysosomes could be a targetable vulnerability, both subtypes were treated with lysosomal inhibitors. Especially for the treatment of mesenchymal neuroblastoma this might be a promising strategy as these cell lines present with high basal level of lysosomes and show a stronger lysosomal adaptation. Hence, a potential strategy for combination treatment addressing the vulnerability of mesenchymal neuroblastoma cells could be the combination of lysosomal inhibitors with MEKi.

There are different options to target lysosomes. The classic ones are increasing the acidic pH, which is specific for lysosomes and necessary for their function. Acidification can be targeted by direct inhibition of vATPase, the proton pump that is responsible for lysosomal acidification, or anti-malaria drugs with weak basic pK_a which accumulate in the lysosome and elevates the acidic pH. Molecules accumulating in lysosomes are described as lysomotropic drugs. The neutralization of lysosomal pH blocks the fusion of autophagosomes and lysosomes[138]. The anti-malaria drugs chloroquine and artesunate are the only drug class that inhibit autophagy and are available in clinics[139,140]. An example for a direct inhibitor of the vATPase is bafilomycin A1 which has its background in antibiotics research, but is not available as an approved drug for anti-cancer treatment[141,142].

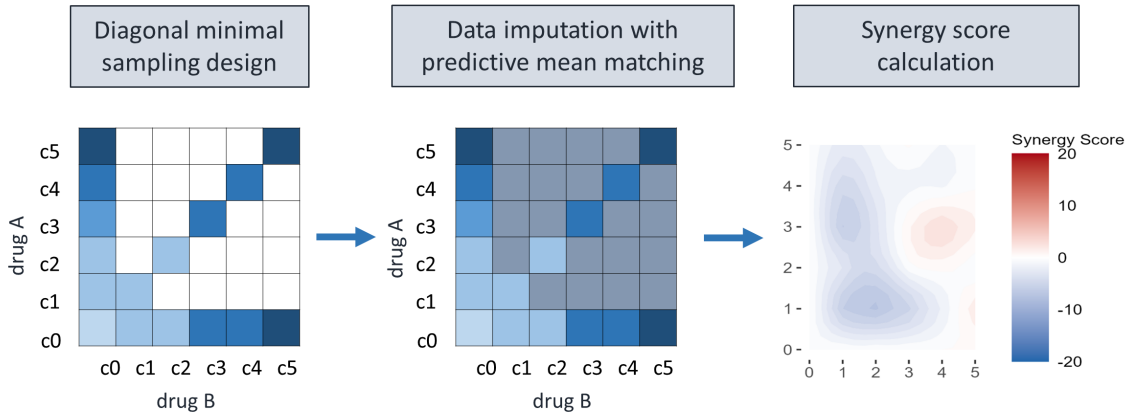

Figure 15: Experimental set up of diagonal minimal sampling design synergy screen. Schematic of diagonal minimal sampling design, blue colored squares are the concentration combinations that were measured in the combination screen. Grey colored squares were imputed and mean synergy scores calculated with the ZIP model.

As an experimental setting for the combination treatment, I chose a diagonal reduced matrix design (**Figure 15)**. With this method, information about synergistic effects are analyzed. Calculating synergy means to compare the combinatorial treatment response to an expected calculated one[120]. The synergy matrix layout combines each concentration of drug A with each concentration of drug B, forming a grid with all possible combinations. In a high throughput drug screen, the focus lies on testing multiple combinations to identify hits which are then further validated by subsequent experiments. In

the diagonal reduced matrix design, the selected concentration combinations as depicted in **Figure 15** are tested. The remaining combinations are imputed by an algorithm[121].

The single drug curves (**Figure 16A**) of the metabolic activity screens showed the expected pattern for MEKis trametinib and selumetinib and ERKi ulixertinib. The mesenchymal cell lines were more sensitive than the adrenergic cell lines. For the lysosomal inhibitors, no difference in reaction between the subtypes could be observed. The synergy screen revealed, that the combination of the MEKis and the ERKi with the lysosomal inhibitors reached high combined sensitivity scores (CSS), indicating a high efficacy of the combination treatment. However, the synergy scores, which evaluate the degree of interaction between the drugs, were mostly below 0, indicating a rather antagonistic interaction (**Figure 16B**). The combination of artesunate with selumetinib was synergistic in some cell lines of both subtypes. The synergy sensitivity plot separated the mesenchymal and adrenergic cell lines which is most likely attributed to the single drug effect of the MAPKis (**Figure16C**).

The widespread application of these classical lysosomal inhibitors is limited. Bafilomycin is quite toxic also to non-malignant cells and is therefore rather used as a tool compound to study mechanistical effects of vATPase inhibition rather than being a treatment option for clinical trials[143]. Inhibiting autophagy is challenging because it can be both, beneficial and detrimental for cancer cell growth[144]. Chloroquine was tested in clinical trials as an add-on to cancer therapy in different entities such as glioblastoma, ductal carcinoma and breast cancer, however with mixed results[145,146]. Long term use of chloroquine shows toxicity such as retinopathy and neurological defects[75,147].

Another strategy to target lysosomes is disrupting lysosomal membrane integrity. When lysosomes are stressed, lysosomal membrane permeabilization occurs and leaks cathepsins into the cytosol, which results in cell death[60]. One strategy to induce lysosomal membrane permeabilization is the inhibition of acid sphingomyelinase (ASM) which causes sphingomyelin accumulation and destabilizes the lysosomal membrane. Amphiphilic cationic molecules have been identified to inhibit ASM[148]. They can also be described as lysomotropic drugs since they accumulate in the lysosome as well. A well-studied group of drugs that show ASM inhibition are fluoxetine, amitriptyline and nortriptyline, all already approved and used in clinic as anti-depressants. The main advantages of these drugs are their safety and accessibility that has been established by long term clinical use[79].

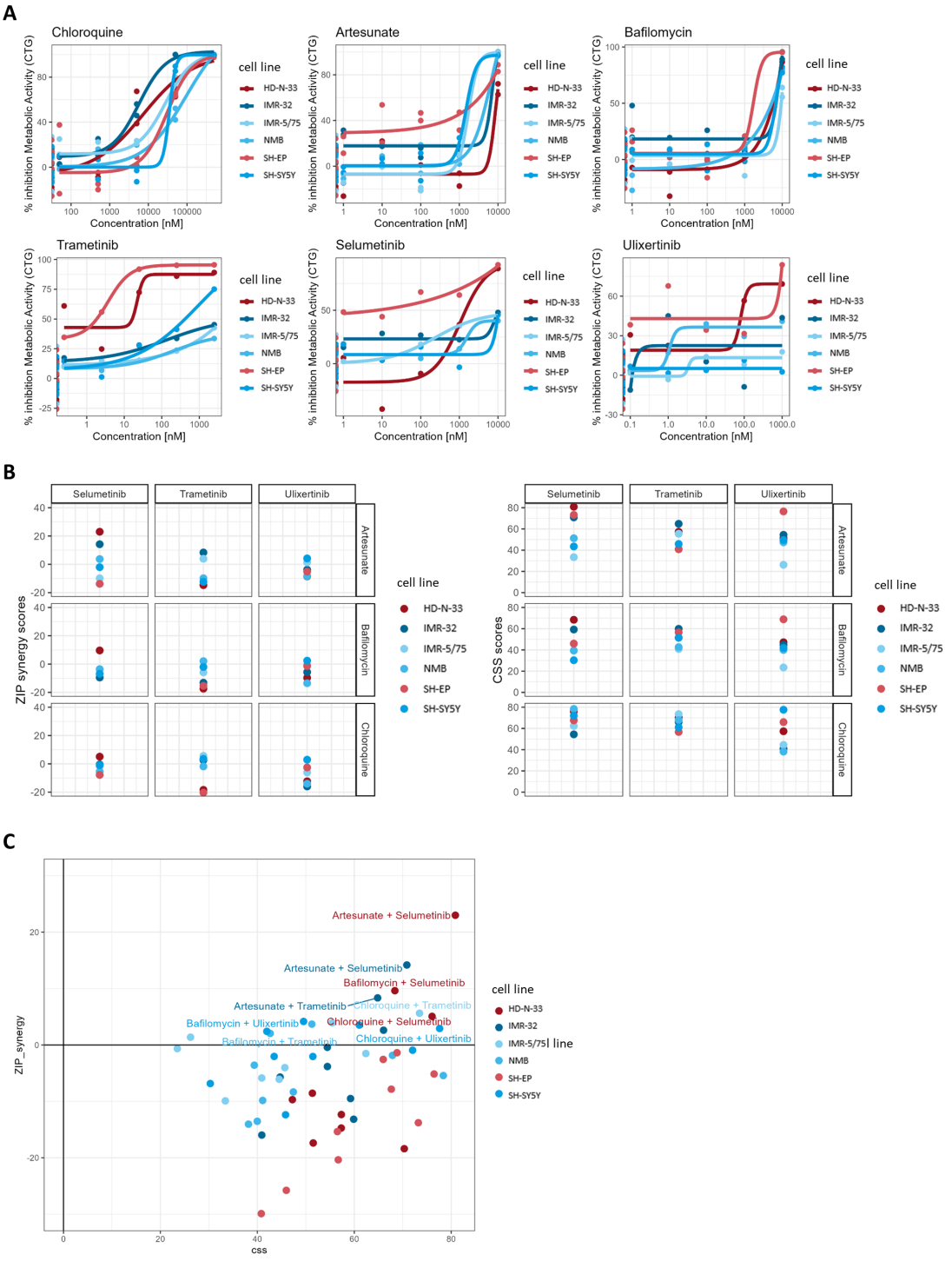

Figure 16: Combination treatment of lysosomal inhibitors and MAPKi. (A) Dose response curves of single drug treatment of two mesenchymal (SH-EP, HD-N-33) and four adrenergic (NMB, IMR-32, IMR-5/75, SH-SY5Y) cell lines treated for 72h. Percent inhibition calculated from metabolic activity measurement with DMSO treated cells as negative and benzethonium chloride treated cells as positive control. (B) ZIP synergy and CSS scores for each tested drug combination (C) Synergy sensitivity plot, combinations with positive ZIP scores are labeled. Mesenchymal cell lines are colored in red, adrenergic in blue.

4.4.1 ASM inhibition leads to an increase of lysosomal numbers in mesenchymal neuroblastoma

To analyze lysosomal adaptation to ASMi in comparison with MAPKi, lysosomal changes were examined in the mesenchymal cell line SH-EP. Treatment with ASMi increased the number of lysosomes per cell, similar to treatment with MEKi (**Figure 17**). The sudden drop in lysosomal numbers occurred due to cell death, which is reflected by a decrease in nuclei numbers.

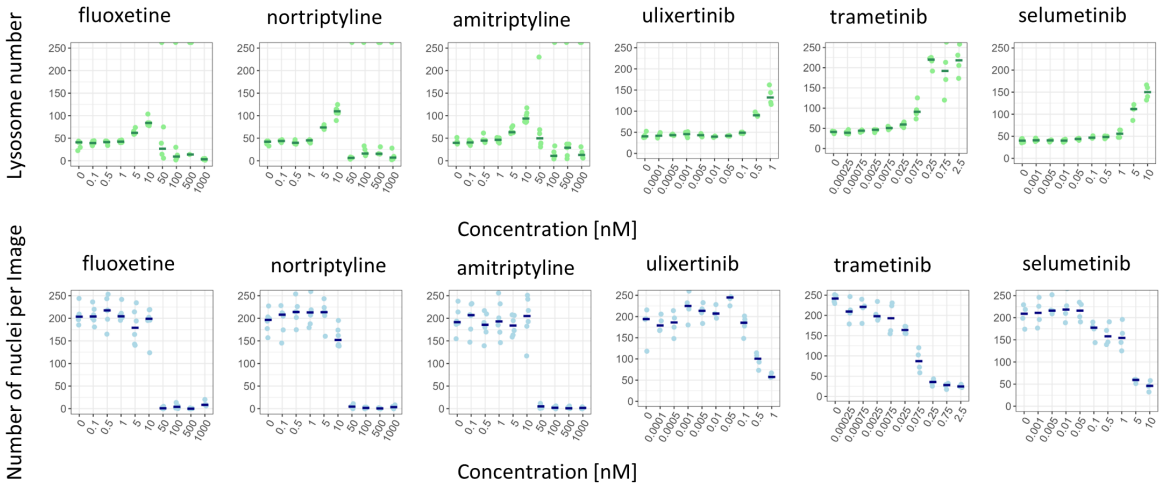

Figure 17: Changes in lysosomal numbers in response to inhibition of lysosomal acid sphingomyelinase. Mesenchymal SH-EP cell line treated with MAPKi (trametinib, selumetinib, ulixertinib) and ASMi (fluoxetine, amitriptyline, nortriptyline) for 72h, lysosomal number per nucleus and number of nuclei was measured.

4.4.2 Synergy screen for the combination of AMSi and MAPKi

Inhibition of MAPK pathway and ASMi both result in lysosomal stress and propose a promising combination strategy and were therefore tested in a synergy screen with metabolic activity and spheroid size as readouts. Regarding the single ASMi drug treatments, no difference can be observed between the two tumor subtypes in both metabolic activity and spheroid growth (**Figure 18A**). The DSSasym also did not differ between mesenchymal and adrenergic cells (**Supplemental Figure 7**).

The adrenergic cell lines had the highest synergy scores for the metabolic readout, although none of the scores exceeded 10 (**Figure 18B**). In the spheroid area readout, the adrenergic cells mostly achieved synergy scores below zero. This indicates, that the combination therapy effect might be cytostatic, meaning the drug show synergism for inhibition of metabolism and the effect on tumor shrinkage is not synergistic. The CSS for the spheroid area readout were all below 40 for the adrenergic cells and separated them from the mesenchymal cell lines (**Figure18C**). This indicated that the efficacy of the combination is in general much higher for mesenchymal cells. For the mesenchymal cells, the synergy scores were higher in the spheroid area readout compared to the metabolic readout. This can be explained because the spheroid shrinkage is caused by dying cells which is a drug effects that occurs after the metabolic activity decrease. Therefore, the single drug effect is lower for spheroid area. The

estimated effect that has to be reached by a drug combination to be considered synergistic is also lower. Hence, this effect is reached faster for the spheroid area compared to metabolic activity.

To validate the combinations of trametinib and fluoxetine as well as trametinib and amitriptyline for two mesenchymal cell lines, a full matrix screen was done. A synergistic effect for spheroid shrinkage could be confirmed with positive ZIP scores for the combination of trametinib and amitriptyline for both cell lines. The HD-N-33 had for this combination a ZIP score of 8.42, the SK-N-AS had 1.12 (**Figure 19**).

In conclusion, lysosomes can be targeted by various different lysomotropic drugs. In addition to chloroquine, which was already tested in clinical trials and has a rather unspecific drug effect, I showed, that artesunate, which has a very similar application as chloroquine might be an alternative. Furthermore, lysomotropic compounds such as fluoxetine or amitriptyline, which inhibit ASM could be repurposed for lysosomal inhibition since these compounds have been used in clinic for other diseases for a long time. However, the overall synergistic effects of the lysosome targeting drugs is rather small. Alternative strategies for combination treatment should also be explored.

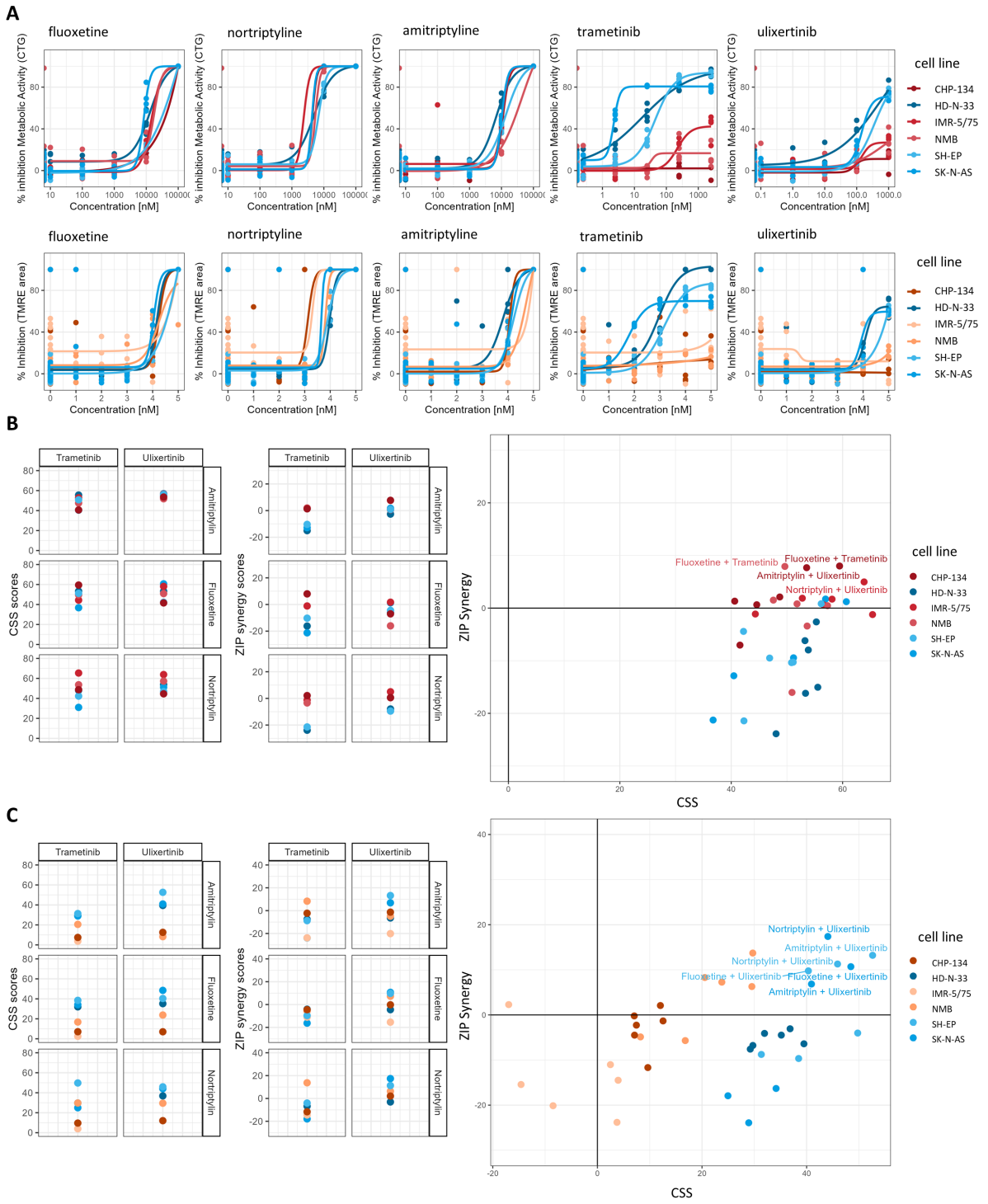

Figure 18: ASMi and MAPKi synergy screen. (A) Dose response curves of single drug treatment of three mesenchymal (SH-EP, HD-N-33, SKNAS) and three adrenergic (NMB, CHP-134, IMR-5/75) cell lines treated for 72h. Percent inhibition calculated from metabolic activity measurement with DMSO treated cells as negative and benzethonium chloride treated cells as positive control. Percent inhibition for TMRE area measurement was calculated with the same controls. If no spheroid was detected, the spheroid area was considered 0. (B) ZIP synergy and CSS scores for each tested drug combination, synergy sensitivity plot for metabolic activity readout. (C) ZIP synergy and CSS scores for each tested drug combination, synergy sensitivity plot for spheroid area readout.

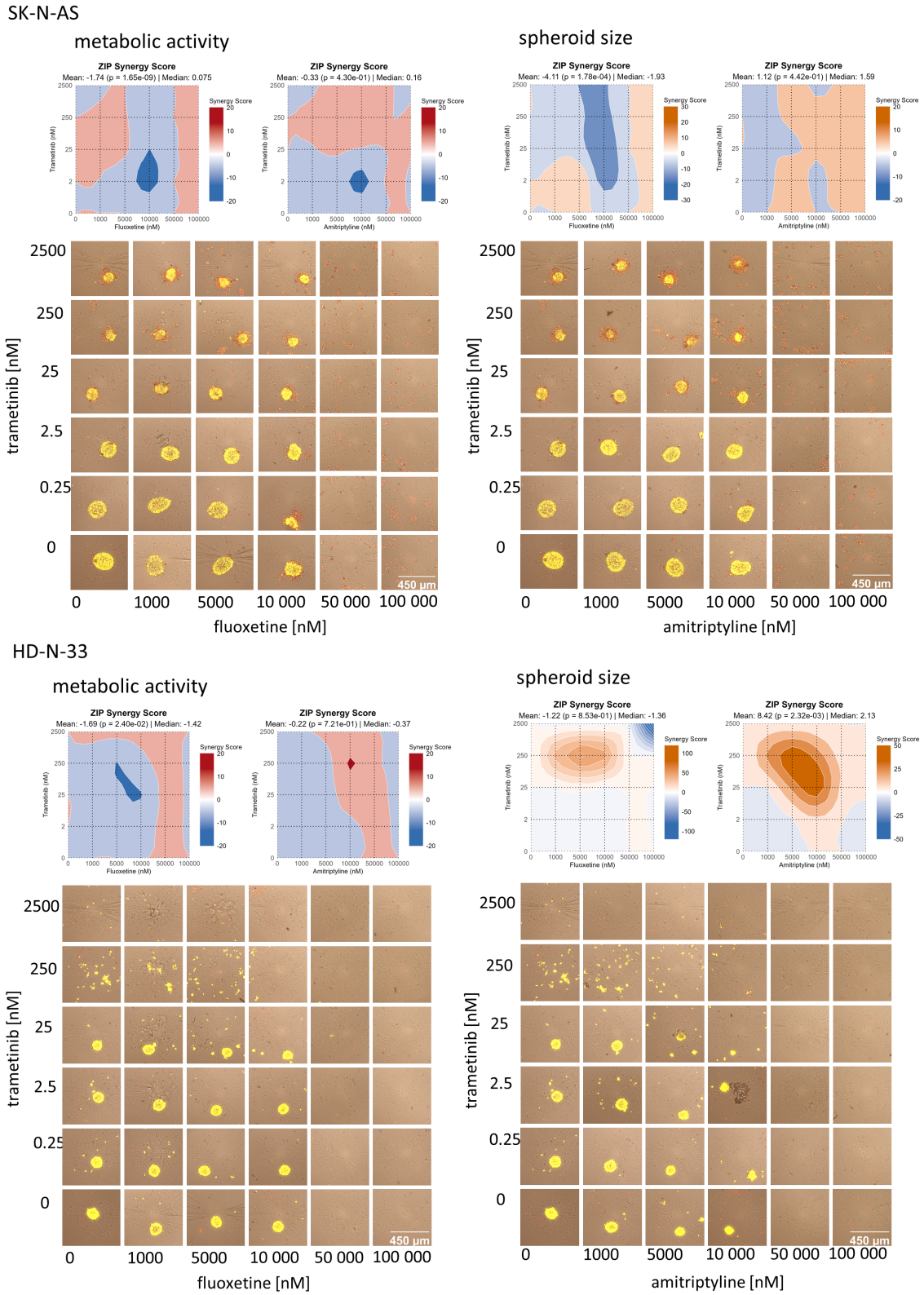

Figure 19: MAPKi and ASMi synergy validation screen. Surface plots of combination treatments with fluoxetine and trametinib and fluoxetine and amitriptyline. Red colored plots show surface plot of metabolic activity, orange plots show surface plot of spheroid size readout, example images for each concentration combination of the matrix, yellow = TMRE staining for viable cells, red = reddot staining for dead cells, top panel shows results of cell line SK-N-AS, bottom panel shows results of cell line HD-N-33.

4.5 Mesenchymal neuroblastomas show characteristics of pre-senescent cells

The previous phenotypic analysis revealed that mesenchymal neuroblastoma cells exhibits a larger, more flattened phenotype compared to adrenergic cells. Interestingly, this mirrors the phenotype of senescent cells, which are distinct in morphological appearance from proliferating cells and also are more flattened and enlarged[149-151]. Similarly, the number of lysosomes per cell is higher for mesenchymal neuroblastoma, which is also observed in senescent cells as they adapt to changes in metabolic conditions[152-154]. Hence, I explored the senescence associated characteristics in the mesenchymal neuroblastoma subtype and tested drugs targeting senescence.

4.5.1 Single sample gene set enrichment analysis for senescence associated gene sets reveales upregulation of SASP in the mesenchymal neuroblastoma subtype

To analyze subtype specific senescence regulation, I examined the gene expression profiles of neuroblastoma subtypes concerning senescence-associated pathways using single-sample gene set enrichment analysis (ssGSEA). The gene sets belonging to the canonical senescence pathways did not show a correlation with the mes/adr score calculated for the cell lines (**Figure 20A**).

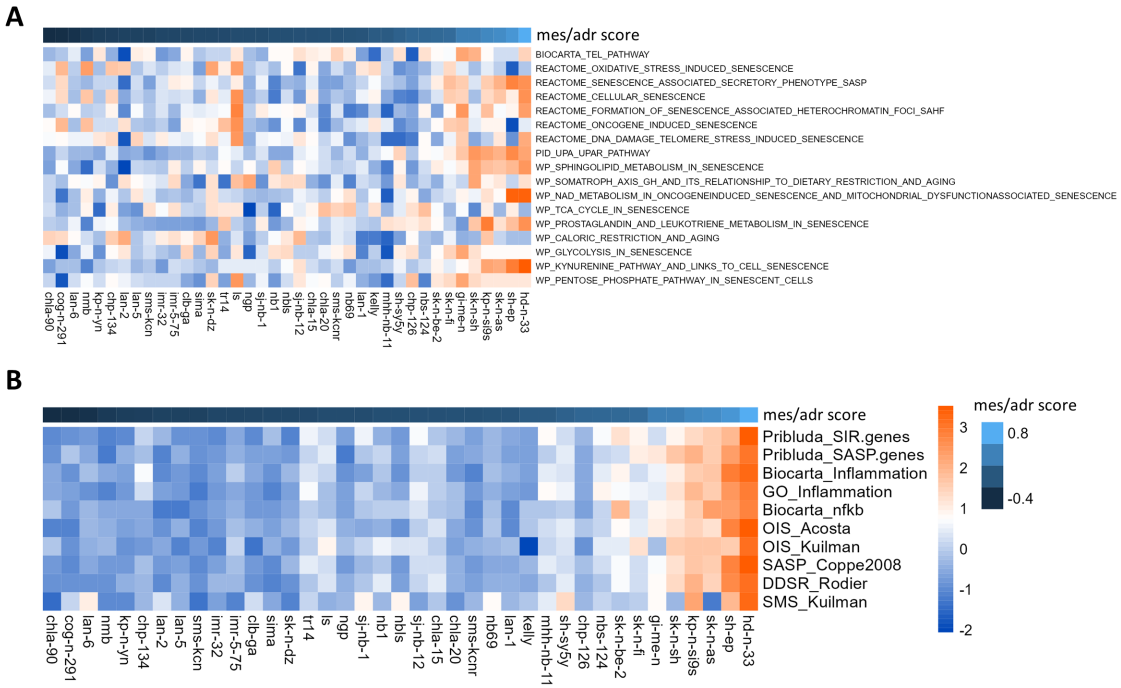

Figure 20: ssGSEA of senescence associated gene sets. (A) Heatmap representing ssGSEA scores for gene set collection of canonical pathways senescence, cells are ordered based on mes/adr score. (B) Heatmap representing the ssGSEA scores for gene sets connected with senescence associated secretome signaling, cells are ordered based on mes/adr score.

However, pathways associated with the Senescence-Associated Secretory Phenotype (SASP) exhibited a distinct pattern of upregulation in the mesenchymal neuroblastoma cell lines (**Figure 20B**).

4.5.2 Upregulation of SASP in mesenchymal neuroblastoma is also relevant in patient-derived fresh tissue tumoroids

To validate the upregulation of SASP associated pathways in mesenchymal neuroblastoma in patient data, I analyzed gene expression data from 223 patient samples obtained from the INFORM registry. INFORM is an international pediatric precision oncology program which provides comprehensive molecular diagnostics including RNA sequencing and drug sensitivity profiling data of relapsed pediatric patients[155]. Remarkably, the patient samples confirm the previous pattern, the ones with high mes/adr score show upregulation of SASP pathways compared to the more adrenergic samples (**Figure 21 A**). For five of the patient samples, *ex vivo* drug sensitivity profiling from fresh tissue cultures was available. This confirms, that samples with higher mes/adr score are more sensitive to MEKi (**Figure 21B**).

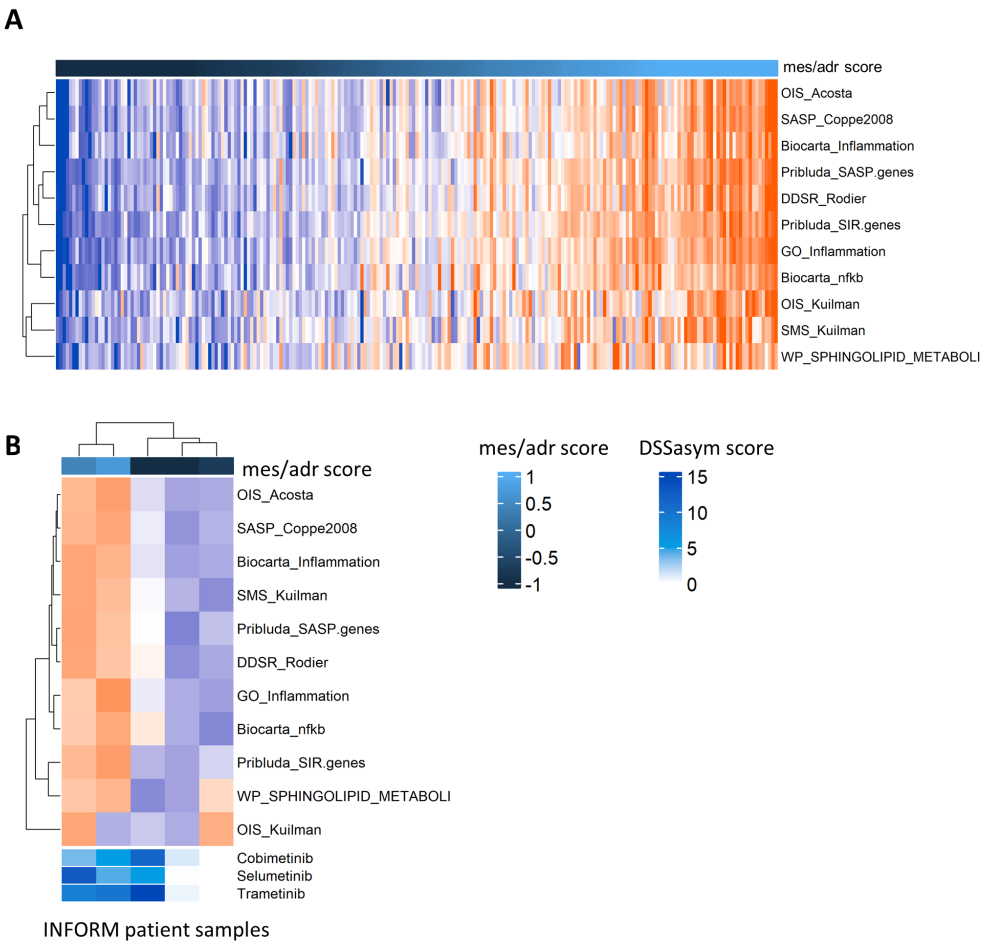

Figure 21: Senescence secretome associated gene expression and drug sensitivity of INFORM patient samples. (A) Heatmap representing ssGSEA scores for gene sets collection of canonical pathways senescence in 223 patient samples of the INFORM cohort, samples are ordered based mes/adr score (B) Heatmap representing the ssGSEA scores for gene sets connected with senescence associated secretome signaling in five INFORM patient samples, DSSasym scores for three MEKi in bottom annotation.

4.5.3 MAPKi treatment induces senescence in mesenchymal neuroblastoma cell line

The elevated basal lysosomal levels, along with increased expression of SASP in mesenchymal neuroblastoma cells compared to adrenergic neuroblastoma, are hallmarks of senescence. Despite these indications, these cells are not considered senescent because they lack the key characteristic of senescent cells, which is proliferation arrest. The upregulation of these pathways, however, could suggest that the mesenchymal cells are primed for senescent signaling and may potentially enter senescence state faster than the adrenergic cells. Indeed, mesenchymal cells showed an increase in senescence associated β-gal staining when treated with MEKi compared to adrenergic cells (**Figure22**). Doxorubicin, which promotes therapy induced senescence, was used as a positive control[156].

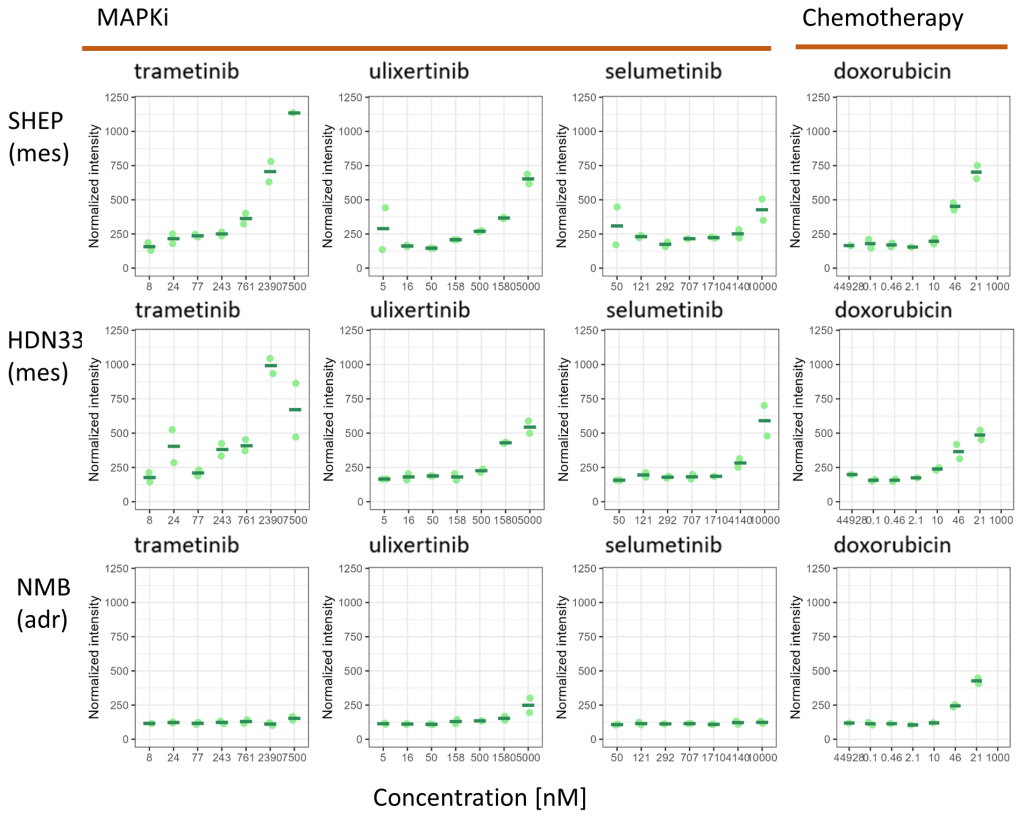

Figure 22: Senescence induction in neuroblastoma subtypes. Intensity of fluorescent β-gal staining for multiple concentrations of three MAPKi and one chemotherapy drug normalized to DMSO treated control. Cells were exposed to drug treatment for 6 days.

4.5.4 Sequential combination treatment of senescence inducing drugs and senolytics shows synergy in both subtypes

Given the increase in β-gal activity in mesenchymal neuroblastoma in response to MEKi, I hypothesized that this increase might create a potential new vulnerability that could be targeted with senolytic drugs. However, analysis of drug screen data from **Figure 1** and **Supplemental Figure 2** did not show high sensitivity of mesenchymal cell lines to senolytic drugs such as navitoclax, venetoclax, A-1331852 and A-1210477. To investigate if a senolytic treatment could be more effective with prior senescence induction, a sequential synergy screen was done with a diagonal minimal sampling design. The tumor spheroids of neuroblastoma cell lines were treated with the senescence inducing drug for three days. Then, the senolytic drugs were added for another three days before analysis (**Figure 23**). As senescence inducers, classic chemotherapy drugs such as doxorubicin and etoposide as well as the MAPKi ulixertinib, cobimetinib, selumetinib, trametinib, and binimetinib were used.

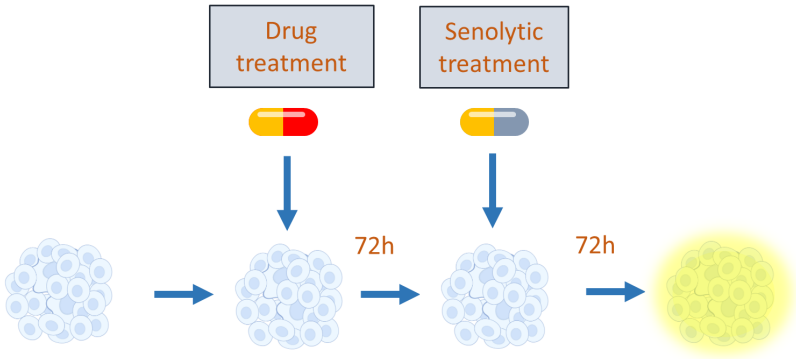

Figure 23: Experimental set up of sequential combination treatment with MEKi and senolytics. Graphical description of the experimental design, cells were seeded and treated with the first drug directly after seeding. After 72h cells were treated with senolytics drugs. Metabolic activity readout and spheroid size analysis was done after another 72h incubation.

The senolytic drugs that were chosen in this experiment include the first discovered senolytic drug dasatinib, which was developed as BCR-ABL inhibitor and inhibits multiple tyrosine kinases including Scr kinases which act in anti-apoptotic pathways[157]. BCL family inhibitors and especially BCL-X_L inhibitors target pro survival pathways that are upregulated in senescent cells to evade apoptosis. Targeting BCL-2 alone is not showing the same senolytic effects as targeting BCL-X_L [158,159]. As BCL-2 inhibitor I applied venetoclax. For BCL-X_L inhibition, A-1210477, A-1331852, and navitoclax were used[160]. BET inhibition also has been reported to have senolytic effects, therefore the BET inhibitors iBET-151 and mivebresib were included in this experiment[161].

The single drug curves do not show a difference in sensitivity between the neuroblastoma subtypes towards any senolytic drug in both metabolic and spheroid size readouts (**Supplemental figure 8 & 9**). To show the differences between combination of chemotherapy and MEKi with senolytics, the results for the drug classes were plotted separately in synergy sensitivity plots. The combination of the senescence inducing drugs and the senolytics showed overall high scores in the whole cell line cohort

for CSS and especially for the synergy score where 21 combinations for the metabolic readout showed mean synergy score above 20 (**Figure 24B**). The imaging readout confirmed this result with 6 combinations having a higher ZIP score than 20 (**Figure 25 B**). The lower number of hits is expected, as shrinkage of the tumor spheroid is a sign of cell death and occurs as a much later drug response than decrease in metabolic activity.

Looking at the subtypes separately, the combination of chemotherapy with senolytics showed high scores for the mesenchymal cell lines, whereas for the combination with MEKi, high synergy scores were found for both subtypes. Comparing the mean synergy score between the subtypes, the combination of MEKi and senolytics is higher for the adrenergic subtypes (CHP134, IMR5/75) and the combination of chemotherapy and senolytic has higher ZIP scores for the mesenchymal cell lines (SKNAS and SHEP) (**Figure 24 B and Figure 25 B**). Following the hypothesis, that mesenchymal cell lines show senescence induction with MEKi treatment and therefore are more sensitive to the combination of MEKi and senolytic therapy, this was an unexpected result. Since the mesenchymal cells show also a strong senescence induction this might benefit the combination treatment at a higher extend than the adrenergic cells, which matches the results depicted in **Figure 24B** and **Figure 25B**.

In conclusion, mesenchymal neuroblastoma cell lines upregulate senescence secretome pathways although they are not in proliferation arrest. This upregulation and the elevated sensitivity of mesenchymal cells towards MEKi could be validated in a patient data set obtained from the INFORM registry. This shows, that the findings are not an artifact of cell lines but also relevant in patient samples. Further, MEKi treatment induces senescence in mesenchymal cells compared to adrenergic cells indicating, that the upregulation of senescence signaling in the mesenchymal cells might prime them for senescence induction. Senescence upregulation could be a potential target in neuroblastoma, as both subtypes showed high synergy and sensitivity scores for the combination treatment of senescence inducing drugs and senolytics.

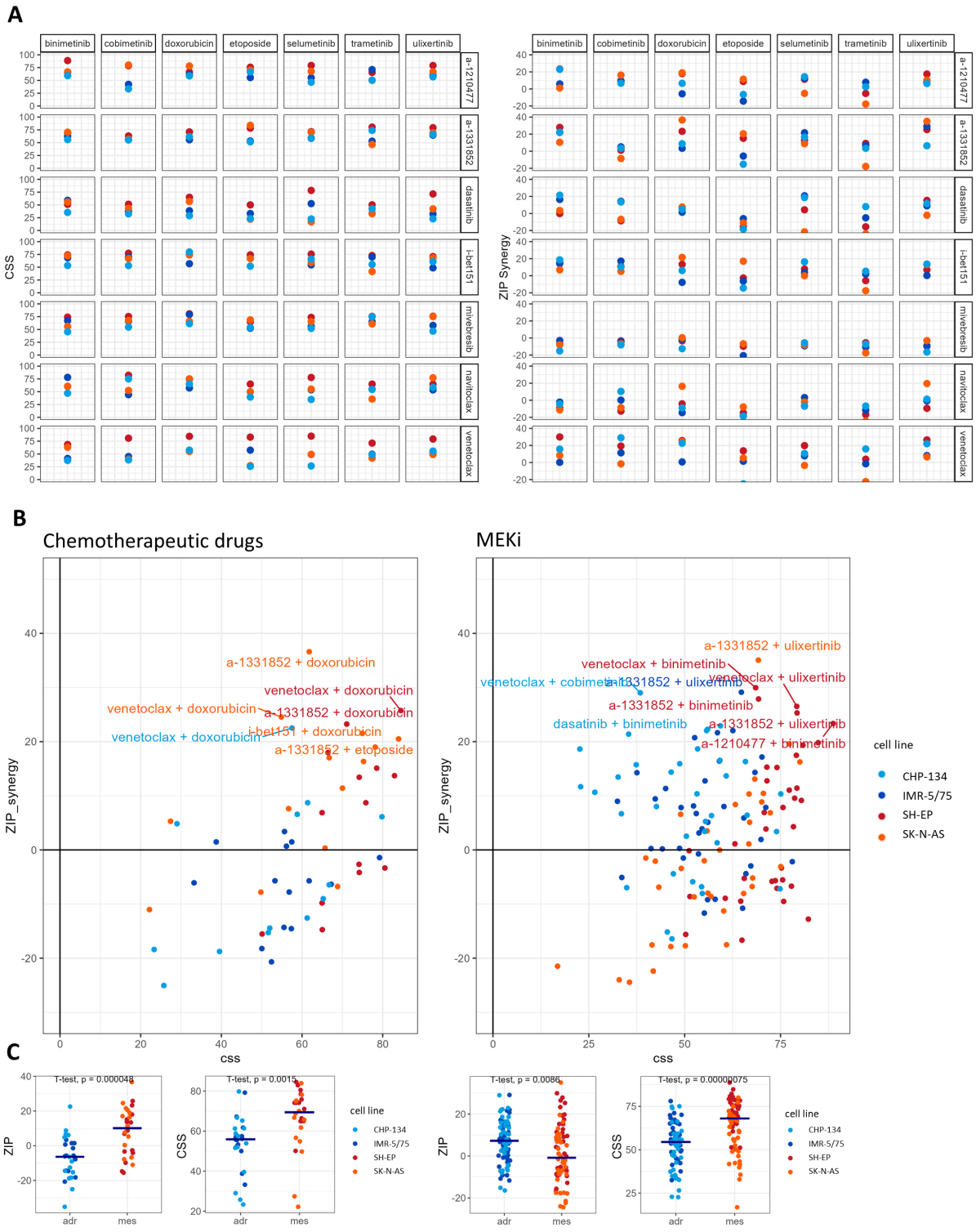

Figure 24: Sequential senolytic combination screen metabolic readout. (A) ZIP synergy and CSS scores for each tested drug combination, for metabolic activity readout. (B) ZIP synergy and CSS scores for each tested drugcombination separated by drug class of the senescence inducing combination partner in a synergy sensitivity plot. (C) Comparison of mean ZIP and CSS scores between neuroblastoma cell lines separated by drug class.

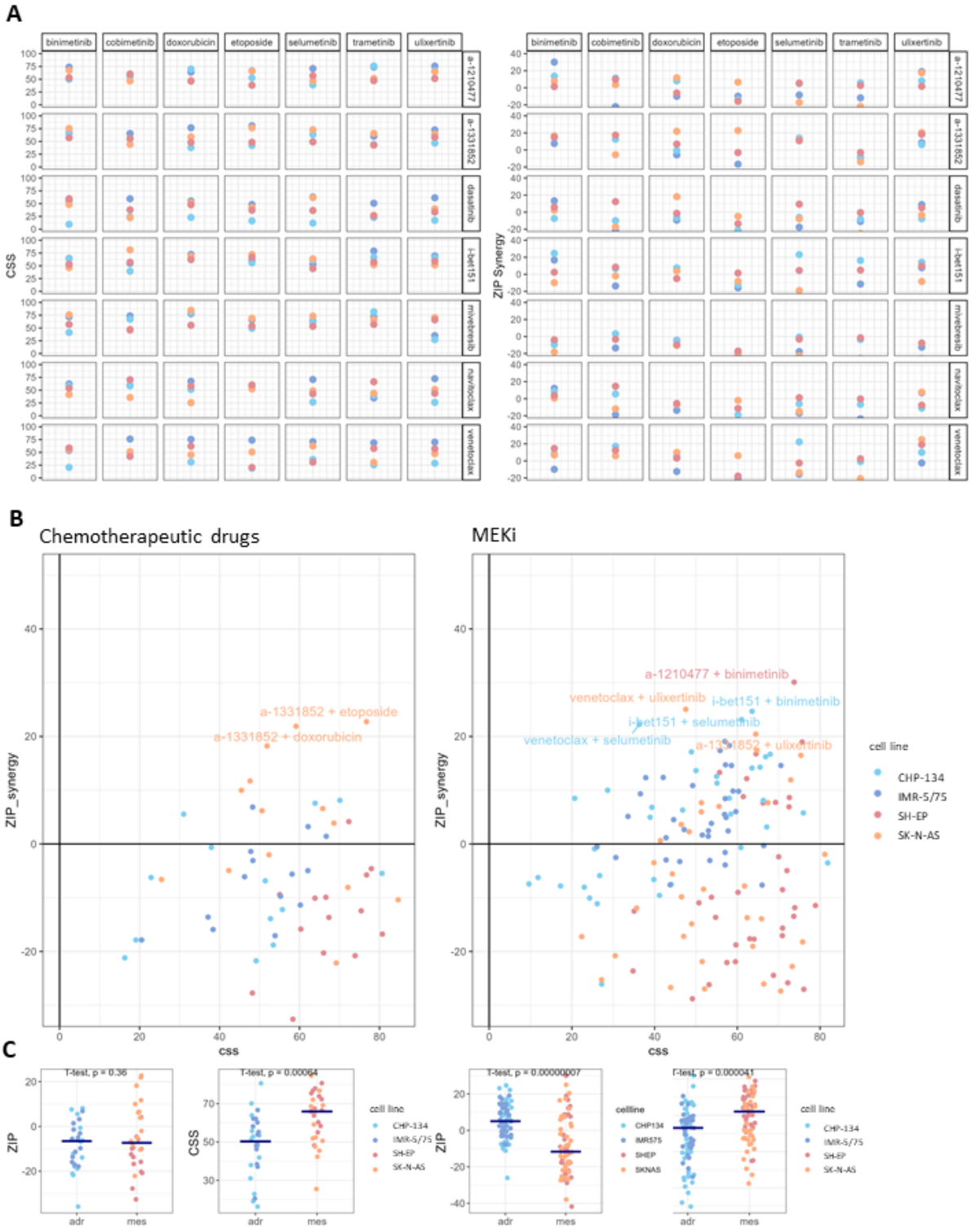

Figure 25: Sequential senolytic combination screen spheroid area. (A) ZIP synergy and CSS scores for each tested drug combination, for spheroid area. (B) ZIP synergy and CSS scores for each tested drug combination separated by drug class of the senescence inducing combination partner in a synergy sensitivity plot. (C) Comparison of mean ZIP and CSS scores between neuroblastoma cell lines separated by drug class.

4.6 Mixed neuroblastoma cell line containing cells with adrenergic and mesenchymal identity confirms described characteristics of the subtypes

One of the established neuroblastoma cell lines shows a mixed phenotype and contains both subtypes[37,162]. This model offers the great opportunity to compare how both subtypes with the same genetic background in a heterogeneous population react to drug treatment.

4.6.1 Single cell gene expression analysis confirms upregulation of SASP associated genes in mesenchymal cells

Single cell gene expression data from this mixed phenotype cell line was analyzed and classified into mesenchymal, adrenergic and intermediate subtype by Jansky et al[32]. Using this classification, I compared the expression of the SASP gene set, showing, that the mesenchymal cells show higher expression of these genes compared to the adrenergic ones. This confirms my data from the ssGSEA of the cell line cohort.

4.6.2 Immunofluorescence co-staining confirms a higher lysosomal quantity for mesenchymal cells

To distinguish between the subtypes in the mixed culture, several antibodies against marker proteins were tested for immunofluorescence staining. The markers that were tested are: PRRX1, SNAI2, YAP1 and PHOX2B[36]. PRRX1 and PHOX2B are key transcription factors, PRRX1 is a transcription factor that commits progenitor cells to mesenchymal tumors and PHOX2B to adrenergic one[163]. YAP1 and SNAI2 are also markers associated with the mesenchymal subtype[36]

The immunofluorescence staining was performed in a panel of 17 cell lines. Nuclei of the cells were segmented and intensity was measured. With a machine learning tool, the cells were classified into staining positive and negative cells (**Supplemental Figure10**). Confusion matrix scores were highest for YAP1 staining, showing this marker is best for distinguishing adrenergic and mesenchymal cells. To test how lysosomes, change in the mesenchymal and adrenergic cells of the mixed cell line, cells were treated for 72 and immunofluorescence co-staining of YAP1 and LAMP1 was performed (**Figure 26 B**). Cells were than classified into YAP1 staining positive and negative and lysosomes were counted. For chemotherapeutic drugs, the percentage of adrenergic cells decreased with increasing drug concentration (**Figure 26C and Supplemental Figure 11**). Treatment with MEKi, however did not lead to an enrichment of adrenergic cells. Lysosome numbers were, at all drug concentrations, higher in the YAP1 classified cells. (**Figure 26D and Supplemental Figure 12**).

In conclusion, the experiments with the mixed phenotype neuroblastoma cell line confirmed the previous findings. The mesenchymal cells upregulated the SASP genes, contain more lysosomes and are more resistant to chemotherapy treatment.

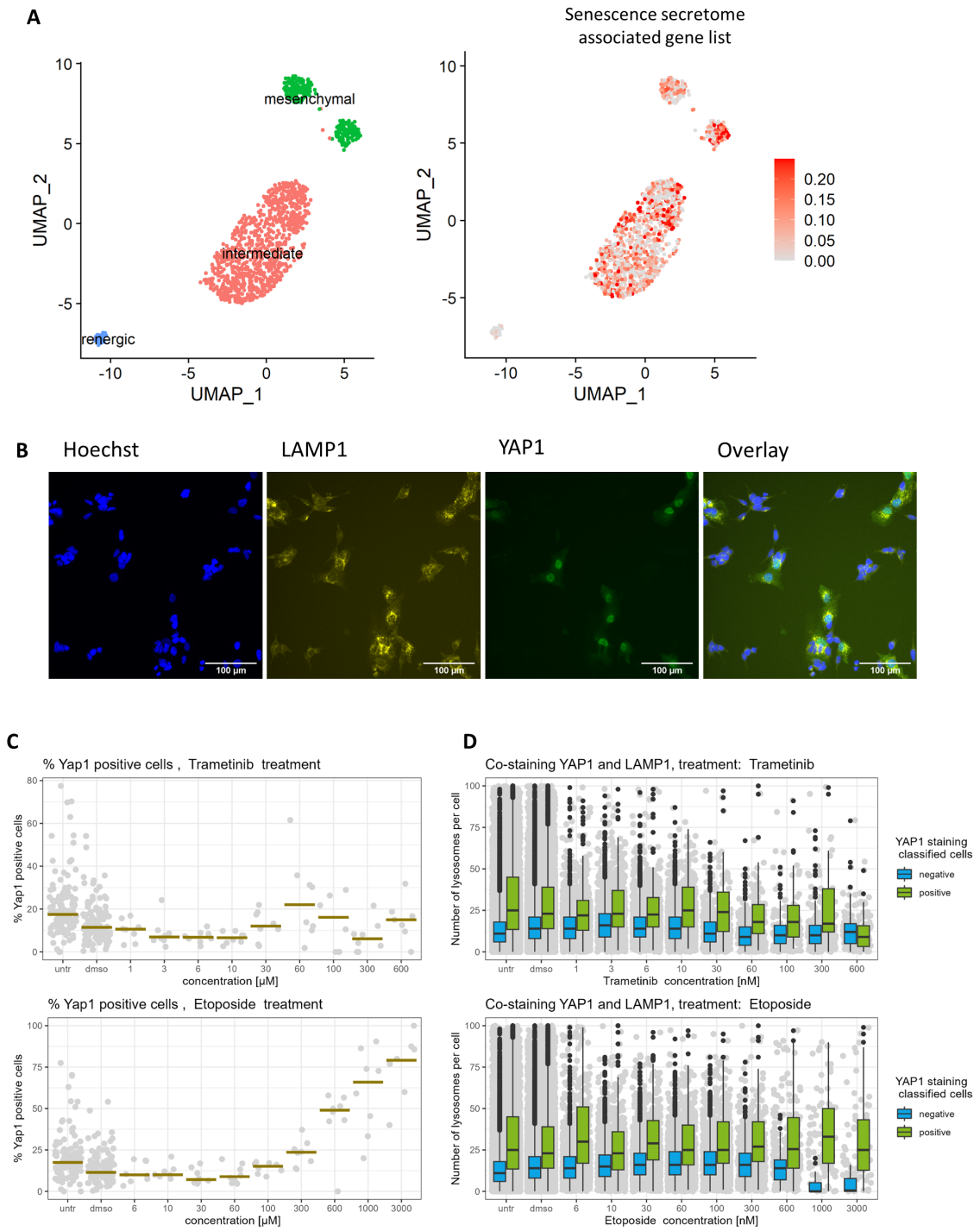

Figure 26: Mixed neuroblastoma cell line. (A) Uniform manifold approximation and projection (UMAP) embedding of single cell data of the cell line SK-N-SH. Neuroblastoma subtypes are annotated on the left plot based on Jansky et al 2021. Expression of SASP associated gene list shown on right plot. (B)Example images of immunofluorescence co-staining with LAMP1 (yellow) and YAP1 (green) antibodies. Nuclei are stained with Hoechst (blue). (C) Fraction of YAP1 positive cells of SK-N-SH cell line for trametinib and etoposide treatment. Cells were treated for 3 days. (D) Number of lysosomes per cell for cells classified as YAP1 positive or negative for multiple treatment concentrations.

5 Discussion

Neuroblastoma is a tumor entity with high inter and intra tumoral heterogeneity that translates to diverse clinical outcomes. Additional difficulties to identify effective treatments are proposed by low mutational burden and complex biological processes such as chromosomal instability, tumor micro environment and epigenetic regulation in the tumor. Recently, epigenetically regulated neuroblastoma subtypes have been identified. Cells of the adrenergic subtype are more committed to the adrenal lineage, cells of the mesenchymal subtype are more undifferentiated and show stem cell like characteristics. The two main subtypes can be further divided due to their molecular alterations and gene expressions[41]. The subtypes have clinical relevance as cells with mesenchymal characteristics are enriched in relapsed tumors, have higher immunogenicity and are considered a factor for treatment failure[164,41,165]. Other groups intensively analyzed the gene expression of the tumor subtypes to describe the connection between the epigenetically regulated subtypes, genetic alterations and clinical outcomes. However, identifying specific drug vulnerabilities and targeting the subtypes remains a challenge.

5.1 Drug sensitivity profiling of neuroblastoma subtypes identifies MEKi as specific sensitivity in mesenchymal neuroblastoma

The drug sensitivity profiling of this project identified a substantial difference in drug response between mesenchymal and adrenergic neuroblastomas. I demonstrated, that adrenergic neuroblastomas are more sensitive to chemotherapeutic drugs compared to the mesenchymal subtype, confirming previous studies[35,36]. The mesenchymal subtype is more sensitive towards MEKi. This sensitivity of the mesenchymal subtype suggests a higher activity of MAPK signaling pathway, which was confirmed by the correlation of mes/adr score and MAPK activity score. The MSS score, which predicts sensitivity towards MEKi was also correlating with the mes/adr score and matches the observed MEKi sensitivity of mesenchymal cell lines.

MAPK pathway is a signaling cascade that transmits signal form the surface of the cell to the nucleus and is activated by external stimuli such as growth factors, cytokines and environmental stress. It plays a role in a lot of cellular processes like proliferation, differentiation and is often deregulated in cancer[166,167]. The RAS-MAPK pathway is usually activated by receptor tyrosine kinases such as ALK, EGFR and FGFR1[168]. Activation of these receptors leads to RAS activation, which then activates RAF and subsequently the MAPK cascade. Here, MEK1/2 gets phosphorylated and activates ERK1/2[169]. These kinases serve as drug targets and can be inhibited by small molecules[170]. Phosphorylated ERK translocates to the nucleus and activates transcription factors.[171]

Activating somatic alterations of the RAS-MAPK pathway are relevant in neuroblastoma and occur especially in relapsed tumors that received chemotherapy treatment[172-174]. Because mutations in the RAS-MAPK pathway do not necessarily reflect signaling activity, activity of the pathways is evaluated

with target gene expression analysis [173,175]. The mesenchymal subtype, same as RAS-pathway gene expression, is enriched in relapsed tumors and a correlation between the mesenchymal signature and the RAS activation signature was demonstated[37]. In my project, I also analyzed correlation between signatures of MPAS and mes/adr score to confirm MAPK activity. The underlying gene sets did not overlap, which demonstrates the independence of this correlation. Because of the high MAPK pathway activity and MEKi sensitivity, targeting RAS-MAPK pathway can be a potential treatment option for especially the mesenchymal subtype.

Other research groups also investigated the sensitivity of neuroblastoma towards MEKi. The novel MEKi CI-1040 was successfully tested in six neuroblastoma cell lines in vitro and demonstrated reduced proliferation and apoptosis induction[176]. Another group tested a set of MAPKi in a panel of nine cell lines and showed varying sensitivity, which could not be explained by mutational status[177]. These authors did not distinguish between epigenetically regulated subgroups, which could have explained the variance in sensitivity. As seen in other entities, it is very likely that neuroblastoma develops resistance against MAPKi when exposed to long term treatment [178,179]. To avoid this, inhibitors of the RAS-MAPK pathway are used in drug combinations. Currently, MEKi such as trametinib, cobimetinib, selumetinib and binimetinib are tested in clinical trials for neuroblastoma, in single treatment or in combination with CDK4/6 inhibitor ribociclib and BRAFi dabrafenib[168,180]. MAPK pathway can also be activated by ALK, which is mutated in 6-10% of sporadic neuroblastoma and ALKi such as crizotinib, ceritinib and lorlatinib are tested in combination with mTOR inhibitors or cyclin D inhibitors[168,181].

5.2 Phenotypic differences in neuroblastoma subtypes

One of the features that varies between the subtypes is their morphology. The mesenchymal cells, display larger and more rounded cell bodies and the adrenergic cells have a smaller and more elongated phenotype. This variation can be attributed to the level of differentiation, with the mesenchymal cells presenting more stem cell like features and the adrenergic ones resembling more differentiated cells[162]. These differentiation stages resemble linage development stages[32,36]. This was also observed for other tumor entities such as glioblastoma where single cell studies identified mesenchymal and proneural subtypes which also display different morphologies[182].

Morphology of cells is closely connected to their function and metabolism, so I also examined lysosomes, which are key organelles for altered metabolism in cancer cells. As hypothesized, I was able to identify differences in the lysosomal compartment between the subtypes. The mesenchymal cells showed higher amounts of lysosomes per cell than adrenergic cells. Like the mes/adr score, which is based on gene expression, the microscopically acquired lysosomal score is also a continuous variable between the subtypes. Both scores correlate with each other. Therefore, the quantity of lysosomes could be a possible image-based biomarker for identification of the mesenchymal subtype.

A high number of lysosomes has various implications for cancer cells. One of the main roles of lysosomes is autophagy. Autophagy is necessary to maintain cellular homeostasis, however for cancer cells, this process could either be benefiting or inhibiting tumor progression[183,184]. In tumor initiation, autophagy protects cells against oncogenic processes and prevents malignant transformation by

removing damaged organelles or oncogenic proteins. It also reduces genotoxic stress by preventing overproduction of reactive oxygen species[185,186]. On the other hand, autophagy is a stress response mechanism and supports enhanced metabolic needs of malignant cancer cells to provide nutrients to sustain the enhanced proliferation rate[187]. Lysosomes also control cancer progression by limiting the amount of receptor tyrosine kinases and their growth promoting signaling on the plasma membrane by endocytic internalization and degradation of these receptors[188]. Additionally, cathepsin release from lysosomes reshape the tumor microenvironment to promote invasive growth and metastasis[189]. Considering these various roles of lysosomes in cancer progression, it is difficult to conclude the consequence of a higher number of lysosomes in mesenchymal neuroblastoma.

Lysosomes are also discussed for their role in drug resistance[190]. Lysosome-mediated drug resistance involves active or passive sequestration of drug molecules. Molecules with a lipophilic weak basic chemical structure passively cross the lysosomal membrane and get protonated in the acidic lysosomal lumen. Due to this additional charge the molecules cannot pass the lysosomal membrane again and are therefore trapped in the lysosome and cannot reach their molecular target anymore, which for many drugs relevant in cancer treatment is in the nucleus[74,76,191]. Active sequestration is mediated by p-glycoprotein, which pumps the drug molecules into the lysosome[191,192]. Following this line of arguments, increased lysosomal biomass would render cells more resistant to drug treatment and serve as a biomarker for resistance to lipophilic weak basic drugs.

In my experiments I could not demonstrate a general higher resistance to weak basic, lipophilic drugs across all drug classes in cell lines with higher lysosomal scores. Drug effects seem rather specific for the mechanism of action than the molecular structure. This could be observed because all the MEKi showed efficacy in mesenchymal cells with high lysosomal score and chemotherapeutic drugs were more effective in adrenergic cells with low lysosomal score. For all the other drugs, there was no in-class effect regarding the correlation between drug sensitivity and lysosomal score. Passive drug sequestration might not be the dominant effect of an increased number of lysosomes in the cell.

5.3 Lysosomal compartment adapts to drug treatment

Due to their relevance in maintaining cellular metabolic homeostasis, lysosomes are very sensitive to cellular stress factors and adapt accordingly[193]. Processes, that induce lysosomal stress, are changes in cellular pH levels, destabilization of the lysosomal membrane and reactive oxygen species[194]. Lysosomes, that are affected by these changes show a lysosomal stress response including adaptive mechanisms like increase in lysosomal pH, increase in lysosome size, repositioning in the cells and increased lysosomal biogenesis[195]. Further increase of the stress factors can lead to lysosomal membrane permeabilization, redox catastrophe and bioenergetic collapse[194]. For cancer cells, it is acknowledged that they have a higher quantity of lysosomes due to the increased metabolic demand. However, changes in lysosomal numbers upon cancer drug treatment are poorly characterized.

In my experiments, I analyzed the changes of the lysosomal compartment as a response to drug treatment and showed in a clustering analysis, that mesenchymal and adrenergic cell lines cluster together based only on the quantified changes of lysosomal numbers. Interestingly, despite the

clustering of the subtypes, there was no drug class that exhibited specific in-class effects or correlated with the mes/adr score in this experiment.

Analysis of lysosomal quantity in response to MAPKi treatment at different timepoints presents a more prominent lysosomal adaptation at the later timepoints such as 24h and 72h. Increase in lysosomal biogenesis and therefore a resulting increase in the lysosomal compartment as an immediate adaptation mechanism is mostly discussed for changed levels of nutrients rather than as a drug response, which results in increased lysosomal mass at a later timepoint[196-199]. In conclusion, the observed lysosomal adaptation is most likely a stress response of the cells.

Looking deeper into differences in lysosomal adaptation for chemotherapeutic drugs and MEKi at later timepoints revealed some more specific differences between the subtypes. In this project, mesenchymal cells showed a very strong increase of lysosome numbers in response to chemotherapy treatment, most likely a response to accumulating DNA damage. Adrenergic cells also exhibited an increase but the extend was much smaller. A high basal number of lysosomes could, in this case, be an indicator of a stronger lysosomal response. For the MAPKi this result was very heterogeneous, as there is no pattern or connection between decrease in nuclei numbers and increase in lysosomes observable. The increase in lysosomes for MAPKi is therefore not only happening in the cases where cell die. Out of the six tested MAPKi, five increased the number of lysosomes in the mesenchymal cell line. The increase in lysosomal levels in the adrenergic cell line for Cobimetinib treatment is very unexpected since none of the other MAPKi caused such a strong response for this cell line.

5.4 Targeting lysosomes in combination with MEKi did not reveal differences between subtypes

In line with the argumentation, that lysosomes contribute to drug resistance, an increase in lysosomal biomass in response to drug treatment would be considered a mechanism of adaptive drug resistance and further increase the resistance to the treated drug. This was observed in previous studies and fostered the idea of combining the drug that induces the lysosomal adaptation with drugs targeting the lysosome[76,79,190,200].

Since this approach provides promising results in these studies, I also tested lysosomal inhibitors in my project. Due to the higher basal lysosomal levels of mesenchymal neuroblastoma cell lines, I expected higher effects of lysosomal inhibitors in these cell lines, especially in combination with MEKi that showed high response in mesenchymal cells.

The first approach I used in this project to target lysosomes as a combination treatment with MEKi, were the repurposed anti-malaria compounds chloroquine and artesunate and the tool compound bafilomycin A1, which inhibits lysosomal vATPase. The results of these combination screens were not overwhelmingly synergistic and also the drugs are not novel translational compounds. Chloroquine as an autophagy inhibitor had great translational potential and was already tested in clinical trials to enhance cancer drug effects, however the results were not as successful as expected[143]. The reason

for this, besides unspecific drug effects of chloroquine, could be the dual role of autophagy in cancer, as its inhibition does not necessarily have a beneficial effect for suppression of tumor growth[201].

5.5 Targeting lysosomal acid sphingomyelinase as alternative strategy to inhibit lysosomes

Another approach to target lysosomes is using other lysomotropic drugs that accumulate in the lysosome and disrupt lysosomal functions. Compounds, that usually are used as antidepressants in psychiatric diseases show lysomotropic behavior and their accumulation in lysosomes lead to inhibition of the enzyme lysosomal acid sphingomyelinase (ASM)[148]. ASM is an enzyme that plays an important role in sphingolipid metabolism by catalyzing the hydrolysis of sphingomyelin into ceramide[202].

Sphingolipids are essential bioactive lipids involved in many critical cellular processes. They serve as structural components of the plasma membrane, maintaining its fluidity and integrity. Sphingolipids gather within lipid rafts on the plasma membrane, playing a pivotal role in regulating signaling pathways that influence growth, apoptosis, senescence, inflammation, and cell migration[203,204]. Dysregulation of sphingolipid metabolism is implicated in diseases such as cancer, neurodegeneration, cardiovascular issues, and immune dysfunction[203,205].

Determining the role of ASM in cancer is complex, because of its dual effects on tumor growth. On the one hand, processing sphingomyelin to ceramide increases accumulation of ceramide, which is a pro apoptotic molecule. Inhibition of ASM could appear counterintuitive because this would prevent ceramide accumulation and protect cancer cells from apoptotic cell death which is an unfavorable outcome in cancer therapy[206]. In fact, there are strategies using recombinant ASM to increase ceramide production to increase apoptosis[207].

Contrary to this approach, there are studies demonstrating that ASM facilitates tumor cell proliferation and tumor evasion and inhibition could have tumor suppressing effects[208]. Inhibiting ASM causes accumulation of sphingomyelin in the lysosomal membrane, increases membrane rigidity and subsequently leads to membrane destabilization[61,209]. This causes leaking of cathepsins into the cytosol which subsequently kills the cells. The detergent capacity of the lysomotropic drugs, that inhibit ASM, could further support this effect[209]. A study, which is applying this theory, identified *SMPD1*, the gene coding for ASM, as a dependence of glioblastoma and showed tumor regression *in vitro* and *in vivo* with fluoxetine treatment[210]. Inhibiting ASM is a suitable alterative to interrupt lysosomal processes and to induce lysosomal cell death.

In this project, treatment with fluoxetine, amitriptyline and nortriptyline were effective in neuroblastoma treatment. Single compound treatments were not specific for one of the neuroblastoma subtypes. Combination of ASMi with MAPKi separated the subtypes regarding their reactivity. The adrenergic cell lines showed synergy for the metabolic readout but a low CSS score and low synergy scores for the spheroid size readout. The drug combinations for these cell lines therefore display cytostatic effects. The reason for synergistic effect of ASM inhibition in the adrenergic cell lines

could be a higher susceptibility due to lower lysosomal quantity. Lysosomal inhibitors could have stronger effects in this case because of the lower number of available targetable organelles. The mesenchymal cell lines showed synergy in spheroid shrinkage, however no synergy in the metabolic readout. This is unexpected since the cell death occurs after decrease of metabolic activity. An important consideration here is that synergy reflects the extend of the interaction between the drugs and as a mathematical model depends on assumptions about the drug interactions. Although the ZIP synergy model currently is favored because it harmonizes the loewe and bliss models, its results still need to be interpreted in context[120]. Since cell death is the preferred outcome in cancer drug treatment, it can be concluded, that the combination of MAPKi and ASMi were most successful in mesenchymal cell lines.

In conclusion, targeting lysosomes by inhibiting lysosomal acidification and targeting lysosomal membrane integrity might be potential strategies for neuroblastoma treatment. Lysosomal inhibition especially with ASMi display synergistic effects. However, due to the various processes lysosomes are involved in, it is hard to predict the effect of lysosomal inhibition. This can be seen in the dual role autophagy has in cancer and in the mixed results chloroquine showed in clinical cancer trials. This duality is also observed for ASM inhibition since both, inhibition of ASM and treatment with recombinant ASM, are successful strategies to target tumor cells in cell culture experiments. More research is done to identify additional strategies to target lysosomes, including inhibiting lysosomal cathepsins and targeting calcium signaling[79].

5.6 Targeting senescent signaling with sequential senolytic treatment

In this project, I could demonstrate some characteristics of senescent cells for mesenchymal neuroblastoma cell lines, including high number of lysosomes and a flattened cell phenotype. Analysis of gene expression data showed upregulation of SASP pathways for mesenchymal neuroblastoma cell lines. Conversely, these cells lack the main characteristic of senescent cells because they still divide. Cellular senescence is characterized by a permanent cell cycle arrest, where cells stop proliferating but remain metabolically active[82].

Proinflammatory SASP is also an important hallmark of senescence and reinforces senescence in an autocrine manner and also affects surrounding cells and tissues. This has an important function in tissue repair, where the immune cells get recruited to remove senescent fibroblasts[211]. Senescence and SASP, like many other complex biological processes, can be beneficial for tumor growth or inhibit it. For example, in early cancer stages SASP adds immune surveillance and in later stages suppresses anti-tumor immune reaction[212,213]. Although gene expression data strongly matches the measured proteins of the secretome[214], antibody arrays of mesenchymal neuroblastoma would be necessary to analyze the secretome and to determine the extent of SASP secretion.

Senescence is a gradual process rather than a one-step event[215,216]. Cells in that process can be influenced by various stimuli to further undergo senescent transition or exit and reenter the cell cycle[212,217,218]. The senescent transition can be accelerated by cellular stresses such as DNA damage resulting in therapy induced senescence[85]. Following this line of arguments, mesenchymal cells could

be in a pre-senescent state and therefore more susceptible for senescence inducing stimuli. The senescence induction experiments in my project support this hypothesis, as mesenchymal cells show higher senescence induction than the adrenergic cells.

In my project, senescence was induced in mesenchymal cells with MEKi and ERKi treatment. Inhibition of the MAPK pathway is not known to directly induce senescence, it rather mediates pro inflammatory reprogramming in cells that already are in senescent transitions[219]. This is also an argument for a pre-senescent state in mesenchymal cells.

A rather new discovery is the association of senescence with stemness, where it was shown that stem cell signature is enriched in senescence cells of multiple induced senescence models[218]. This gives them tumor initiation potential that could enhance tumor aggressiveness upon reactivation of proliferation and especially play a role in relapses[220]. This theory would be interesting to test in neuroblastoma since the neuroblastoma tumor cells resemble the differentiation stages of neuroblast differentiation trajectory with the most undifferentiated ones bearing the worst prognosis[32].

Since MEKi and chemotherapy treatment are inducing senescence, the strategy of the sequential senolytic screen in this project was to induce senescent signaling with these drugs and then apply senolytic therapy. Senolytic drugs mainly target pro-survival anti-apoptotic pathways that are upregulated in senescence[88].

Regarding the results of the synergy screen, the combination of chemotherapy and senolytics showed higher synergy scores in mesenchymal than in adrenergic cells. Notably, the combination of MEKi and senolytics had higher synergy scores for adrenergic cells. However, the scores have quite a wide spread in sensitivity and synergy scores so the effect of the combination therapy is very dependent of the exact drug combination and the cell line. Other factors like molecular alteration and off-target effects can be responsible for this spread.

An alternative strategy to target senescent cells are senomorphic drugs. These drugs inhibit the signaling pathways that regulate SASP. Since SASP mediates a majority of tumor-promoting, pathologic roles of senescent cells, targeting SASP is a promising strategy to target tissue inflammation and tumor progression[221]. Targeting SASP is a challenge itself, because SASP is a complex mixture of secreted cytokines, proteases, vesicles and growth factors and its composition varies between tumor and tissue types[222]. Efforts are made to target upstream signaling to inhibit SASP at the translational level by interfering with the NF-κB pathway[88]. This could be a promising strategy to target this pre-senescent state of mesenchymal neuroblastoma cells where SASP is upregulated.

5.7 Confirming the connection between SASP upregulation and MEKi sensitivity in mesenchymal neuroblastoma with patient derived tumor samples

Established neuroblastoma cell lines are valuable model systems, however these cell lines may not accurately represent the physiology and behavior of patient tumors due to genetic and epigenetic changes and lack of heterogeneity. Therefore, I compared the results from the cell line experiments

with data of the INFORM registry, a pediatric precision medicine program that biologically characterizes tumor samples of relapsed diseases[223]. Comparing ssGSEA and drug screening data from *ex vivo* drug sensitivity profiling of fresh tissue cultures, it could be confirmed, that samples with mesenchymal characteristics have upregulated SASP signaling as well as heightened MEKi sensitivity. Unfortunately, of the 223 samples with available gene expression data, only five samples could have been submitted to the drug screening pipeline. More samples would be necessary to confirm this trend. For future experiments it would be interesting to asses if the senolytic combinations are also successful in fresh tissue samples or long-term cultures established from these samples.

5.8 Subtypes in mixed Neuroblastoma cell line confirm previous findings

The cell line SK-N-SH is an isogenic cell line that contains both subtypes and can be kept in cell culture maintaining both subtypes throughout passages[37,224]. The cells already show a morphological difference in culture with some cells being flatter and more spread and others with a smaller, more elongated shape, that grow in clusters in the cell culture flask. In order to distinguish between the subtypes in culture, the mesenchymal marker YAP1 was stained and cells were classified into staining positive and negative, representing mesenchymal and adrenergic cells. In exposure to chemotherapeutic drugs, the mesenchymal cells enrich. This suggests differences in drug sensitivity. Cells of the adrenergic subtype die and mesenchymal cells, which are more resistant to chemotherapy treatment survive. This argument is supported by the measured differences in DSSasym. With MEKi treatment, selective cell death of mesenchymal cells was expected, however this could not be observed in this experiment.

Another explanation for the enrichment of mesenchymal cells with chemotherapy treatment could be the plasticity of the subtypes and their ability to transdifferentiate into one another[39,225]. This transition can already happen in 48h however in the study of Thirant et al. it was stimulated with EGF and TFNalpha[39]. This group also observed spontaneous transitions, however, over weeks of observation. To uncover, if drug treatment could induce this transition remains to be studied.

Looking into the number of lysosomes, the mesenchymal cells continuously showed a higher number of lysosomes for all drug treatments and drug concentrations. For some drugs, a slight increase in lysosomal numbers can be observed. Regarding the gene expression data, the mesenchymal and intermediate population of the cell line displayed upregulation of the SASP gene list compared to the adrenergic group. This is in line with my previous findings where I revealed upregulation of SASP associated pathways in mesenchymal cells. This demonstrates that both subtypes can exist next to each other showing their specific characteristics. This is also the case in tumors where cells with characteristics of each subtype can be found[164].

6 Conclusions and future perspectives

In this project I analyzed drug sensitivities, morphology and gene expression of 24 neuroblastoma cell lines representing the range of epigenetically regulated subtypes. I showed, that neuroblastoma subtypes have differences in drug sensitivity, specifically mesenchymal neuroblastomas are more sensitive towards MEKi. Additionally, I demonstrated, that MAPK pathway activity is higher in mesenchymal neuroblastomas than the adrenergic subtype.

High content image-based analysis of cell morphology revealed a larger and more rounded phenotype and a higher lysosomal content for mesenchymal cells. I established a lysosomal score based on the imaging data that correlates with the gene expression based mes/adr score. Drug screens with lysosomal changes as readout further highlighted the different reactions to drug treatment. In combination screens with MEKi and drugs targeting the lysosomes, I could also see the differences between the subtypes and slightly synergistic effects when combining MEKi with ASMi.

Examining gene expression data, I revealed an upregulation of SASP signaling associated genes in mesenchymal neuroblastomas compared to the adrenergic ones and hypothesized these mesenchymal cells might be in a pre-senescent state, in which senescence could be induced easier than in adrenergic cells. A combination drug screen of senescence inducing drugs and senolytics revealed, that this combination strategy is effective in both subtypes and it is the most promising combination strategy of this project regarding the synergy scores. I could confirm the upregulation of SASP genes and MEKi sensitivity in a panel of patient samples obtained from the INFORM registry, demonstrating the translational relevance of this project.

Current developments in image-based classification of tumors rely more and more on morphological features of label free images such as shape and texture rather than specific markers. Rising use of AI and deep learning applications in biomedical research are paving the way for drug screens in this direction. Image based drug screens depend on morphological features as readout rather than classical endpoint readouts like metabolic activity or caspase assays. Cellular changes in morphology happen at earlier timepoints of drug treatment and give information about cellular states that are associated with morphological changes such as senescence or differentiation.

Repurposing lysomotropic drugs from other diseases for cancer treatment looks promising for other entities, so this might also have a future in neuroblastoma treatment. As research is advancing, other mechanisms of action for well-established drugs are identified, as discussed above for the anti-depressant drugs used in this project. The single drug effects of these compounds might be lower than the effect of the standard of care treatment but they could potentially have enhancing effects in tumor reduction while having low toxicity.

Senolytic drugs have growing applications in cancer treatment, and show great potential. Targeting senescent signaling especially SASP could not only kill the senescent cancer cells but also reduce the impact of the inflammatory environment created by the SASP on the neighboring tissue and prevent tumor progression and metastatic growth. Future advances in drug development targeting SASP might also be beneficial for targeting the mesenchymal neuroblastoma subtypes especially in the relapsed tumors.

7 Acknowledgements

I am so incredibly grateful to all of the people who I met and who supported me during the last years and contributed to this story. Thank you a lot:

Apl.-Prof Dr. Ina Oehme, for being my supervisor in this project. Ina, thank you for selecting me in the Spring 2020 the corona year selection and for trusting me with this project. You gave me the opportunity to learn, to develop this project and to find my path and place in your group.

Prof. Dr. Olaf Witt, for the opportunity to work in this highly cooperative department, the chance to participate in inspiring collaborations, to experience pediatric cancer research outside of my own project.

Prof. Dr. Peter Angel, for providing valuable scientific expertise during the last years as my TAC member and for being the first examiner of this project.

Assoc. Prof. Anne Brady for her expertise in lysosomes and mitochondria as a TAC member, which always resulted in fruitful discussions.

Prof. Dr. Stefan Wölfl and Dr. Ana Banito for agreeing to participate in my defense committee.

Prof. Dr. Frank Westermann for all collaborations and support with expertise in the neuroblastoma field, data and materials.

Thank you also to Dr. Johannes Ridinger for trusting the pharmacist with a biology project that in the end turned out to be more pharmaceutical than anticipated.

My scientific friends and mentors, Dr. Julia Zaman and Dr. Heike Peterziel who are true role models for me that helped me grow as a person and as a scientist. Thank you for discussing all aspects of my project with me countless times, for your guidance and encouragement. Thank you, Heike, for our microscope business trips where we dreamed about the endless possibilities and cool projects we could do, for your support in hard times and the occasional personal crisis meeting. Julia, thank you for reminding me about the fun of science and for our collaboration projects, entertaining lunches and also your support outside of the lab and everything that goes beyond the DKFZ.

This journey was by far not easy and the rollercoaster that is the PhD life sure also happened to me. Special thanks to all the people who were in there with me:

My wonderful colleagues for all the support and scientific discussions, fun and educational retreats and conferences. Thank you for cheering for me in and outside of the lab. Thank you to all the B310 members, current and former: Till M, Anna K, Ginny, Romain, Jonas, Flo, Nora, Isabel, Pauline, Leo, Simon, Elisabeth, Till S, Michael, Rabia, Sara, Eugene and Sonja B. So many thanks to the special force, for your skills and experience Aileen, Marko, Anette, Ina and especially Alex for your tremendous

support and for fixing all my lab related problems. I am very grateful for Anna, Kyriaki, Marta, Simay, Olga and Lisa as my fellow and former PhD colleagues, this is an AGICC appreciation moment.

Special thanks to Charlotte for real talk glass box moments, Daniela for your organizational skills and for reminding me always about the things I missed. Natja thank you for teaching me communication skills, explaining me how to prepare good coffee and sharing life's wisdom. Lisa thank you for your kind personality and patience, Simay for being from start to end with me in this journey, for finding our paths and growing up together in this group. Anna and Kyriaki for metal support in microscope crash moments and general PhD downs. Thank you also to my lunch friends Julia, Lars, David, Caro und Amelie. Words can hardly describe how grateful I am for Coco and Marta, my dear and lovely elevator girls. I could not have been luckier working every day next to you two. Thank you, for always sharing all thoughts and worries with me, for listening, for laughing, for crying, for the occasional office get together and especially for sticking with me at my lowest, for picking me up and encouraging me to change. Thank you so much.

This massive outburst in appreciation and gratitude would never be complete without you, my friends outside of the lab, my Heidelberg family, you truly changed my life for the better. I can't thank you enough for your continuous support and your friendship. Thank you, Cristina, Sandra, Marta, Johannes, Maria, Paula, Chase, David, Dani and Enrique. Thank you, Ferdinand, for everything we shared and experienced together. I would not be the person that I am today without you.

And I want to say thank you to the people who are in my life since before my PhD journey started, who grew up and navigated life with me and stayed close to me no matter the distance between us, Tim, Katze, Nicole, Melina and Sabine, you mean a lot to me.

Thank you to my family Wiebke, Fabi and Laszlo. I love you.

9 Supplementary figures

Supplemental figure 1: Cohort plots of drug screen. Dot plots of DSS scores for each drug of the library. Colors indicate tumor entity.

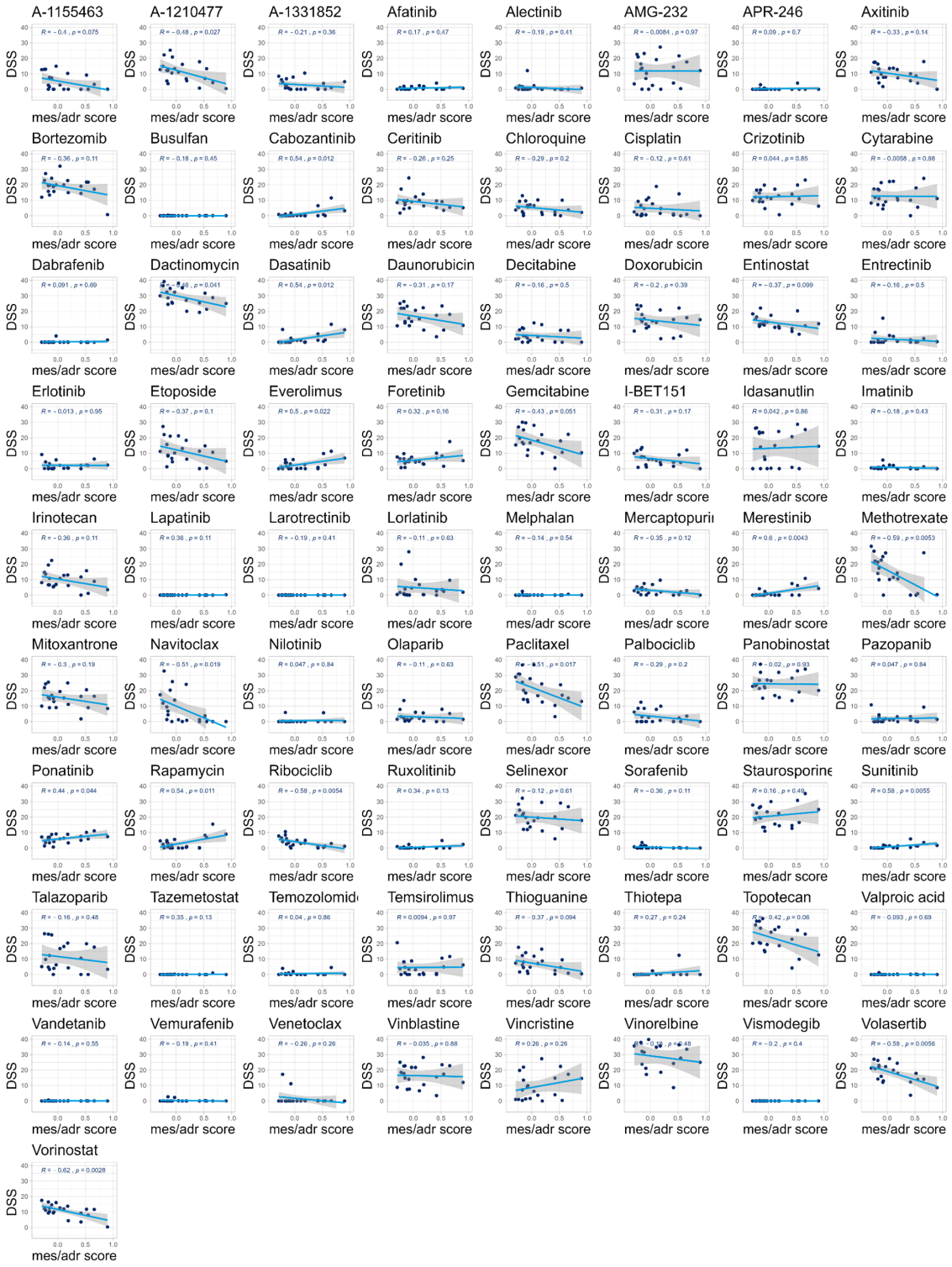

Supplemental figure 2: Correlation DSS and mes/adr score. Correlation plots of mes/adr score and DSS score for 73 drugs of the library for n = 24 neuroblastoma cell lines.

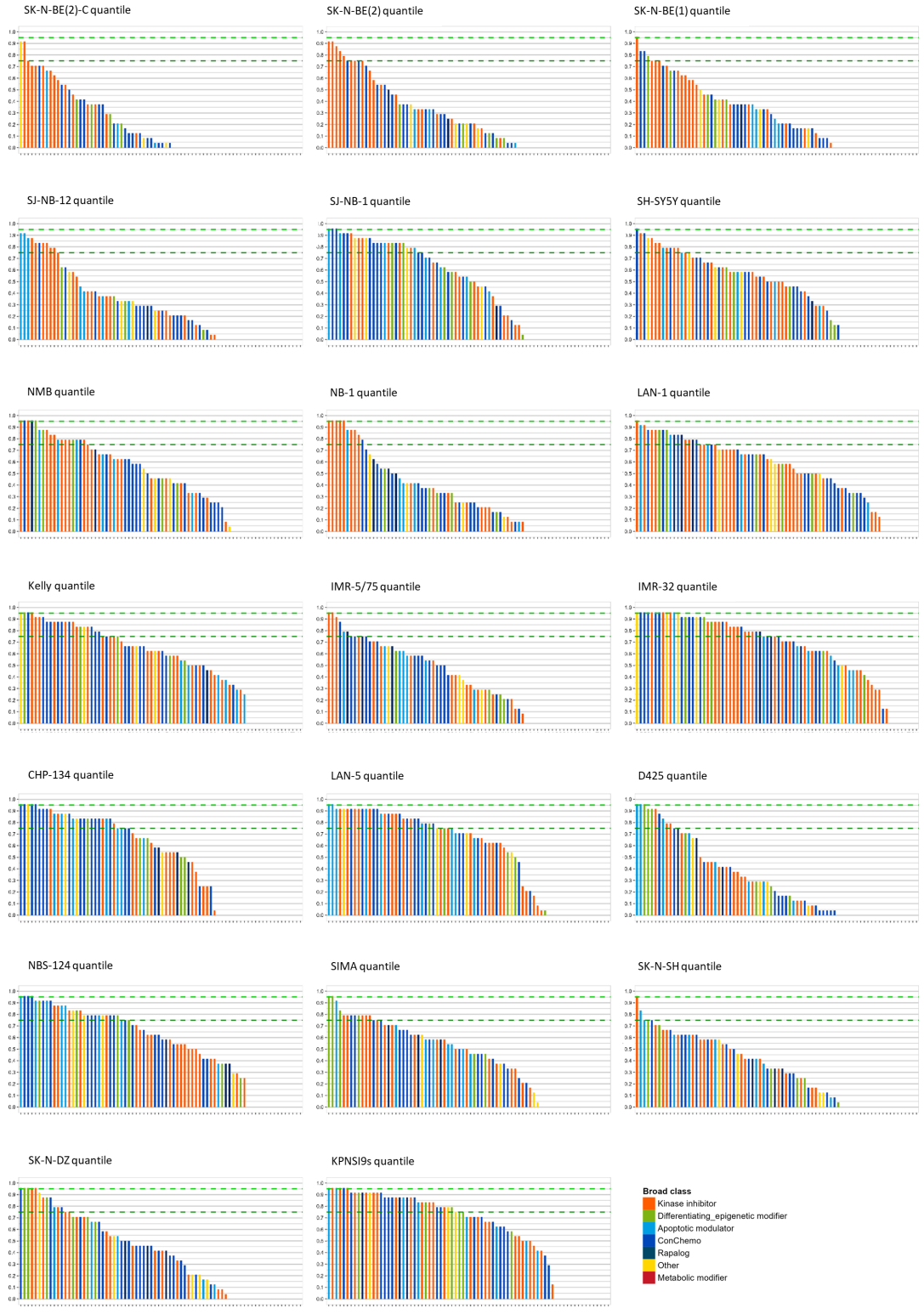

Supplemental figure 3: Cohort comparison of quantile scores. Waterfall plots of neuroblastoma cell lines with drugs ranked based on their quantile score. The quantile score of each drug represents the drug response of the cell line to that drug compared to the drug reaction of all the 24 neuroblastoma cell lines in the cohort and allows a comparison of the drugs in one cell line.

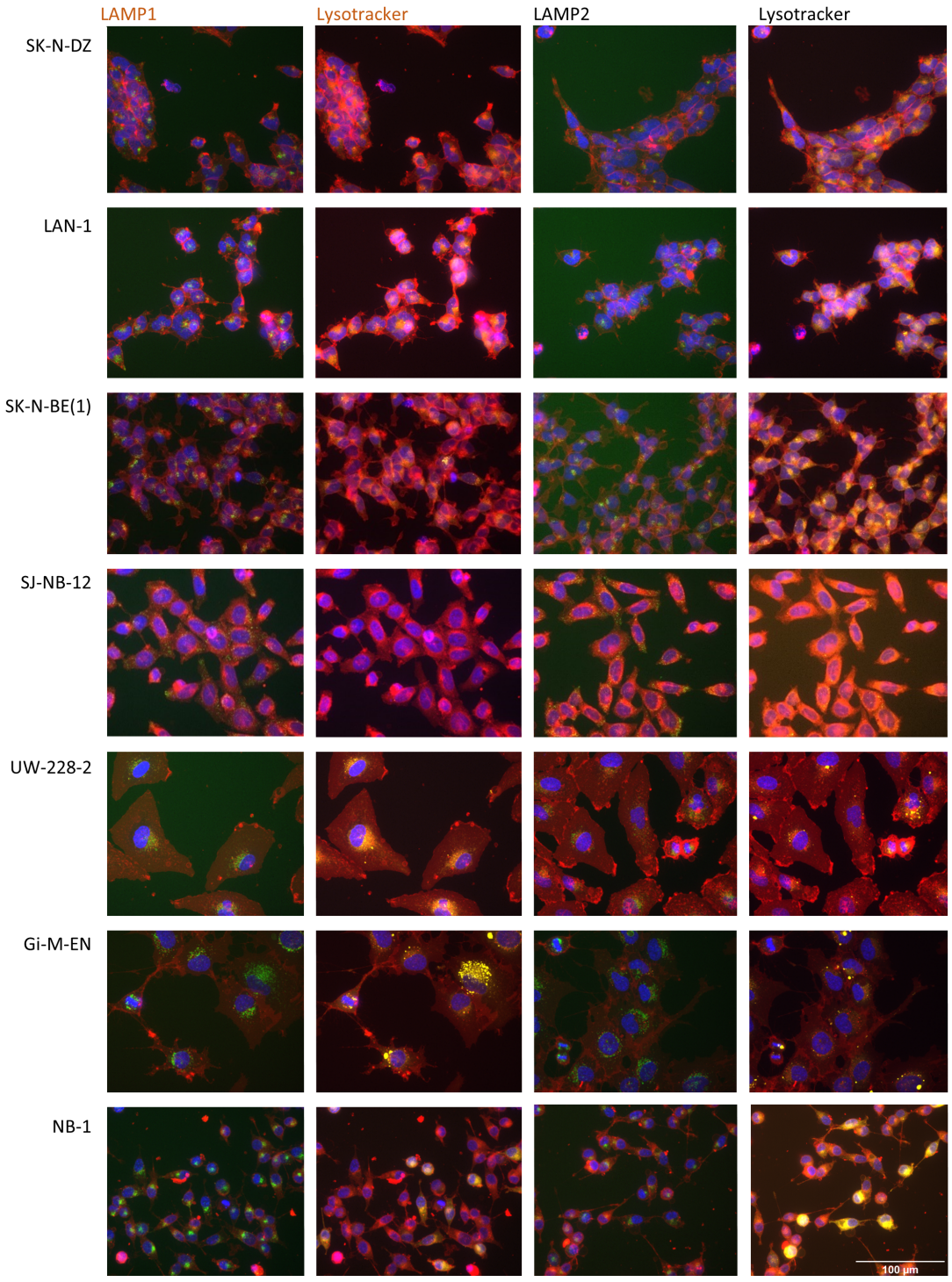

Supplemental figure 4: Staining of lysosomes in pediatric cancer cell lines. Immunofluorescence staining for LAMP1 and LAMP2 (green), complimentary stain of lysotracker (yellow) in composite with cell membrane stain (red) and nuclei (blue).

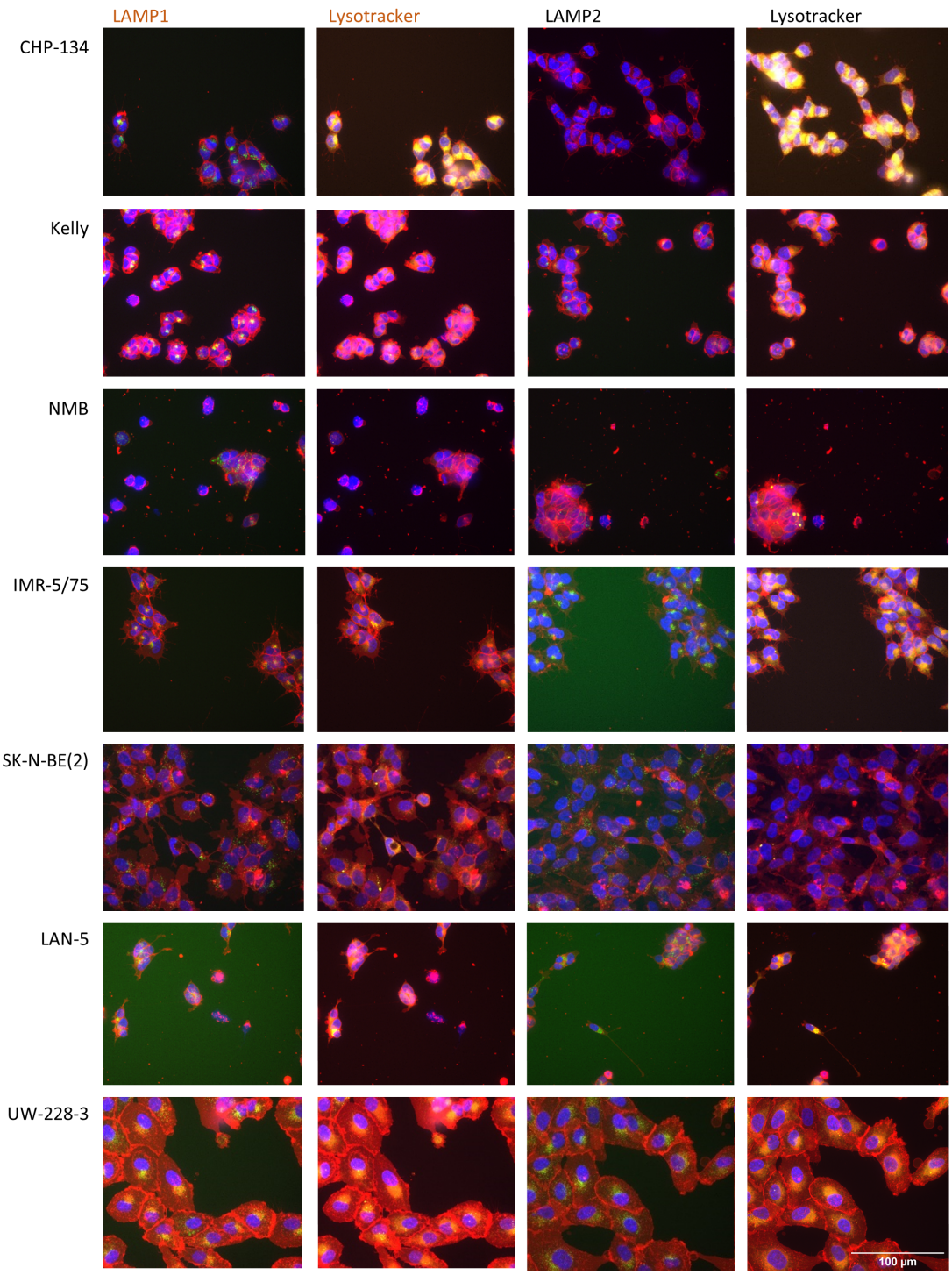
LAMP1
Lysotracker
LAMP2
Lysotracker
CHP-134
Kelly
NMB
IMR-5/75
SK-N-BE(2)
LAN-5
UW-228-3
100 µm

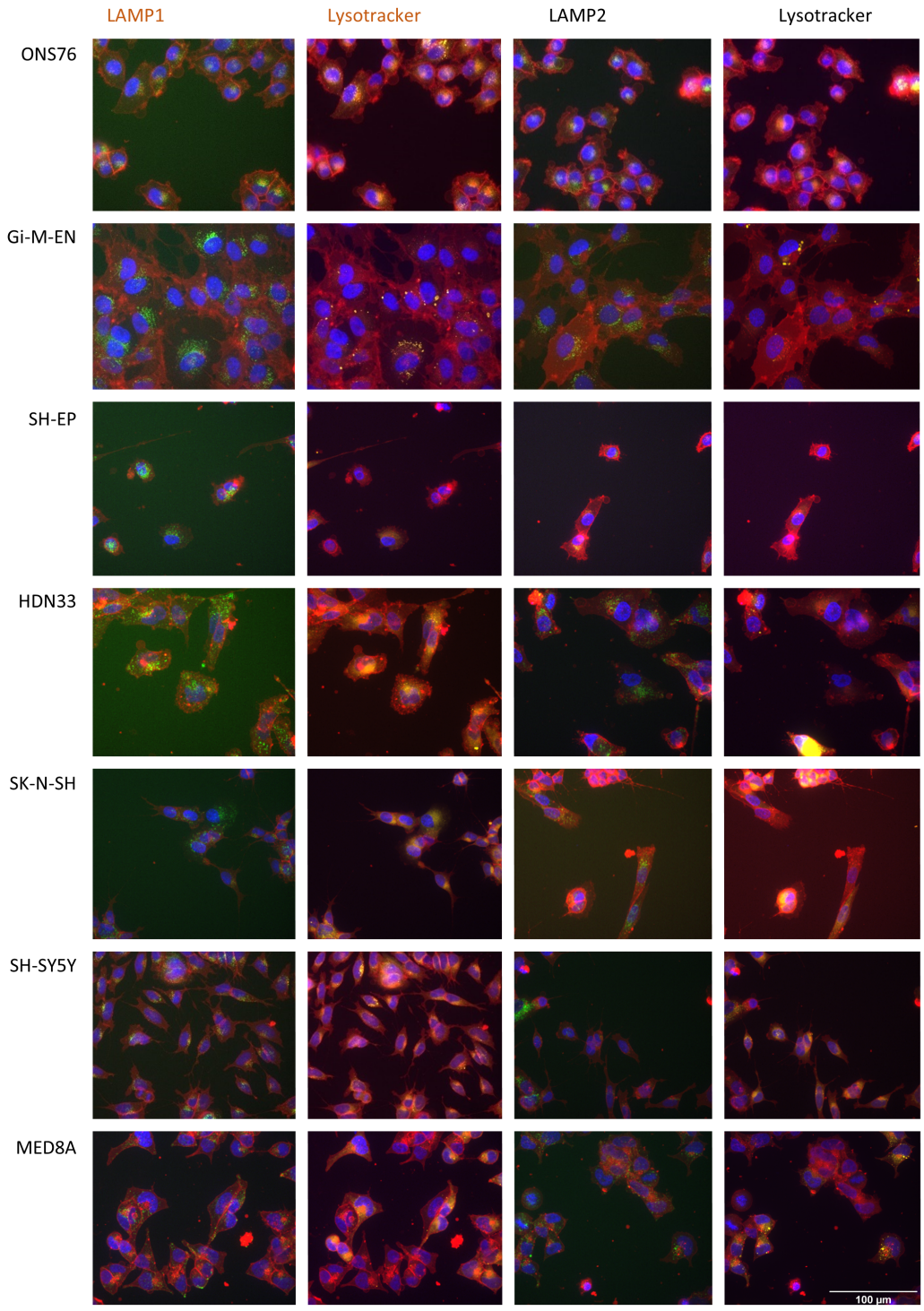
LAMP1
Lysotracker
LAMP2
Lysotracker
ONS76
Gi-M-EN
SH-EP
HDN33
SK-N-SH
SH-SY5Y
MED8A
100 µm

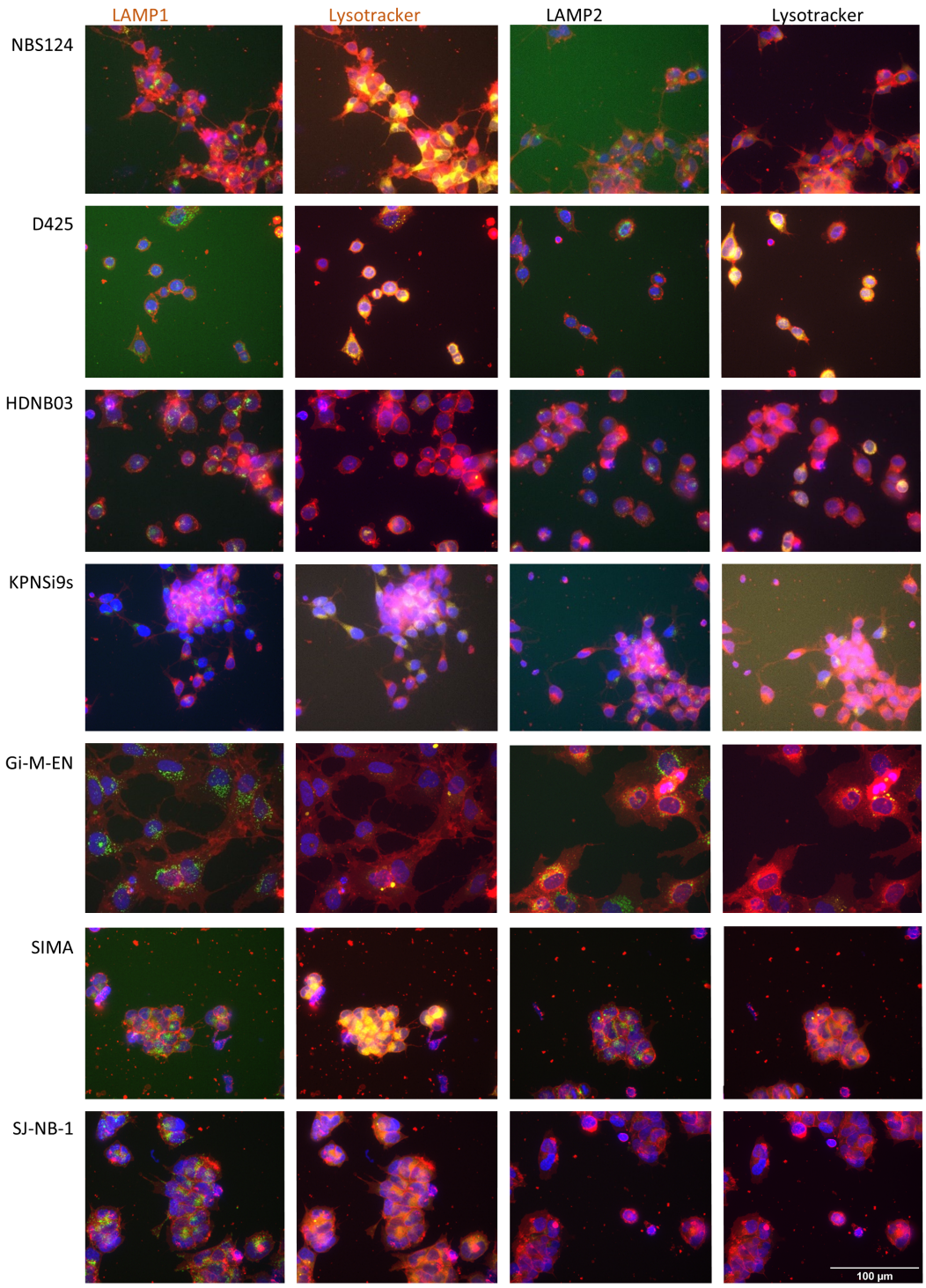
LAMP1
Lysotracker
LAMP2
Lysotracker
NBS124
D425
HDNB03
KPNSi9s
Gi-M-EN
SIMA
SJ-NB-1
100 µm

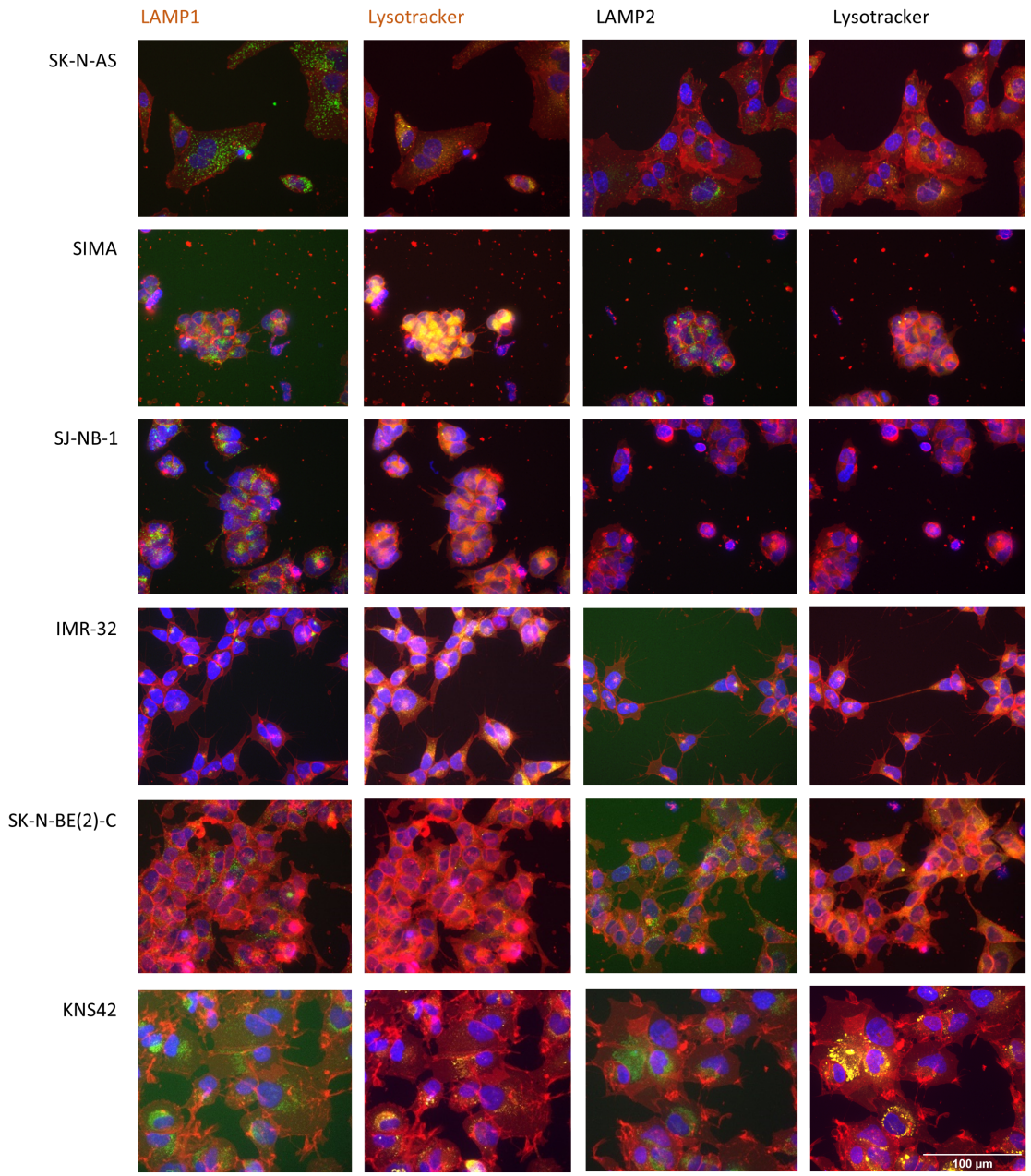
LAMP1
Lysotracker
LAMP2
Lysotracker
SK-N-AS
SIMA
SJ-NB-1
IMR-32
SK-N-BE(2)-C
KNS42
100 µm

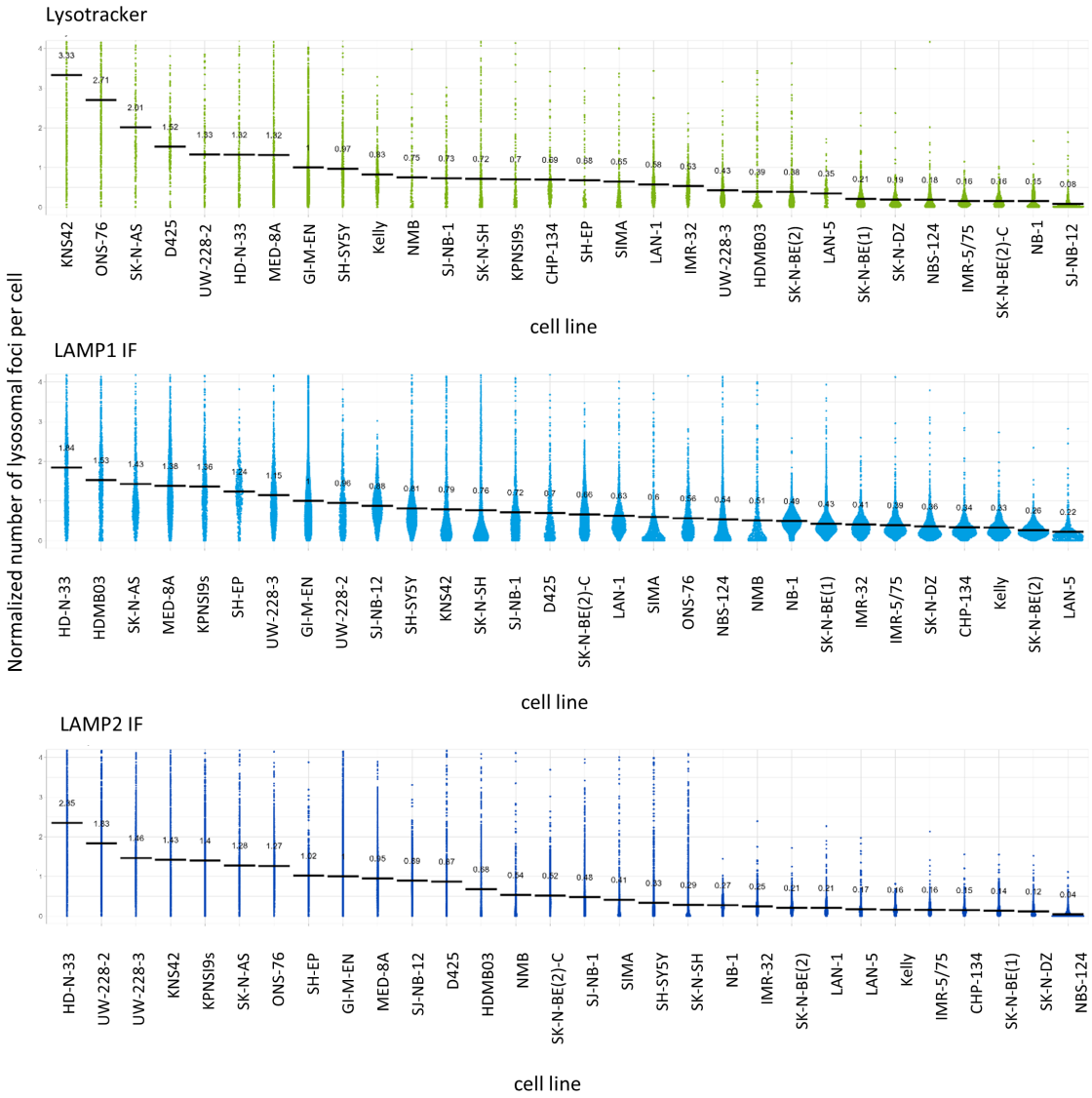

Supplemental figure 5: Calculation of basal lysosomal score. Dot plots of number of lysosomes per cell of three lysosomal measurements normalized to the cell line Gi-M-EN. Each dot represents lysosomal number of one cell. Mean values were calculates for each cell line.

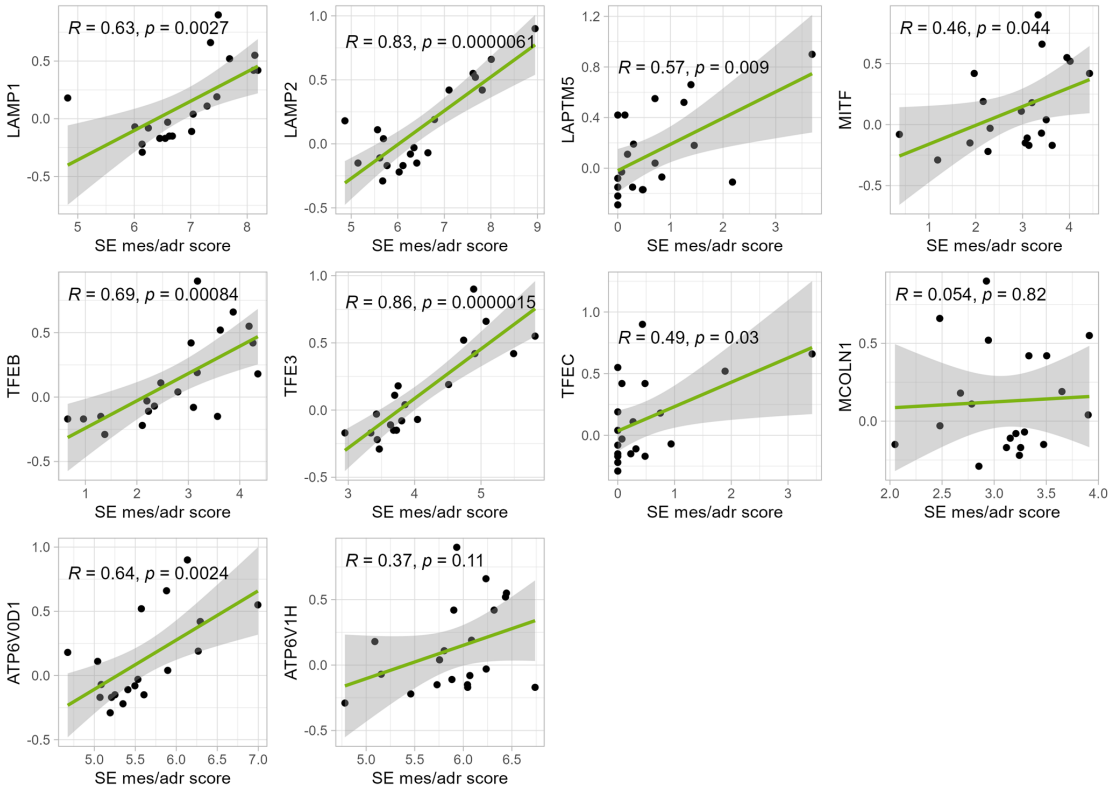

Supplemental figure 6: Correlation of lysosomal genes and mes/adr score. Pearson's correlation of mes/adr score and gene expression of selected genes involved in lysosomal function, regulation and biogenesis.

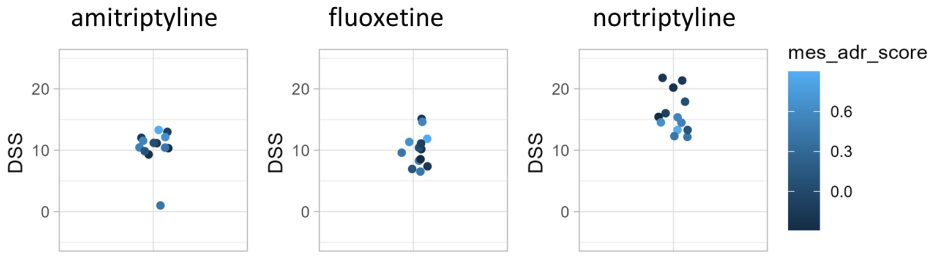

Supplemental figure 7: DSS scores for ASM inhibitors. Dot plot of DSS scores for 13 neuroblastoma cell lines, cell lines were treated for 72h.

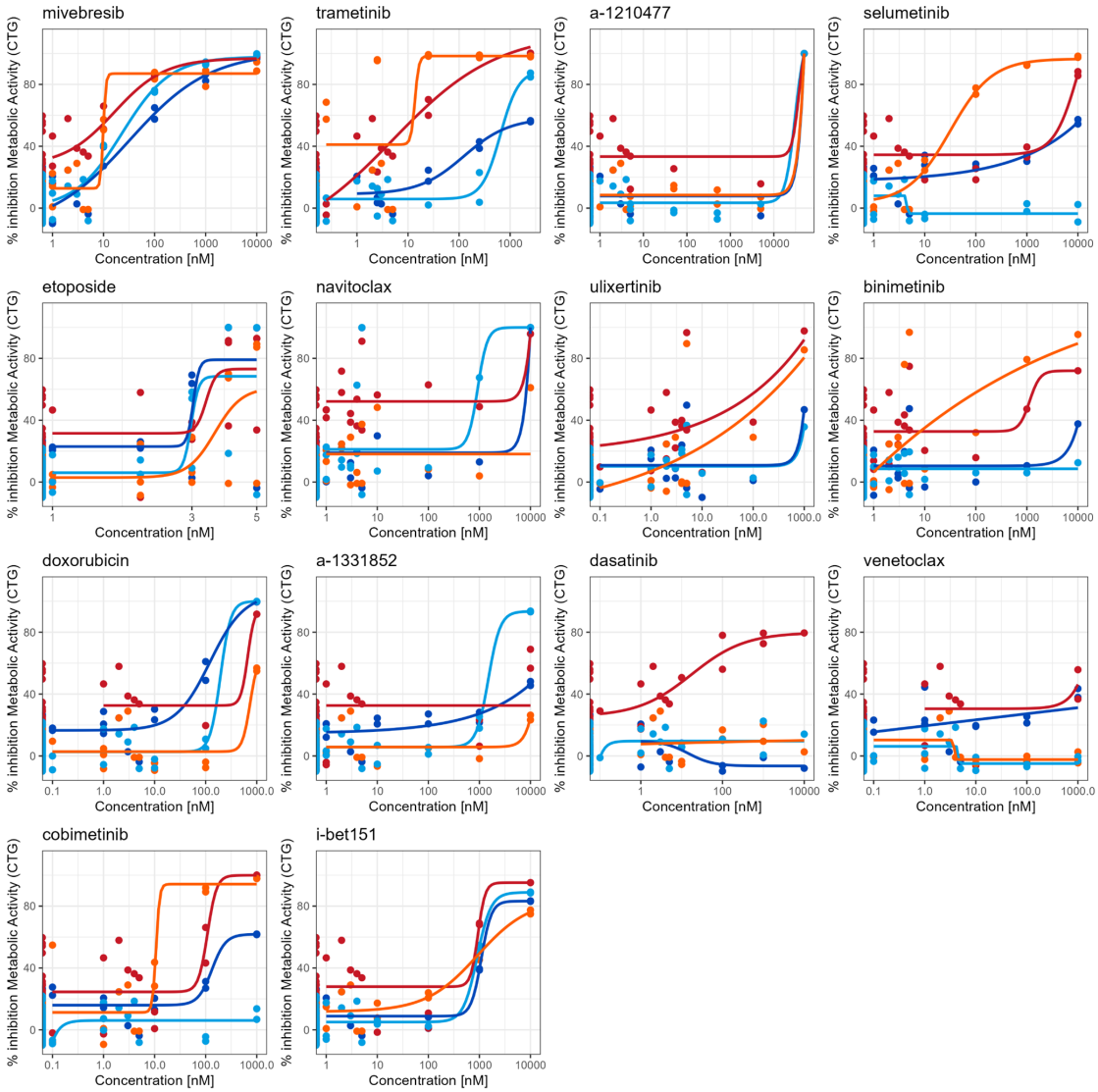

Supplemental figure 8: Single drug curves senolytic screen metabolic readout. Dose response curves of single drug treatment of 2 mesenchymal (SH-EP, SKNAS) and 2 adrenergic (CHP134, IMR5/75) cell lines treated for 72h. Percent inhibition calculated from metabolic activity measurement with DMSO treated cells as negative and benzethonium chloride treated cells as positive control.

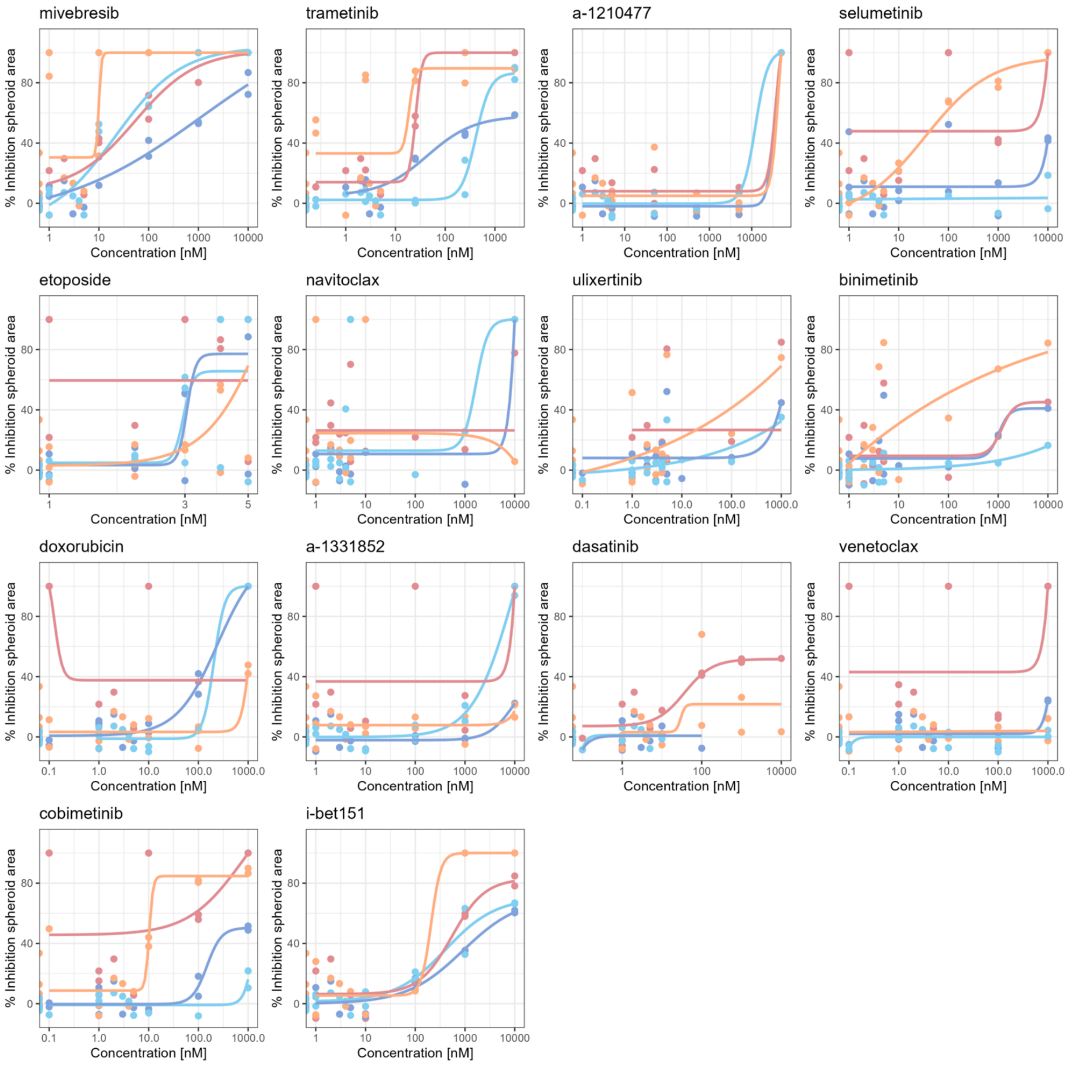

Supplemental figure 9: Single drug curves senolytic screen spheroid area readout. Dose response curves of single drug treatment of 3 mesenchymal (SH-EP, HDN33, SKNAS) and 4 adrenergic (NMB, CHP134, IMR5/75) cell lines treated for 72h. Percent inhibition calculated from metabolic activity measurement with DMSO treated cells as negative and benzethonium chloride treated cells as positive control. Percent inhibition for TMRE area measurement was calculated with the same controls. If no spheroid was detected, the spheroid area was considered 0.

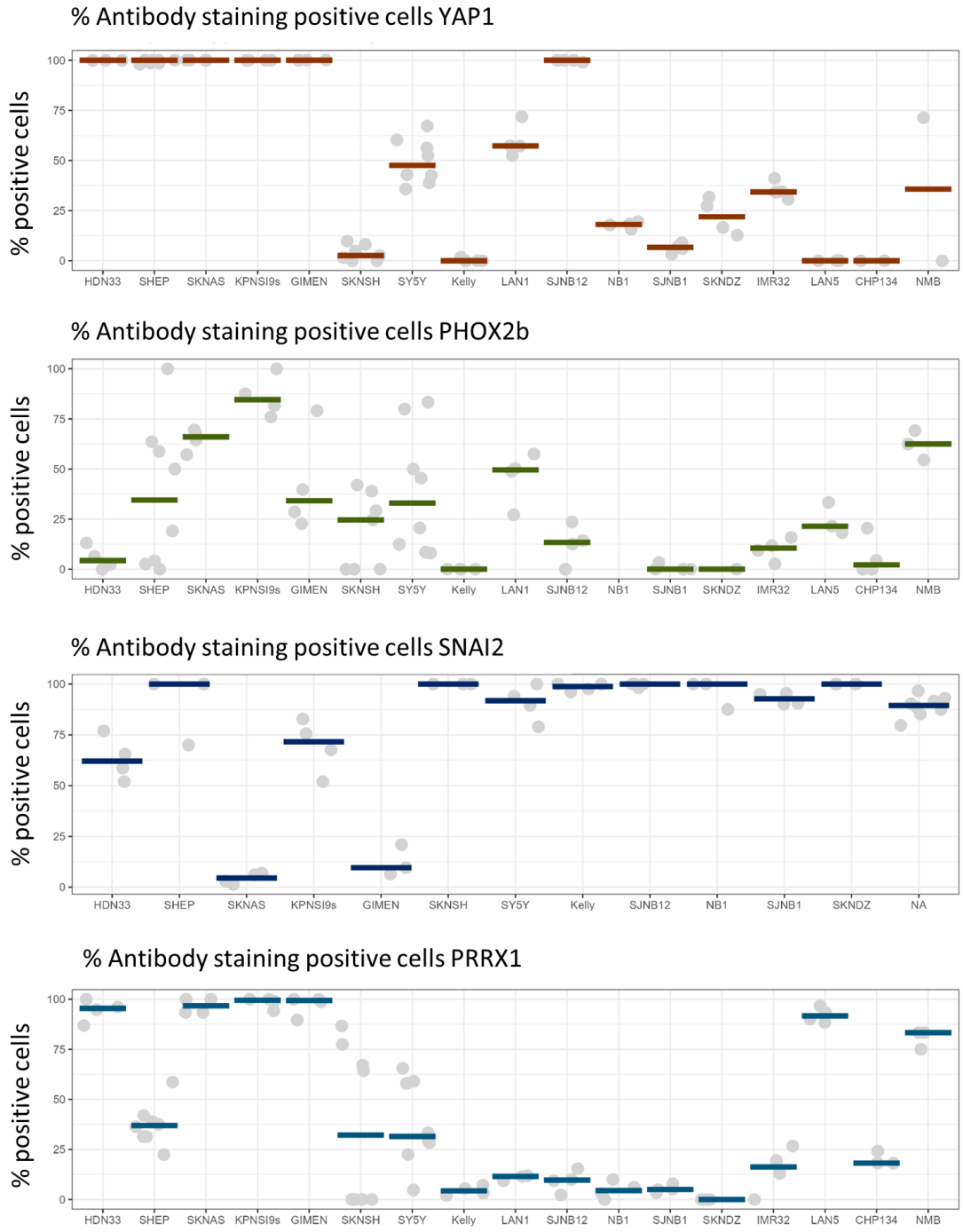

Supplemental figure 10: Classification of Immunofluorescence staining of mesenchymal and adrenergic markers. Result of the classification of immunofluorescence staining of mesenchymal and adrenergic markers percentage of positively classified cells for 8 images per cell line.

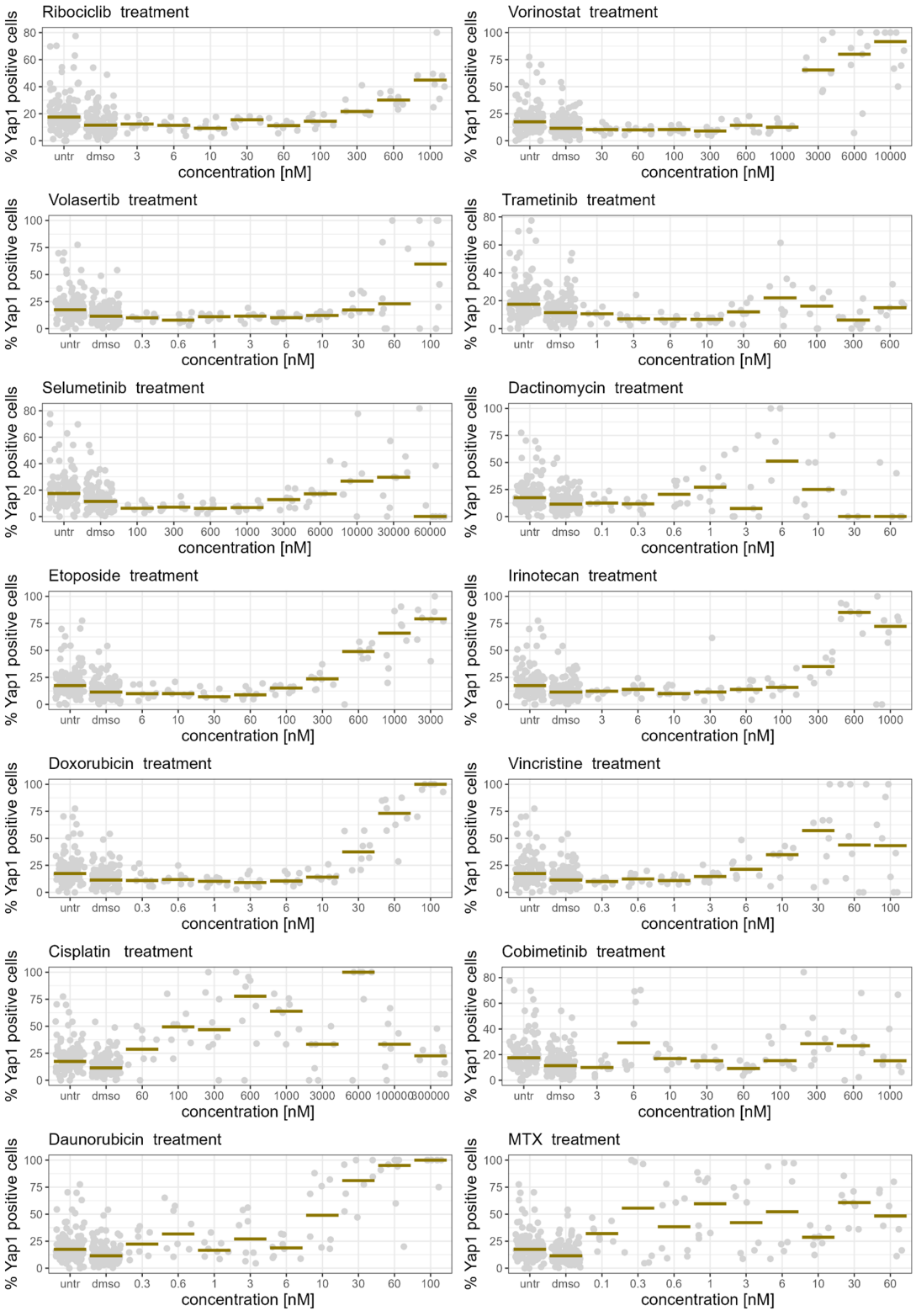

Supplemental figure 11 Classification of YAP1 positive cells in response to drug treatment.

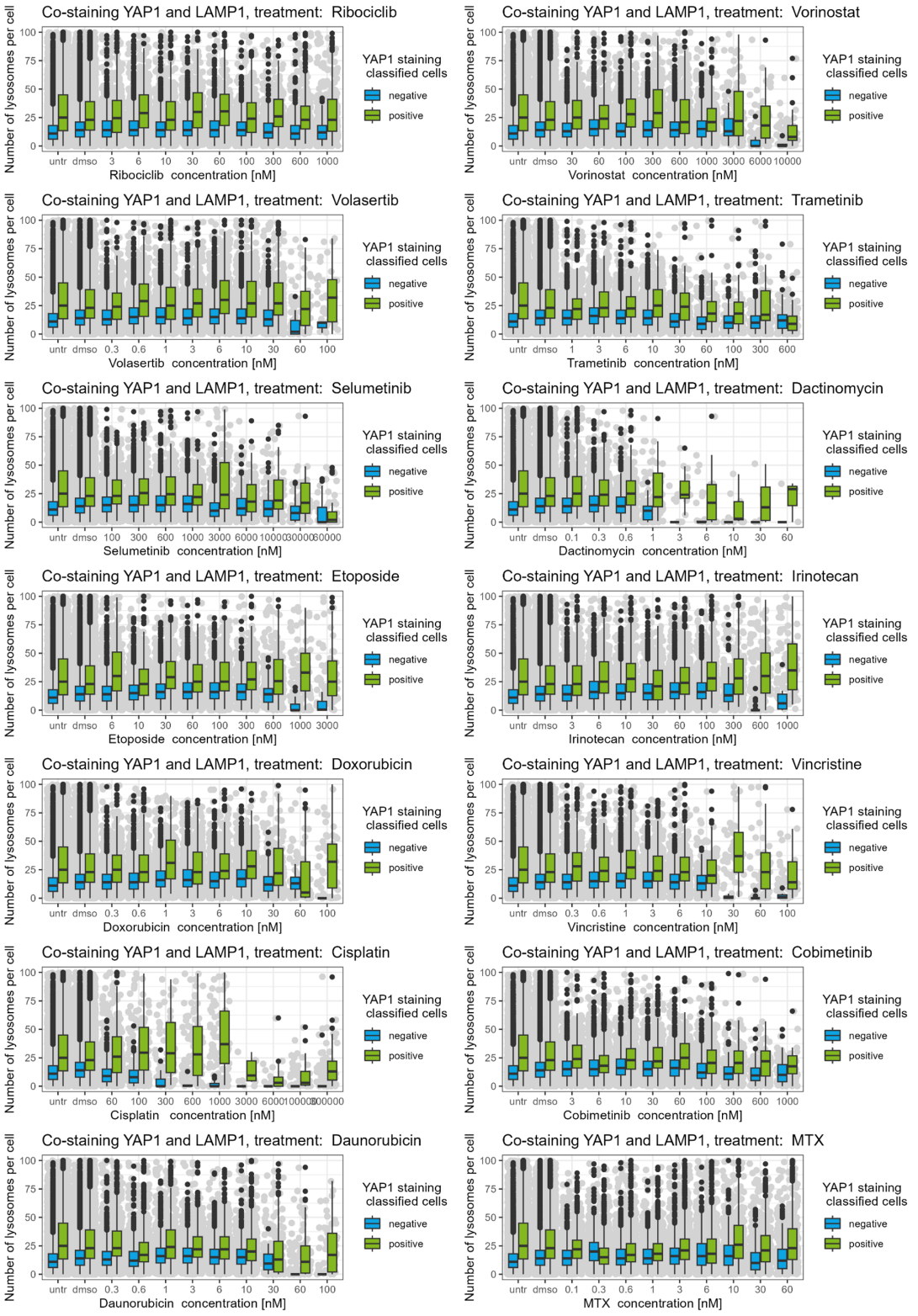

Supplemental figure 12: Changes in lysosomal numbers in YAP1 classified cells in response to drug treatment.

10 References

1. Qiu, B. & Matthay, K.K. Advancing therapy for neuroblastoma. *Nat Rev Clin Oncol* **19**, 515-533 (2022).

2. Maris, J.M. Recent advances in neuroblastoma. *N Engl J Med* **362**, 2202-11 (2010).

3. Screening, P.D.Q. & Prevention Editorial, B. Neuroblastoma Screening (PDQ®): Health Professional Version. in *PDQ Cancer Information Summaries* (National Cancer Institute (US), Bethesda (MD), 2002).

4. DuBois, S.G. et al. Metastatic sites in stage IV and IVS neuroblastoma correlate with age, tumor biology, and survival. *J Pediatr Hematol Oncol* **21**, 181-9 (1999).

5. Shimada, H. et al. Histopathologic prognostic factors in neuroblastic tumors: definition of subtypes of ganglioneuroblastoma and an age-linked classification of neuroblastomas. *J Natl Cancer Inst* **73**, 405-16 (1984).

6. Ambros, P.F. et al. International consensus for neuroblastoma molecular diagnostics: report from the International Neuroblastoma Risk Group (INRG) Biology Committee. *Br J Cancer* **100**, 1471-82 (2009).

7. Brodeur, G.M. et al. Revisions of the international criteria for neuroblastoma diagnosis, staging, and response to treatment. *J Clin Oncol* **11**, 1466-77 (1993).

8. Monclair, T. et al. The International Neuroblastoma Risk Group (INRG) staging system: an INRG Task Force report. *J Clin Oncol* **27**, 298-303 (2009).

9. Cohn, S.L. et al. The International Neuroblastoma Risk Group (INRG) classification system: an INRG Task Force report. *J Clin Oncol* **27**, 289-97 (2009).

10. Irwin, M.S. et al. Revised Neuroblastoma Risk Classification System: A Report From the Children's Oncology Group. *J Clin Oncol* **39**, 3229-3241 (2021).

11. Mossé, Y.P. et al. Identification of ALK as a major familial neuroblastoma predisposition gene. *Nature* **455**, 930-5 (2008).

12. Trochet, D. et al. Germline mutations of the paired-like homeobox 2B (PHOX2B) gene in neuroblastoma. *Am J Hum Genet* **74**, 761-4 (2004).

13. Janoueix-Lerosey, I. et al. Overall genomic pattern is a predictor of outcome in neuroblastoma. *J Clin Oncol* **27**, 1026-33 (2009).

14. Depuydt, P. et al. Genomic Amplifications and Distal 6q Loss: Novel Markers for Poor Survival in High-risk Neuroblastoma Patients. *J Natl Cancer Inst* **110**, 1084-1093 (2018).

15. Bartolucci, D. et al. MYCN Impact on High-Risk Neuroblastoma: From Diagnosis and Prognosis to Targeted Treatment. *Cancers (Basel)* **14**(2022).

16. Huang, M. & Weiss, W.A. Neuroblastoma and MYCN. *Cold Spring Harb Perspect Med* **3**, a014415 (2013).

17. Brodeur, G.M., Seeger, R.C., Schwab, M., Varmus, H.E. & Bishop, J.M. Amplification of N-myc in untreated human neuroblastomas correlates with advanced disease stage. *Science* **224**, 1121-4 (1984).

18. Seeger, R.C. et al. Association of multiple copies of the N-myc oncogene with rapid progression of neuroblastomas. *N Engl J Med* **313**, 1111-6 (1985).

19. Bellini, A. et al. Frequency and Prognostic Impact of ALK Amplifications and Mutations in the European Neuroblastoma Study Group (SIOPEN) High-Risk Neuroblastoma Trial (HR-NBL1). *J Clin Oncol* **39**, 3377-3390 (2021).

20. O'Donohue, T. et al. Differential Impact of ALK Mutations in Neuroblastoma. *JCO Precis Oncol* **5**(2021).

21. Tucker, E.R. et al. Combination Therapies Targeting ALK-aberrant Neuroblastoma in Preclinical Models. *Clin Cancer Res* **29**, 1317-1331 (2023).

22. Shreenivas, A. et al. ALK fusions in the pan-cancer setting: another tumor-agnostic target? *NPJ Precis Oncol* **7**, 101 (2023).

23. Goldsmith, K.C. et al. Lorlatinib with or without chemotherapy in ALK-driven refractory/relapsed neuroblastoma: phase 1 trial results. *Nat Med* **29**, 1092-1102 (2023).

24. Heaphy, C.M. et al. Prevalence of the alternative lengthening of telomeres telomere maintenance mechanism in human cancer subtypes. *Am J Pathol* **179**, 1608-15 (2011).

25. Wienke, J. et al. The immune landscape of neuroblastoma: Challenges and opportunities for novel therapeutic strategies in pediatric oncology. *Eur J Cancer* **144**, 123-150 (2021).

26. Kennedy, P.T., Zannoupa, D., Son, M.H., Dahal, L.N. & Woolley, J.F. Neuroblastoma: an ongoing cold front for cancer immunotherapy. *J Immunother Cancer* **11**(2023).

27. Anderson, J., Majzner, R.G. & Sondel, P.M. Immunotherapy of Neuroblastoma: Facts and Hopes. *Clin Cancer Res* **28**, 3196-3206 (2022).

28. Markham, A. Naxitamab: First Approval. *Drugs* **81**, 291-296 (2021).

29. Del Bufalo, F. et al. GD2-CART01 for Relapsed or Refractory High-Risk Neuroblastoma. *N Engl J Med* **388**, 1284-1295 (2023).

30. Furlan, A. et al. Multipotent peripheral glial cells generate neuroendocrine cells of the adrenal medulla. *Science* **357**(2017).

31. Huber, K. The sympathoadrenal cell lineage: specification, diversification, and new perspectives. *Dev Biol* **298**, 335-43 (2006).

32. Jansky, S. et al. Single-cell transcriptomic analyses provide insights into the developmental origins of neuroblastoma. *Nat Genet* **53**, 683-693 (2021).

33. Ross, R.A., Spengler, B.A. & Biedler, J.L. Coordinate morphological and biochemical interconversion of human neuroblastoma cells. *J Natl Cancer Inst* **71**, 741-7 (1983).

34. La Quaglia, M.P. & Manchester, K.M. A comparative analysis of neuroblastic and substrate-adherent human neuroblastoma cell lines. *J Pediatr Surg* **31**, 315-8 (1996).

35. Boeva, V. et al. Heterogeneity of neuroblastoma cell identity defined by transcriptional circuitries. *Nat Genet* **49**, 1408-1413 (2017).

36. van Groningen, T. et al. Neuroblastoma is composed of two super-enhancer-associated differentiation states. *Nat Genet* **49**, 1261-1266 (2017).

37. Gartlgruber, M. et al. Super enhancers define regulatory subtypes and cell identity in neuroblastoma. *Nat Cancer* **2**, 114-128 (2021).

38. Zeineldin, M., Patel, A.G. & Dyer, M.A. Neuroblastoma: When differentiation goes awry. *Neuron* **110**, 2916-2928 (2022).

39. Thirant, C. et al. Reversible transitions between noradrenergic and mesenchymal tumor identities define cell plasticity in neuroblastoma. *Nat Commun* **14**, 2575 (2023).

40. Westerhout, E.M. et al. Mesenchymal-Type Neuroblastoma Cells Escape ALK Inhibitors. *Cancer Res* **82**, 484-496 (2022).

41. Sengupta, S. et al. Mesenchymal and adrenergic cell lineage states in neuroblastoma possess distinct immunogenic phenotypes. *Nat Cancer* **3**, 1228-1246 (2022).

42. Mabe, N.W. et al. Transition to a mesenchymal state in neuroblastoma confers resistance to anti-GD2 antibody via reduced expression of ST8SIA1. *Nat Cancer* **3**, 976-993 (2022).

43. Chung, C. et al. Neuroblastoma. *Pediatr Blood Cancer* **68 Suppl 2**, e28473 (2021).

44. Pinto, N.R. et al. Advances in Risk Classification and Treatment Strategies for Neuroblastoma. *J Clin Oncol* **33**, 3008-17 (2015).

45. Chan, G.C. & Chan, C.M. Anti-GD2 Directed Immunotherapy for High-Risk and Metastatic Neuroblastoma. *Biomolecules* **12**(2022).

46. Fischer, M. et al. Ceritinib in paediatric patients with anaplastic lymphoma kinase-positive malignancies: an open-label, multicentre, phase 1, dose-escalation and dose-expansion study. *Lancet Oncol* **22**, 1764-1776 (2021).

47. Saftig, P. & Klumperman, J. Lysosome biogenesis and lysosomal membrane proteins: trafficking meets function. *Nat Rev Mol Cell Biol* **10**, 623-35 (2009).

48. Ballabio, A. & Bonifacino, J.S. Lysosomes as dynamic regulators of cell and organismal homeostasis. *Nat Rev Mol Cell Biol* **21**, 101-118 (2020).

49. de Duve, C. The lysosome turns fifty. *Nat Cell Biol* **7**, 847-9 (2005).

50. Appelqvist, H., Wäster, P., Kågedal, K. & Öllinger, K. The lysosome: from waste bag to potential therapeutic target. *J Mol Cell Biol* **5**, 214-26 (2013).

51. Lawrence, R.E. & Zoncu, R. The lysosome as a cellular centre for signalling, metabolism and quality control. *Nat Cell Biol* **21**, 133-142 (2019).

52. Saftig, P., Schröder, B. & Blanz, J. Lysosomal membrane proteins: life between acid and neutral conditions. *Biochem Soc Trans* **38**, 1420-3 (2010).

53. Perera, R.M. & Zoncu, R. The Lysosome as a Regulatory Hub. *Annu Rev Cell Dev Biol* **32**, 223-253 (2016).

54. Medina, D.L. TRPML1 and TFEB, an Intimate Affair. *Handb Exp Pharmacol* **278**, 109-126 (2023).

55. Yang, C. & Wang, X. Lysosome biogenesis: Regulation and functions. *J Cell Biol* **220**(2021).

56. Puertollano, R., Ferguson, S.M., Brugarolas, J. & Ballabio, A. The complex relationship between TFEB transcription factor phosphorylation and subcellular localization. *Embo j* **37**(2018).

57. Machado, E.R., Annunziata, I., van de Vlekkert, D., Grosveld, G.C. & d'Azzo, A. Lysosomes and Cancer Progression: A Malignant Liaison. *Front Cell Dev Biol* **9**, 642494 (2021).

58. Schwake, M., Schröder, B. & Saftig, P. Lysosomal membrane proteins and their central role in physiology. *Traffic* **14**, 739-48 (2013).

59. Schröder, B.A., Wrocklage, C., Hasilik, A. & Saftig, P. The proteome of lysosomes. *Proteomics* **10**, 4053-76 (2010).

60. Aits, S., Jäättelä, M. & Nylandsted, J. Methods for the quantification of lysosomal membrane permeabilization: a hallmark of lysosomal cell death. *Methods Cell Biol* **126**, 261-85 (2015).

61. Kirkegaard, T. & Jäättelä, M. Lysosomal involvement in cell death and cancer. *Biochim Biophys Acta* **1793**, 746-54 (2009).

62. Yamamoto, H. & Matsui, T. Molecular Mechanisms of Macroautophagy, Microautophagy, and Chaperone-Mediated Autophagy. *J Nippon Med Sch* **91**, 2-9 (2024).

63. Tekirdag, K. & Cuervo, A.M. Chaperone-mediated autophagy and endosomal microautophagy: Joint by a chaperone. *J Biol Chem* **293**, 5414-5424 (2018).

64. Jeger, J.L. Endosomes, lysosomes, and the role of endosomal and lysosomal biogenesis in cancer development. *Mol Biol Rep* **47**, 9801-9810 (2020).

65. Yim, W.W. & Mizushima, N. Lysosome biology in autophagy. *Cell Discov* **6**, 6 (2020).

66. Dielschneider, R.F., Henson, E.S. & Gibson, S.B. Lysosomes as Oxidative Targets for Cancer Therapy. *Oxid Med Cell Longev* **2017**, 3749157 (2017).

67. Tang, T. et al. The role of lysosomes in cancer development and progression. *Cell Biosci* **10**, 131 (2020).

68. Eriksson, I. & Öllinger, K. Lysosomes in Cancer-At the Crossroad of Good and Evil. *Cells* **13**(2024).

69. Min, K.J. & Kwon, T.K. Induction of Lysosomal Membrane Permeabilization Is a Major Event of FTY720-Mediated Non-Apoptotic Cell Death in Human Glioma Cells. *Cancers (Basel)* **12**(2020).

70. Vanden Berghe, T., Linkermann, A., Jouan-Lanhouet, S., Walczak, H. & Vandenabeele, P. Regulated necrosis: the expanding network of non-apoptotic cell death pathways. *Nat Rev Mol Cell Biol* **15**, 135-47 (2014).

71. Boya, P. & Kroemer, G. Lysosomal membrane permeabilization in cell death. *Oncogene* **27**, 6434-51 (2008).

72. Wang, F., Gómez-Sintes, R. & Boya, P. Lysosomal membrane permeabilization and cell death. *Traffic* **19**, 918-931 (2018).

73. Gotink, K.J. et al. Lysosomal sequestration of sunitinib: a novel mechanism of drug resistance. *Clin Cancer Res* **17**, 7337-46 (2011).

74. Zhitomirsky, B. & Assaraf, Y.G. Lysosomes as mediators of drug resistance in cancer. *Drug Resist Updat* **24**, 23-33 (2016).

75. Hraběta, J. et al. Drug Sequestration in Lysosomes as One of the Mechanisms of Chemoresistance of Cancer Cells and the Possibilities of Its Inhibition. *Int J Mol Sci* **21**(2020).

76. Geisslinger, F., Müller, M., Vollmar, A.M. & Bartel, K. Targeting Lysosomes in Cancer as Promising Strategy to Overcome Chemoresistance-A Mini Review. *Front Oncol* **10**, 1156 (2020).

77. Piao, S. & Amaravadi, R.K. Targeting the lysosome in cancer. *Ann N Y Acad Sci* **1371**, 45-54 (2016).

78. Ellegaard, A.M., Bach, P. & Jäättelä, M. Targeting Cancer Lysosomes with Good Old Cationic Amphiphilic Drugs. *Rev Physiol Biochem Pharmacol* **185**, 107-152 (2023).

79. Cao, M., Luo, X., Wu, K. & He, X. Targeting lysosomes in human disease: from basic research to clinical applications. *Signal Transduct Target Ther* **6**, 379 (2021).

80. Hayflick, L. & Moorhead, P.S. The serial cultivation of human diploid cell strains. *Exp Cell Res* **25**, 585-621 (1961).

81. Roger, L., Tomas, F. & Gire, V. Mechanisms and Regulation of Cellular Senescence. *Int J Mol Sci* **22**(2021).

82. Hernandez-Segura, A., Nehme, J. & Demaria, M. Hallmarks of Cellular Senescence. *Trends Cell Biol* **28**, 436-453 (2018).

83. Muñoz-Espín, D. & Serrano, M. Cellular senescence: from physiology to pathology. *Nat Rev Mol Cell Biol* **15**, 482-96 (2014).

84. d'Adda di Fagagna, F. Living on a break: cellular senescence as a DNA-damage response. *Nat Rev Cancer* **8**, 512-22 (2008).

85. Prasanna, P.G. et al. Therapy-Induced Senescence: Opportunities to Improve Anticancer Therapy. *J Natl Cancer Inst* **113**, 1285-1298 (2021).

86. Petrova, N.V., Velichko, A.K., Razin, S.V. & Kantidze, O.L. Small molecule compounds that induce cellular senescence. *Aging Cell* **15**, 999-1017 (2016).

87. Birch, J. & Gil, J. Senescence and the SASP: many therapeutic avenues. *Genes Dev* **34**, 1565-1576 (2020).

88. Schmitt, C.A., Wang, B. & Demaria, M. Senescence and cancer - role and therapeutic opportunities. *Nat Rev Clin Oncol* **19**, 619-636 (2022).

89. Kumari, R. & Jat, P. Mechanisms of Cellular Senescence: Cell Cycle Arrest and Senescence Associated Secretory Phenotype. *Front Cell Dev Biol* **9**, 645593 (2021).

90. Kim, Y.H. & Park, T.J. Cellular senescence in cancer. *BMB Rep* **52**, 42-46 (2019).

91. Herranz, N. & Gil, J. Mechanisms and functions of cellular senescence. *J Clin Invest* **128**, 1238-1246 (2018).

92. Ou, H.L. et al. Cellular senescence in cancer: from mechanisms to detection. *Mol Oncol* **15**, 2634-2671 (2021).

93. Kurz, D.J., Decary, S., Hong, Y. & Erusalimsky, J.D. Senescence-associated (beta)-galactosidase reflects an increase in lysosomal mass during replicative ageing of human endothelial cells. *J Cell Sci* **113 (Pt 20)**, 3613-22 (2000).

94. Yang, N.C. & Hu, M.L. The limitations and validities of senescence associated-beta-galactosidase activity as an aging marker for human foreskin fibroblast Hs68 cells. *Exp Gerontol* **40**, 813-9 (2005).

95. Rossiello, F., Herbig, U., Longhese, M.P., Fumagalli, M. & d'Adda di Fagagna, F. Irreparable telomeric DNA damage and persistent DDR signalling as a shared causative mechanism of cellular senescence and ageing. *Curr Opin Genet Dev* **26**, 89-95 (2014).

96. Huang, W., Hickson, L.J., Eirin, A., Kirkland, J.L. & Lerman, L.O. Cellular senescence: the good, the bad and the unknown. *Nat Rev Nephrol* **18**, 611-627 (2022).

97. Wang, L., Lankhorst, L. & Bernards, R. Exploiting senescence for the treatment of cancer. *Nat Rev Cancer* **22**, 340-355 (2022).

98. Kirkland, J.L. & Tchkonia, T. Cellular Senescence: A Translational Perspective. *EBioMedicine* **21**, 21-28 (2017).

99. Zhang, L., Pitcher, L.E., Prahalad, V., Niedernhofer, L.J. & Robbins, P.D. Targeting cellular senescence with senotherapeutics: senolytics and senomorphics. *Febs j* **290**, 1362-1383 (2023).

100. Laberge, R.M. et al. MTOR regulates the pro-tumorigenic senescence-associated secretory phenotype by promoting IL1A translation. *Nat Cell Biol* **17**, 1049-61 (2015).

101. Lelarge, V., Capelle, R., Oger, F., Mathieu, T. & Le Calvé, B. Senolytics: from pharmacological inhibitors to immunotherapies, a promising future for patients' treatment. *NPJ Aging* **10**, 12 (2024).

102. Watanabe, S., Kawamoto, S., Ohtani, N. & Hara, E. Impact of senescence-associated secretory phenotype and its potential as a therapeutic target for senescence-associated diseases. *Cancer Sci* **108**, 563-569 (2017).

103. Amor, C. et al. Senolytic CAR T cells reverse senescence-associated pathologies. *Nature* **583**, 127-132 (2020).

104. Tsimberidou, A.M., Fountzilas, E., Nikanjam, M. & Kurzrock, R. Review of precision cancer medicine: Evolution of the treatment paradigm. *Cancer Treat Rev* **86**, 102019 (2020).

105. Wang, Y. & Zheng, D. The importance of precision medicine in modern molecular oncology. *Clin Genet* **100**, 248-257 (2021).

106. Hoelder, S., Clarke, P.A. & Workman, P. Discovery of small molecule cancer drugs: successes, challenges and opportunities. *Mol Oncol* **6**, 155-76 (2012).

107. Napoli, G.C., Figg, W.D. & Chau, C.H. Functional Drug Screening in the Era of Precision Medicine. *Front Med (Lausanne)* **9**, 912641 (2022).

108. Letai, A. Functional precision cancer medicine-moving beyond pure genomics. *Nat Med* **23**, 1028-1035 (2017).

109. Horvath, P. et al. Screening out irrelevant cell-based models of disease. *Nat Rev Drug Discov* **15**, 751-769 (2016).

110. Wang, Y. & Jeon, H. 3D cell cultures toward quantitative high-throughput drug screening. *Trends Pharmacol Sci* **43**, 569-581 (2022).

111. Friedrich, J., Seidel, C., Ebner, R. & Kunz-Schughart, L.A. Spheroid-based drug screen: considerations and practical approach. *Nat Protoc* **4**, 309-24 (2009).

112. Tung, Y.C. et al. High-throughput 3D spheroid culture and drug testing using a 384 hanging drop array. *Analyst* **136**, 473-8 (2011).

113. Choo, N. et al. High-Throughput Imaging Assay for Drug Screening of 3D Prostate Cancer Organoids. *SLAS Discov* **26**, 1107-1124 (2021).

114. Wagle, M.C. et al. A transcriptional MAPK Pathway Activity Score (MPAS) is a clinically relevant biomarker in multiple cancer types. *NPJ Precis Oncol* **2**, 7 (2018).

115. He, L. et al. Methods for High-throughput Drug Combination Screening and Synergy Scoring. *Methods Mol Biol* **1711**, 351-398 (2018).

116. Gilad, Y., Gellerman, G., Lonard, D.M. & O'Malley, B.W. Drug Combination in Cancer Treatment-From Cocktails to Conjugated Combinations. *Cancers (Basel)* **13**(2021).

117. DeVita, V.T., Jr. & Chu, E. A history of cancer chemotherapy. *Cancer Res* **68**, 8643-53 (2008).

118. Bayat Mokhtari, R. et al. Combination therapy in combating cancer. *Oncotarget* **8**, 38022-38043 (2017).

119. Chan, G.K., Wilson, S., Schmidt, S. & Moffat, J.G. Unlocking the Potential of High-Throughput Drug Combination Assays Using Acoustic Dispensing. *J Lab Autom* **21**, 125-32 (2016).

120. Meyer, C.T., Wooten, D.J., Lopez, C.F. & Quaranta, V. Charting the Fragmented Landscape of Drug Synergy. *Trends Pharmacol Sci* **41**, 266-280 (2020).

121. Zheng, S. et al. SynergyFinder Plus: Toward Better Interpretation and Annotation of Drug Combination Screening Datasets. *Genomics Proteomics Bioinformatics* **20**, 587-596 (2022).

122. Greco, W.R., Bravo, G. & Parsons, J.C. The search for synergy: a critical review from a response surface perspective. *Pharmacol Rev* **47**, 331-85 (1995).

123. Loewe, S. The problem of synergism and antagonism of combined drugs. *Arzneimittelforschung* **3**, 285-90 (1953).

124. Yadav, B., Wennerberg, K., Aittokallio, T. & Tang, J. Searching for Drug Synergy in Complex Dose-Response Landscapes Using an Interaction Potency Model. *Comput Struct Biotechnol J* **13**, 504-13 (2015).

125. Tang, J., Wennerberg, K. & Aittokallio, T. What is synergy? The Saariselkä agreement revisited. *Front Pharmacol* **6**, 181 (2015).

126. Malyutina, A. et al. Drug combination sensitivity scoring facilitates the discovery of synergistic and efficacious drug combinations in cancer. *PLoS Comput Biol* **15**, e1006752 (2019).

127. Milde, T. et al. HD-MB03 is a novel Group 3 medulloblastoma model demonstrating sensitivity to histone deacetylase inhibitor treatment. *J Neurooncol* **110**, 335-48 (2012).

128. Peterziel, H. et al. Drug sensitivity profiling of 3D tumor tissue cultures in the pediatric precision oncology program INFORM. *NPJ Precis Oncol* **6**, 94 (2022).

129. ElHarouni, D. et al. iTReX: Interactive exploration of mono- and combination therapy dose response profiling data. *Pharmacol Res* **175**, 105996 (2022).

130. Yadav, B. et al. Quantitative scoring of differential drug sensitivity for individually optimized anticancer therapies. *Sci Rep* **4**, 5193 (2014).

131. Stirling, D.R., Carpenter, A.E. & Cimini, B.A. CellProfiler Analyst 3.0: accessible data exploration and machine learning for image analysis. *Bioinformatics* **37**, 3992-3994 (2021).

132. Dao, D. et al. CellProfiler Analyst: interactive data exploration, analysis and classification of large biological image sets. *Bioinformatics* **32**, 3210-3212 (2016).

133. Barbie, D.A. et al. Systematic RNA interference reveals that oncogenic KRAS-driven cancers require TBK1. *Nature* **462**, 108-12 (2009).

134. Sigaud, R. et al. MAPK inhibitor sensitivity scores predict sensitivity driven by the immune infiltration in pediatric low-grade gliomas. *Nat Commun* **14**, 4533 (2023).

135. Dry, J.R. et al. Transcriptional pathway signatures predict MEK addiction and response to selumetinib (AZD6244). *Cancer Res* **70**, 2264-73 (2010).

136. Alborzinia, H. et al. MYCN mediates cysteine addiction and sensitizes neuroblastoma to ferroptosis. *Nat Cancer* **3**, 471-485 (2022).

137. Lu, S., Sung, T., Lin, N., Abraham, R.T. & Jessen, B.A. Lysosomal adaptation: How cells respond to lysosomotropic compounds. *PLoS One* **12**, e0173771 (2017).

138. Redmann, M. et al. Inhibition of autophagy with bafilomycin and chloroquine decreases mitochondrial quality and bioenergetic function in primary neurons. *Redox Biol* **11**, 73-81 (2017).

139. Li, Z.J. et al. Artesunate synergizes with sorafenib to induce ferroptosis in hepatocellular carcinoma. *Acta Pharmacol Sin* **42**, 301-310 (2021).

140. Ferreira, P.M.P., Sousa, R.W.R., Ferreira, J.R.O., Militão, G.C.G. & Bezerra, D.P. Chloroquine and hydroxychloroquine in antitumor therapies based on autophagy-related mechanisms. *Pharmacol Res* **168**, 105582 (2021).

141. Wang, R. et al. Molecular basis of V-ATPase inhibition by bafilomycin A1. *Nat Commun* **12**, 1782 (2021).

142. Homewood, C.A., Warhurst, D.C., Peters, W. & Baggaley, V.C. Lysosomes, pH and the anti-malarial action of chloroquine. *Nature* **235**, 50-2 (1972).

143. Mauthe, M. et al. Chloroquine inhibits autophagic flux by decreasing autophagosome-lysosome fusion. *Autophagy* **14**, 1435-1455 (2018).

144. Levy, J.M.M., Towers, C.G. & Thorburn, A. Targeting autophagy in cancer. *Nat Rev Cancer* **17**, 528-542 (2017).

145. Verbaanderd, C. et al. Repurposing Drugs in Oncology (ReDO)-chloroquine and hydroxychloroquine as anti-cancer agents. *Ecancermedicalscience* **11**, 781 (2017).

146. Jain, V., Singh, M.P. & Amaravadi, R.K. Recent advances in targeting autophagy in cancer. *Trends Pharmacol Sci* **44**, 290-302 (2023).

147. Yusuf, I.H., Charbel Issa, P. & Ahn, S.J. Hydroxychloroquine-induced Retinal Toxicity. *Front Pharmacol* **14**, 1196783 (2023).

148. Kornhuber, J. et al. Identification of novel functional inhibitors of acid sphingomyelinase. *PLoS One* **6**, e23852 (2011).

149. Greenberg, S.B., Grove, G.L. & Cristofalo, V.J. Cell size in aging monolayer cultures. *In Vitro* **13**, 297-300 (1977).

150. Wallis, R. et al. Senescence-associated morphological profiles (SAMPs): an image-based phenotypic profiling method for evaluating the inter and intra model heterogeneity of senescence. *Aging (Albany NY)* **14**, 4220-4246 (2022).

151. Kusumoto, D. et al. Anti-senescent drug screening by deep learning-based morphology senescence scoring. *Nat Commun* **12**, 257 (2021).

152. Rovira, M. et al. The lysosomal proteome of senescent cells contributes to the senescence secretome. *Aging Cell* **21**, e13707 (2022).

153. Tan, J.X. & Finkel, T. Lysosomes in senescence and aging. *EMBO Rep* **24**, e57265 (2023).

154. Zhang, W. et al. Role of Lysosomal Acidification Dysfunction in Mesenchymal Stem Cell Senescence. *Front Cell Dev Biol* **10**, 817877 (2022).

155. Worst, B.C. et al. Next-generation personalised medicine for high-risk paediatric cancer patients - The INFORM pilot study. *Eur J Cancer* **65**, 91-101 (2016).

156. Faheem, M.M. et al. Convergence of therapy-induced senescence (TIS) and EMT in multistep carcinogenesis: current opinions and emerging perspectives. *Cell Death Discov* **6**, 51 (2020).

157. Nambiar, A. et al. Senolytics dasatinib and quercetin in idiopathic pulmonary fibrosis: results of a phase I, single-blind, single-center, randomized, placebo-controlled pilot trial on feasibility and tolerability. *EBioMedicine* **90**, 104481 (2023).

158. Zhu, Y. et al. New agents that target senescent cells: the flavone, fisetin, and the BCL-X(L) inhibitors, A1331852 and A1155463. *Aging (Albany NY)* **9**, 955-963 (2017).

159. Lew, T.E. & Seymour, J.F. Clinical experiences with venetoclax and other pro-apoptotic agents in lymphoid malignancies: lessons from monotherapy and chemotherapy combination. *J Hematol Oncol* **15**, 75 (2022).

160. Robbins, P.D. et al. Senolytic Drugs: Reducing Senescent Cell Viability to Extend Health Span. *Annu Rev Pharmacol Toxicol* **61**, 779-803 (2021).

161. Wakita, M. et al. A BET family protein degrader provokes senolysis by targeting NHEJ and autophagy in senescent cells. *Nat Commun* **11**, 1935 (2020).

162. Acosta, S. et al. Comprehensive characterization of neuroblastoma cell line subtypes reveals bilineage potential similar to neural crest stem cells. *BMC Dev Biol* **9**, 12 (2009).

163. Soldatov, R. et al. Spatiotemporal structure of cell fate decisions in murine neural crest. *Science* **364**(2019).

164. Gomez, R.L., Ibragimova, S., Ramachandran, R., Philpott, A. & Ali, F.R. Tumoral heterogeneity in neuroblastoma. *Biochim Biophys Acta Rev Cancer* **1877**, 188805 (2022).

165. Louis, C.U. & Shohet, J.M. Neuroblastoma: molecular pathogenesis and therapy. *Annu Rev Med* **66**, 49-63 (2015).

166. Sanchez-Vega, F. et al. Oncogenic Signaling Pathways in The Cancer Genome Atlas. *Cell* **173**, 321-337.e10 (2018).

167. Zhang, W. & Liu, H.T. MAPK signal pathways in the regulation of cell proliferation in mammalian cells. *Cell Res* **12**, 9-18 (2002).

168. Mlakar, V., Morel, E., Mlakar, S.J., Ansari, M. & Gumy-Pause, F. A review of the biological and clinical implications of RAS-MAPK pathway alterations in neuroblastoma. *J Exp Clin Cancer Res* **40**, 189 (2021).

169. Kyriakis, J.M. et al. Raf-1 activates MAP kinase-kinase. *Nature* **358**, 417-21 (1992).

170. Song, Y. et al. Targeting RAS-RAF-MEK-ERK signaling pathway in human cancer: Current status in clinical trials. *Genes Dis* **10**, 76-88 (2023).

171. Guo, Y.J. et al. ERK/MAPK signalling pathway and tumorigenesis. *Exp Ther Med* **19**, 1997-2007 (2020).

172. Padovan-Merhar, O.M. et al. Enrichment of Targetable Mutations in the Relapsed Neuroblastoma Genome. *PLoS Genet* **12**, e1006501 (2016).

173. Eleveld, T.F. et al. Relapsed neuroblastomas show frequent RAS-MAPK pathway mutations. *Nat Genet* **47**, 864-71 (2015).

174. Eleveld, T.F. et al. RAS-MAPK Pathway-Driven Tumor Progression Is Associated with Loss of CIC and Other Genomic Aberrations in Neuroblastoma. *Cancer Res* **78**, 6297-6307 (2018).

175. Bollag, G. et al. Loss of NF1 results in activation of the Ras signaling pathway and leads to aberrant growth in haematopoietic cells. *Nat Genet* **12**, 144-8 (1996).

176. Chilamakuri, R. & Agarwal, S. Direct Targeting of the Raf-MEK-ERK Signaling Cascade Inhibits Neuroblastoma Growth. *Curr Oncol* **29**, 6508-6522 (2022).

177. Dorel, M. et al. Neuroblastoma signalling models unveil combination therapies targeting feedback-mediated resistance. *PLoS Comput Biol* **17**, e1009515 (2021).

178. Takeuchi, Y. et al. In vivo effects of short- and long-term MAPK pathway inhibition against neuroblastoma. *J Pediatr Surg* **53**, 2454-2459 (2018).

179. Kun, E., Tsang, Y.T.M., Ng, C.W., Gershenson, D.M. & Wong, K.K. MEK inhibitor resistance mechanisms and recent developments in combination trials. *Cancer Treat Rev* **92**, 102137 (2021).

180. Hart, L.S. et al. Preclinical Therapeutic Synergy of MEK1/2 and CDK4/6 Inhibition in Neuroblastoma. *Clin Cancer Res* **23**, 1785-1796 (2017).

181. Moore, N.F. et al. Molecular rationale for the use of PI3K/AKT/mTOR pathway inhibitors in combination with crizotinib in ALK-mutated neuroblastoma. *Oncotarget* **5**, 8737-49 (2014).

182. Tirosh, I. et al. Single-cell RNA-seq supports a developmental hierarchy in human oligodendroglioma. *Nature* **539**, 309-313 (2016).

183. Hippert, M.M., O'Toole, P.S. & Thorburn, A. Autophagy in cancer: good, bad, or both? *Cancer Res* **66**, 9349-51 (2006).

184. Mulcahy Levy, J.M. & Thorburn, A. Autophagy in cancer: moving from understanding mechanism to improving therapy responses in patients. *Cell Death Differ* **27**, 843-857 (2020).

185. Galluzzi, L. et al. Autophagy in malignant transformation and cancer progression. *Embo j* **34**, 856-80 (2015).

186. Ariosa, A.R. et al. A perspective on the role of autophagy in cancer. *Biochim Biophys Acta Mol Basis Dis* **1867**, 166262 (2021).

187. Russell, R.C. & Guan, K.L. The multifaceted role of autophagy in cancer. *Embo j* **41**, e110031 (2022).

188. Zhang, Z. et al. Role of lysosomes in physiological activities, diseases, and therapy. *J Hematol Oncol* **14**, 79 (2021).

189. Vidak, E., Javoršek, U., Vizovišek, M. & Turk, B. Cysteine Cathepsins and their Extracellular Roles: Shaping the Microenvironment. *Cells* **8**(2019).

190. Fassl, A. et al. Increased lysosomal biomass is responsible for the resistance of triple-negative breast cancers to CDK4/6 inhibition. *Sci Adv* **6**, eabb2210 (2020).

191. Halaby, R. Influence of lysosomal sequestration on multidrug resistance in cancer cells. *Cancer Drug Resist* **2**, 31-42 (2019).

192. Al-Akra, L. et al. Tumor stressors induce two mechanisms of intracellular P-glycoprotein-mediated resistance that are overcome by lysosomal-targeted thiosemicarbazones. *J Biol Chem* **293**, 3562-3587 (2018).

193. Lim, C.Y. & Zoncu, R. The lysosome as a command-and-control center for cellular metabolism. *J Cell Biol* **214**, 653-64 (2016).

194. Lakpa, K.L., Khan, N., Afghah, Z., Chen, X. & Geiger, J.D. Lysosomal Stress Response (LSR): Physiological Importance and Pathological Relevance. *J Neuroimmune Pharmacol* **16**, 219-237 (2021).

195. Settembre, C. & Ballabio, A. Lysosomal adaptation: how the lysosome responds to external cues. *Cold Spring Harb Perspect Biol* **6**(2014).

196. Karageorgos, L.E. et al. Lysosomal biogenesis in lysosomal storage disorders. *Exp Cell Res* **234**, 85-97 (1997).

197. Bajaj, L. et al. Lysosome biogenesis in health and disease. *J Neurochem* **148**, 573-589 (2019).

198. Settembre, C. et al. TFEB links autophagy to lysosomal biogenesis. *Science* **332**, 1429-33 (2011).

199. Sardiello, M. et al. A gene network regulating lysosomal biogenesis and function. *Science* **325**, 473-7 (2009).

200. Hansen, M.B. et al. Identification of lysosome-targeting drugs with anti-inflammatory activity as potential invasion inhibitors of treatment resistant HER2 positive cancers. *Cell Oncol (Dordr)* **44**, 805-820 (2021).

201. Singh, S.S. et al. Dual role of autophagy in hallmarks of cancer. *Oncogene* **37**, 1142-1158 (2018).

202. Henry, B., Ziobro, R., Becker, K.A., Kolesnick, R. & Gulbins, E. Acid sphingomyelinase. *Handb Exp Pharmacol*, 77-88 (2013).

203. Hannun, Y.A. & Obeid, L.M. Many ceramides. *J Biol Chem* **286**, 27855-62 (2011).

204. Sonnino, S. & Prinetti, A. Membrane domains and the "lipid raft" concept. *Curr Med Chem* **20**, 4-21 (2013).

205. Alaamery, M. et al. Role of sphingolipid metabolism in neurodegeneration. *J Neurochem* **158**, 25-35 (2021).

206. Jenkins, R.W., Canals, D. & Hannun, Y.A. Roles and regulation of secretory and lysosomal acid sphingomyelinase. *Cell Signal* **21**, 836-46 (2009).

207. Savić, R. & Schuchman, E.H. Use of acid sphingomyelinase for cancer therapy. *Adv Cancer Res* **117**, 91-115 (2013).

208. Kachler, K. et al. Enhanced Acid Sphingomyelinase Activity Drives Immune Evasion and Tumor Growth in Non-Small Cell Lung Carcinoma. *Cancer Res* **77**, 5963-5976 (2017).

209. Petersen, N.H. et al. Transformation-associated changes in sphingolipid metabolism sensitize cells to lysosomal cell death induced by inhibitors of acid sphingomyelinase. *Cancer Cell* **24**, 379-93 (2013).

210. Bi, J. et al. Targeting glioblastoma signaling and metabolism with a re-purposed brain-penetrant drug. *Cell Rep* **37**, 109957 (2021).

211. Ohtani, N. The roles and mechanisms of senescence-associated secretory phenotype (SASP): can it be controlled by senolysis? *Inflamm Regen* **42**, 11 (2022).

212. Zingoni, A. et al. The senescence journey in cancer immunoediting. *Mol Cancer* **23**, 68 (2024).

213. Ruhland, M.K. et al. Stromal senescence establishes an immunosuppressive microenvironment that drives tumorigenesis. *Nat Commun* **7**, 11762 (2016).

214. Coppé, J.P. et al. Senescence-associated secretory phenotypes reveal cell-nonautonomous functions of oncogenic RAS and the p53 tumor suppressor. *PLoS Biol* **6**, 2853-68 (2008).

215. Ashraf, H.M., Fernandez, B. & Spencer, S.L. The intensities of canonical senescence biomarkers integrate the duration of cell-cycle withdrawal. *Nat Commun* **14**, 4527 (2023).

216. Lee, S. & Schmitt, C.A. The dynamic nature of senescence in cancer. *Nat Cell Biol* **21**, 94-101 (2019).

217. Pizzul, P., Rinaldi, C. & Bonetti, D. The multistep path to replicative senescence onset: zooming on triggering and inhibitory events at telomeric DNA. *Front Cell Dev Biol* **11**, 1250264 (2023).

218. Milanovic, M. et al. Senescence-associated reprogramming promotes cancer stemness. *Nature* **553**, 96-100 (2018).

219. Brägelmann, J. et al. MAPK-pathway inhibition mediates inflammatory reprogramming and sensitizes tumors to targeted activation of innate immunity sensor RIG-I. *Nat Commun* **12**, 5505 (2021).

220. Dou, Z. & Berger, S.L. Senescence Elicits Stemness: A Surprising Mechanism for Cancer Relapse. *Cell Metab* **27**, 710-711 (2018).

221. Tchkonia, T., Zhu, Y., van Deursen, J., Campisi, J. & Kirkland, J.L. Cellular senescence and the senescent secretory phenotype: therapeutic opportunities. *J Clin Invest* **123**, 966-72 (2013).

222. Coppé, J.P., Desprez, P.Y., Krtolica, A. & Campisi, J. The senescence-associated secretory phenotype: the dark side of tumor suppression. *Annu Rev Pathol* **5**, 99-118 (2010).

223. van Tilburg, C.M. et al. The Pediatric Precision Oncology INFORM Registry: Clinical Outcome and Benefit for Patients with Very High-Evidence Targets. *Cancer Discov* **11**, 2764-2779 (2021).

224. Ciccarone, V., Spengler, B.A., Meyers, M.B., Biedler, J.L. & Ross, R.A. Phenotypic diversification in human neuroblastoma cells: expression of distinct neural crest lineages. *Cancer Res* **49**, 219-25 (1989).

225. Yan, X. et al. Cooperative Cross-Talk between Neuroblastoma Subtypes Confers Resistance to Anaplastic Lymphoma Kinase Inhibition. *Genes Cancer* **2**, 538-49 (2011).